QUANTIFYING THE STRAIN RESPONSE IN THE RAT TIBIA DURING SIMULATED RESISTANCE TRAINING USED AS A DISUSE COUNTERMEASURE

A Thesis

by

JAY MELVIN JEFFERY

Submitted to the Office of Graduate Studies of
Texas A&M University
in partial fulfillment of the requirements for the degree of

MASTER OF SCIENCE

December 2007

Major Subject: Mechanical Engineering

QUANTIFYING THE STRAIN RESPONSE IN THE RAT TIBIA DURING SIMULATED RESISTANCE TRAINING USED AS A DISUSE COUNTERMEASURE

A Thesis

by

JAY MELVIN JEFFERY

Submitted to the Office of Graduate Studies of
Texas A&M University
in partial fulfillment of the requirements for the degree of

MASTER OF SCIENCE

Approved by:

Co-Chairs of Committee,	Harry A. Hogan
	Susan A. Bloomfield
Committee Member,	Anastasia H. Muliana
Head of Department,	Dennis O'Neal

December 2007

Major Subject: Mechanical Engineering

ABSTRACT

Quantifying the Strain Response in the Rat Tibia During Simulated Resistance Training Used as a Disuse Countermeasure. (December 2007)

Jay Melvin Jeffery, B.S., Brigham Young University

Co-chairs of Advisory Committee: Dr. Harry A. Hogan
Dr. Susan A. Bloomfield

Disuse of weight bearing bones has been shown to cause bone loss. This poses a health concern for people exposed to microgravity, such as astronauts. Animal studies are used to study factors related to bone loss and countermeasures to prevent bone loss. This study used a hindlimb unloaded (HU) rat model to simulate microgravity and a muscle stimulation countermeasure to simulate resistive exercise. Uniaxial strain gages were implanted on the antero-medial aspect of the proximal tibia to measure the mechanical strain during a typical exercise session.

In a separate but parallel study, the exercise was shown to be an effective countermeasure to disuse related bone loss. The current study sought to understand the loading of the bone during the exercise. To determine if the strain response changes during a protocol using this countermeasure, strains were measured on a group of weight bearing animals and a group that were hind limb unloaded and received the countermeasure for 21 days. Strain magnitudes and rates were considered and related to torques at the ankle joint. No significant differences in strain magnitudes were noted between the baseline control group and the hindlimb unloaded group that received the countermeasure.

The two kinds of contractions used in an exercise session are isometric and eccentric. The isometric contractions are used to adjust the stimulation equipment for the eccentric contractions, which constitute the exercise. Peak strain levels during the isometric contractions ranged from 900 to 2200 microstrain while the eccentric were 38% lower and ranged from 600 to 1400. Eccentric strain rates were 62% lower than the isometric contractions strain rates. These results indicate that the strain environment

during the isometric contractions may be causing more of the osteogenic response than the eccentric contractions, which have previously been thought to be the primary part of the countermeasure.

ACKNOWLEDGMENTS

I would like to thank all the people who have helped me through my graduate studies. Especially I would like to thank Dr. Harry Hogan and Dr. Susan Bloomfield for teaching me and guiding me in such an unfamiliar field. Also, I would like to thank Brent Vyvial, Jan Stallone, and Michael Murphy for helping me learn the techniques and conduct the study. I extend a special thank you to Lindsay Sumner, Matts Nilsson and Sabrina Macmanus for help with animal care. Most of all I want to thank my family, especially my wife Jennifer, for all the love, help, and support. Thank you all.

TABLE OF CONTENTS

Page

LIST OF FIGURES

Page

Page

Page

LIST OF TABLES

Page

INTRODUCTION

Motivation and Rationale

Like other systems in the body, the skeletal system is adaptive. When exposed to larger than normal loads, weight-bearing bones often increase in strength. The reverse is also true in that, when skeletal loading is reduced, bones can become weaker. Loss of skeletal integrity during periods of disuse poses a health risk to bed ridden patients and people exposed to microgravity.

Two approaches to counteract disuse related bone loss are resistive exercise and administration of antiresorptive medications. The nuances of how these treatments affect bone adaptation are not fully understood. Animal studies play an important role in isolating and studying specific factors related to these treatments. With an understanding of how bones change and how these treatments affect the skeletal system, health professionals will be better equipped to help people maintain skeletal health.

Objectives

This study investigated the electrical muscle stimulation of the leg in rat models as a countermeasure to disuse-related bone loss. Previous work by Brent Vyvial (2006) used strain gages to quantify the loading on the surface of the proximal tibia during a similar protocol[1]. The current study was intended to extend this work using a modified protocol with two basic goals: (1) to characterize the bone strains for the new protocol, and (2) to seek greater statistical power in comparisons between animal groups. In the study by Vyvial, groups at 3 time points during an exercise protocol were compared to see how the protocol affects the strain environment, but the number of animals in each group was too low to permit statistically significant comparisons. The current study paralleled a study by Lindsay Sumner[2], who extended the work of Justin Alcorn (2006)[3] with this modified protocol to investigate the effectiveness of the simulated resistance training countermeasure.

This thesis follows the style of the *Journal of Bone and Mineral Research*.

The hindlimb unloaded rat model is a generally accepted model for microgravity effects on the skeleton[4] and was used for this study. The muscle stimulation protocol utilizes subcutaneous fine wire electrodes to stimulate the sciatic nerve in the leg, causing the lower leg (calf) muscles to contract and rotate the foot in plantarflexion. The foot is attached to a foot plate interfaced with a stepper motor to resist the motion, producing an eccentric (muscle lengthening) contraction as the foot is forced into dorsifelxion, hence simulating a resistance exercise. This simulated exercise is used throughout a period of hindlimb unloading as a possible countermeasure to disuse. Data from a strain gage attached to the tibia was matched with torque data measured at the stepper motor shaft to quantify both the loading and strain response of the bone.

This study was designed to address the following questions

1. What is the strain level experienced on the tibia during the current muscle stimulation exercise and how does this compare to the results of Vyvial (2006)?
2. What is the relationship between strain on the tibia and torque at the ankle? Further, does this relationship change from the very beginning of the study (i.e., before hindlimb unloading plus exercise (HU+Ex) starts, and also after 3 weeks of HU+Ex?
3. What can these tell us about the exercise as a countermeasure to disuse?

The design of this study was not to directly test the efficacy of the countermeasure. The parallel study of Sumner was conducted to investigate the potential of this exercise to prevent bone loss. The objective of the current study is to quantify the strain environment of the tibia during the exercise, and investigate whether the environment changes during the protocol.

The current study is part of a larger investigation by the Bone Biology Lab at Texas A&M University. The goal of the investigation is to learn how dosages of antiresorptive medications and exercise countermeasures interact in preventing bone loss. Muscle stimulation is being tested as a means of dosing resistance exercise.

Bone Structure

The features found in bone are shown in Figure 1. The outer surface is called the periosteum and contains osteoblasts, which are cells capable of forming bone.

Osteocytes are cells situated inside miniature cavities inside bone material which detect mechanical deformation.

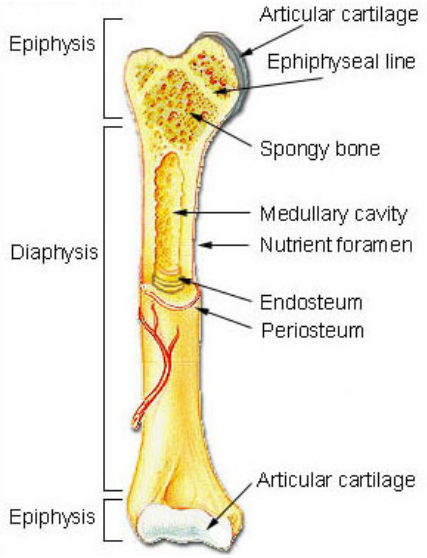

Figure 1 Structure of a typical long bone[5].

There are two basic types of bone in mature mammals: cortical bone and cancellous bone. Cortical bone is dense, stiff and strong. Collagen protein fibers are oriented parallel to the longitudinal axis in what is called lamellar bone. Primary bone resembles a tree trunk with rings of fibers centered on the axis of the bone. This is the bone structure in the long bones of rats. In larger animals, such as humans, fibers form smaller rings within primary bone centered on Haversian canals (Figure 2).

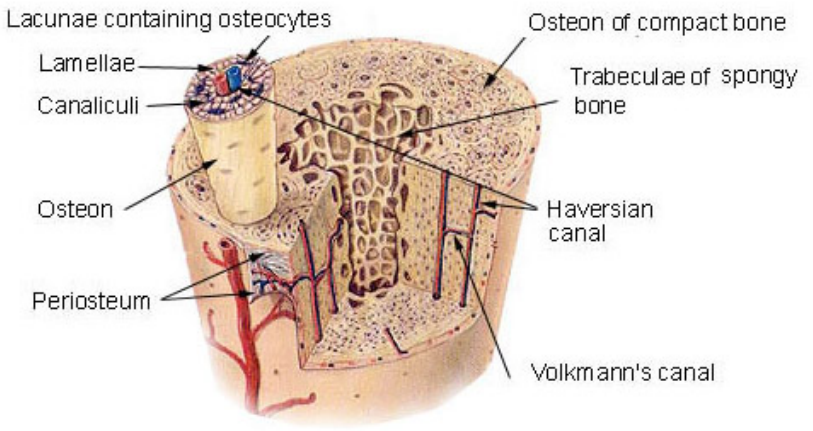

Figure 2 Structure of bone tissue in larger animals[6].

Cancellous bone is found on the inner surfaces of many bones, usually towards the ends of long bones and in bones loaded compressively such as vertebrae. Its structure is made up of connective struts and plates called trabeculae and is often called trabecular bone. Because of its porous structure, is also called spongy bone. This bone is more responsive to disuse and other factors which cause loss of bone.

Mechanical Adaptation

Bone tissue has strain limits which are controlled in a closed loop manner. When strains exceed a certain threshold, octeocyte cells sense this and trigger bone formation. New bone is formed in a region that will strengthen and/or stiffen the bone structure. This can involve removing bone from some areas, while laying down new bone elsewhere to change the shape without adding bone volume. For example, a curved bone may straighten. The bone geometry is adjusted until strains return to the normal range. Because the bone is maintained within certain mechanical limits in a similar way to a thermostat in a thermal system, Howard Frost has termed this closed loop behavior the "mechanostat.[7]"

This closed loop behavior can also cause bone that is not experiencing normal loading to be resorbed, down regulating skeletal mass. Exposure to microgravity has

been shown to degrade the strength of weight bearing bones of astronauts and cosmonauts. Crew members of the International Space Station making 4 to 6 month flights were reported to have lost bone mineral density at a rate of about 1% per month in the hip and spine[8]. In another study, a cosmonaut who flew a 6 month mission to the MIR station was monitored pre and post flight[9]. It was determined that the bone mass lost was not recovered after 6 months of weight bearing activity.

Methods for Studying Skeletal Adaptation

Many approaches have been used to simulate disuse and exercise countermeasures in animal models. Animal models are used to study isolated factors *in vivo* that would be either impractical or unethical to isolate in human subjects. Many of these approaches are reviewed by Alexander G. Robling et al.[10].

Early studies used turkeys with pins attached to long bones to isolate and control bone loading[11]. These pins were glued into holes drilled in the bone. A loader attached to the pins could impose cyclic bending of the bone with rate and magnitude controlled. This method is invasive, which makes factors related to the loading difficult to isolate from artifacts of the implantation. While it does not load the bone in a manner of high physiological relevance, this probably makes the procedure well suited for studying osteogenic thresholds in novel loading.

For rat and mouse models, a four point bending apparatus has been used to load the tibia[12]. Four-point bending puts a section of bone into state of constant bending moment, which is easily calculated from beam theory. Loading is normally cyclical and used to study how bone tissue responds to mechanical factors. The loading is not physiological in nature, which again makes this method ideal for the study of novel loading. This procedure is non-invasive; however, the possibility of inflammation resulting from the pads compressing the soft tissue surrounding the bone and periostium complicate interpretation of the results.

Another approach to mechanical loading is to put the bone in axial compression. This approach has been used for mouse and rat models on both the ulna[13] and tibia[14]. Cups attached to an actuator fit over the upper and lower joints of the limb; cyclical

loading is applied in axial compression. This method more closely approximates the kind of loading the bone would experience in normal physical activity and the sites of contact are removed from the parts of the bone which are studied.

These models all employ external loading that differs from that encountered during locomotion. Ambulatory activities are less attractive for these studies as the intensity cannot be controlled, and training of the animals may be required. A flywheel based resistance exercise has been developed in which the rat uses its muscles to load the bone[15]. A rat is trained to jump against a rotating mass, which gives the researcher control of the timing of the exercise and the work done by the muscles. This has the advantage of the animal's muscle being used to load the bone and is more physiological. The disadvantage is that because the exercise is voluntary, the effort and intensity can be difficult to control with laboratory animals.

The current protocol uses stimulation of the leg muscles of the rat to load the bone in a controlled, involuntary way. This gives the researcher control over the loading, while maintaining physiological relevance. The procedure is noninvasive and requires only mild anesthesia. The mechanics and precedent of the procedure are explained in the Methods section.

Strain Gages

Strain gages have been used in many of these and other studies to understand the response of bone to loads. Strain gages use a foil grid on a polymer substrate to transduce a change in mechanical strain to a change in electrical resistance. For a useful review of strain gage techniques, history and results relating to bone, see Fritton et al (2001)[16].

Strain gages operate on the principle that the resistance of a wire R will change as it is stretched or contracted according to the relationship

$$R = \frac{\rho L}{A} \qquad \text{(Equation 1)}$$

where L is the length of the wire, A is the cross sectional area and ρ is the resistivity of the wire material. Note that Poisson contraction will affect the area, increasing the effectiveness of the gage. A uniaxial strain gage is shown in Figure 3.

Figure 3 A close-up view of a uniaxial strain gage

To fully quantify a strain field requires knowing the strain in three independent directions. Rosette strain gages have 3 separate gage elements in independent directions so that the full strain state can be calculated. Uniaxial strain gages only measure strain in one direction and can only approximate a strain state if the strain gage direction matches the axis of principle strain.

The change in resistance of practical strain gages is several orders of magnitude less than the resistance of the gage, so signal conditioning is required to make a useful output. A Wheatstone bridge is used to turn the change in resistance into a change in voltage, as shown in Figure 4. The anisotropy of the material and irregularity of bone geometry limit the configuration to a quarter bridge. This makes a gage especially susceptible to temperature and environmental factors. A useful equation for the output voltage V_{out} from a Wheatstone bridge is

$$V_{out} = V_{exitation} \frac{R_3 R_1 - R_4 R_2}{(R_2 + R_3)(R_1 + R_4)} \quad \text{(Equation 2)}$$

Where $V_{excitation}$ is the excitation voltage, R_1 is the gage resistance and R_2, R_3 and R_4 are the resistances of the other resistors in the bridge. Amplification, calibration, and filtering are also needed to make the signal readable.

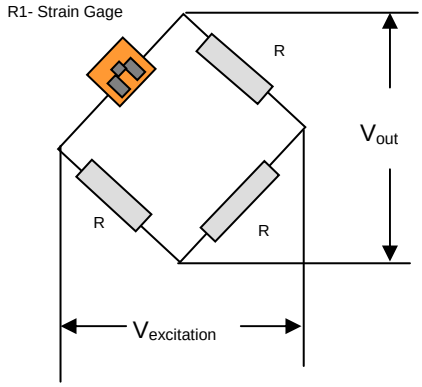

Figure 4 A Wheatstone bridge allows the resistance in a strain gage to be measured as a voltage.

METHODS

Animals

Sixteen male 6-month-old Sprague-Dawley rats were used in this study. This strain and age of rats was used in the previous study of Vyvial and the parallel contemporaneous study of Sumner. The rats were fed ad-libitum and housed singly with a 12-hour light/dark cycle. The animal procedures were approved by the Texas A&M University Laboratory Animal Care Committee under the Animal Use Protocol number 2003-179. The anesthesia administered was inhaled isoflurane for the muscle stimulation, with a higher dose administered for gage surgery, and injected Ketamine/medetomidine for the tail harnessing procedure.

Animals were originally grouped according to body mass and peak isometric torque (PIT) into 2 groups of 7 animals. The first group was baseline control (BL) which had strain gages implanted and strain measurements taken at the beginning of the experiment. Two animals from this group had strain gages placed improperly and 1 had a gage failure, yielding unreliable data. For this reason, 2 animals of the same age and strain were studied separately, and the data was included in the current study. The data from these agreed well with the other BL group animals' data. One animal's isometric data was not usable. In the end, for the BL group the number of animals was n=6 for the eccentric contraction data and n=5 for the isometric data. The experimental group was hindlimb unloaded and received the exercise countermeasure (HU+Ex) for 21 days. After the 21 days, gages were implanted and strain measurements taken. All gages functioned properly and n=7 for both types of contractions in the HU + Ex group.

The duration of 21 days was chosen to match the period of hindlimb unloading used by Vyvial (2006). Typical hindlimb unloading protocols in our lab last for 28 days and this duration generally shows a detectable loss of cancellous bone in the tibia of adult rats[17]. The study Alcorn (2006) conducted to investigate the efficacy of the previous exercise countermeasure protocol, and the study Sumner (2007) conducted to investigate the current protocol both used 28 days of hindlimb unloading.

Muscle Stimulation

The muscle stimulation was performed on a miniature isokinetic dynamometer. The system was first used to test muscle function in mice[18] and has been adapted for the rat[19]. It has been in use by the Bone Biology Lab at Texas A&M University for several years, primarily in the study of muscle function[20]. The system consists of 3 basic parts. An Aurora Scientific 305B stepper motor (Aurora, Ontario, Canada) with an aluminum foot pedal controls the position of the foot and rotates about the axis of the ankle of the rat. It has both position and torque feedback. A Grass S48 stimulator with an SIU-5 stimulus isolation unit (Grass-Telefactor, MA) administers a small electric pulse to stimulate muscle contraction by means of 2 fine wire electrodes. A computer controls the motor and the stimulator while recording data using a program in Test Point (SuperLogics Inc., MA) . The Test Point programs control data acquisition and synchronization of the electrical stimulation signal and the foot pedal position.

The left leg was shaved and antiseptic applied to the skin where the electrodes would be placed. The electrodes are thin, solid wire (Stablohm 800B size 0.003, California Fine Wire Company, Grover Beach, CA). The insulation was burned off the ends using a standard cigarette lighter and the electrodes were put into 27.5 gage guide needles. The needles were inserted into the upper leg on either side of the sciatic nerve and the needles were withdrawn, leaving the electrodes. This is shown in Figure 5. A clamp held the knee to keep the leg from moving while the foot rotated.

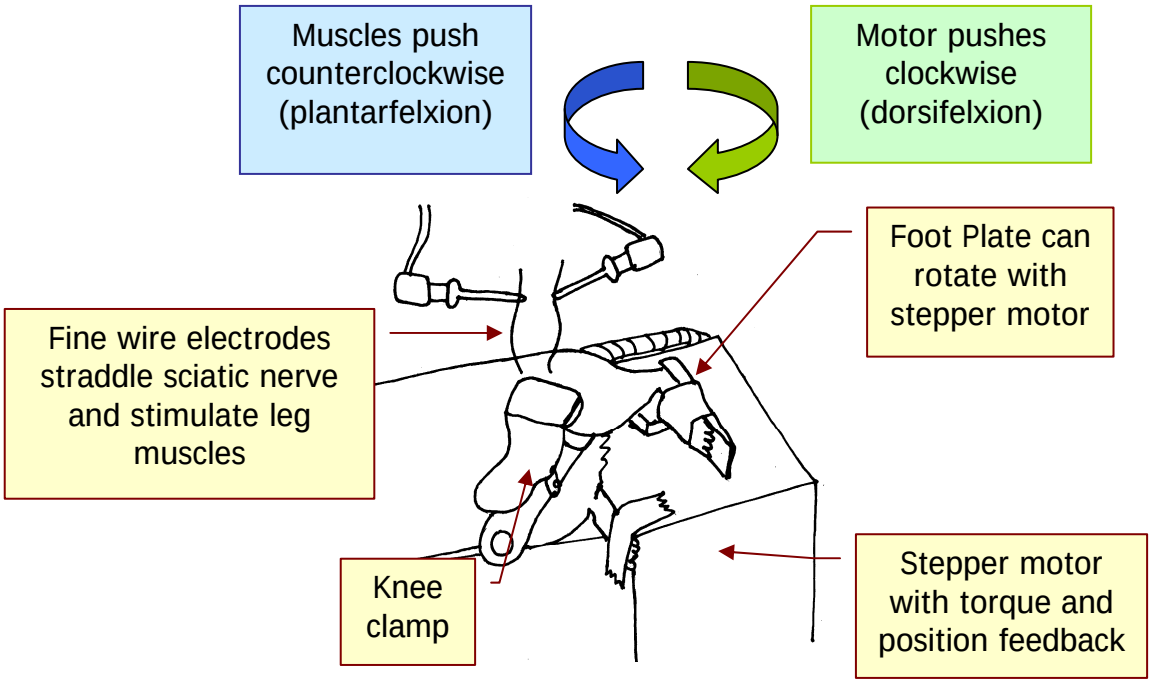

Figure 5 Muscle stimulation set up. Fine wire electrodes stimulate the muscles of the lower limb causing the foot to try to rotate at the ankle in plantarflexion. The foot is taped to a footplate on a stepper motor that controls the angular position of the foot. The motor resists the rotation of the foot by holding it stationary or forces a dorsifelxion rotation. The leg is held in place with a knee clamp.

The muscle stimulation procedure consists of 2 types of contractions. The first is an isometric contraction where the foot is held in stationary and muscle length is not allowed to change. The stepper motor records the torque required to keep the foot from rotating. The stimulus is applied at 175 Hz for 200ms. The purpose of these contractions is to find the peak isometric torque (PIT) and the stimulation voltage needed to attain it. This contraction is illustrated in Figure 6.

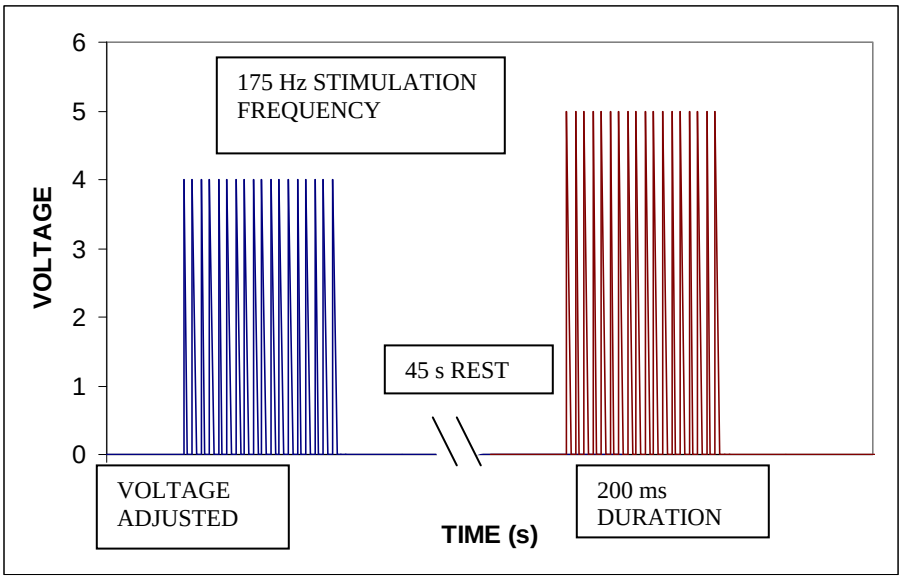

Figure 6 Two isometric contraction stimulations for voltage optimization. This is done by increasing the voltage until the peak isometric torque (PIT) is found. This diagram only illustrates attributes of the stimulation and does not represent actual machine output.

The second type of muscle contraction is an eccentric contraction and is the type used in the exercise. The motor moves the foot through 40 degrees of dorisiflexor rotation while the leg applies force in the opposite rotational direction (tending to plantarflex the joint). The motor torque required for the movement was recorded. The stimulation and rotation duration are 1 second. These contractions are done at the voltage at which PIT was observed. The frequency which gives the same torque in eccentric contractions as the PIT is found by trial and error and is then used for the exercise. The eccentric contraction stimulus is illustrated in Figure 7 and the role of both contractions is illustrated in Figure 8 Stages of an exercise sessionFigure 8.

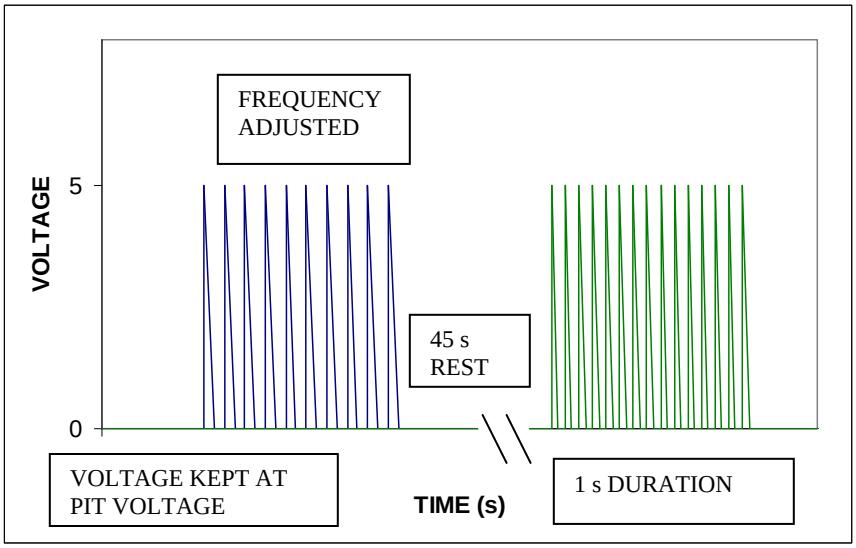

Figure 7 Eccentric contraction stimulation. Voltage is kept at the same level used to achieve PIT. Frequency is adjusted until the peak torque matches PIT. This frequency is used for the exercise and with more eccentric contractions. This diagram only illustrates attributes of the stimulation and does not represent actual machine output.

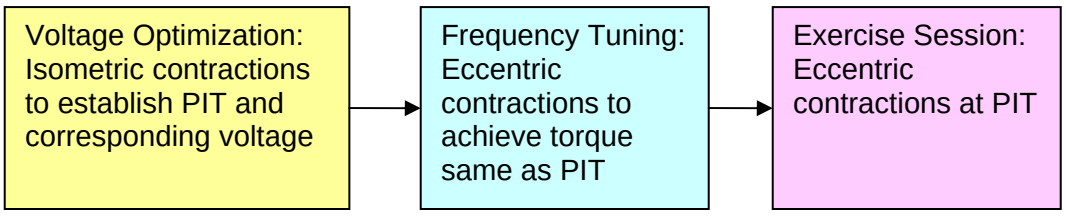

Figure 8 Stages of an exercise session

Differences between the protocol employed in this study and the previous protocol employed by Alcorn (2006) and Vyvial (2006) are in the angle through which the pedal travels, the duration of the eccentric contraction, and the number of repetitions in each set. In the previous protocol, isometric contractions were done with the foot at a right angle to the leg. Changes to the angles are illustrated in Figure 9 and 10. The angle has been changed to 20^{o} from this position towards the shin (i.e., more dorsiflexion). The eccentric contractions swept from -20^{o} to 20^{o} towards the shin in the

previous study (Figure 9 left). In the current study, the eccentric contraction swept from the position perpendicular to the leg to 40° towards the shin (Figure 9 right).

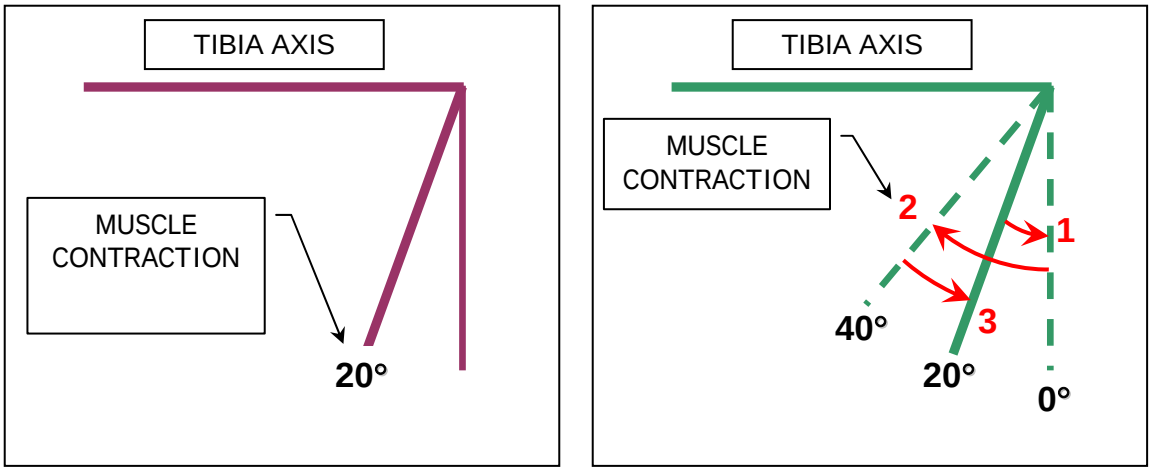

Figure 9 The current protocol. The isometric contractions (left) were done at 20°. Eccentric contractions (right) started with the foot 20° towards the tibia, swept to 0° (1), swept towards the tibia 40° (2-the muscle contracts during this motion), and returns to the starting position (3).

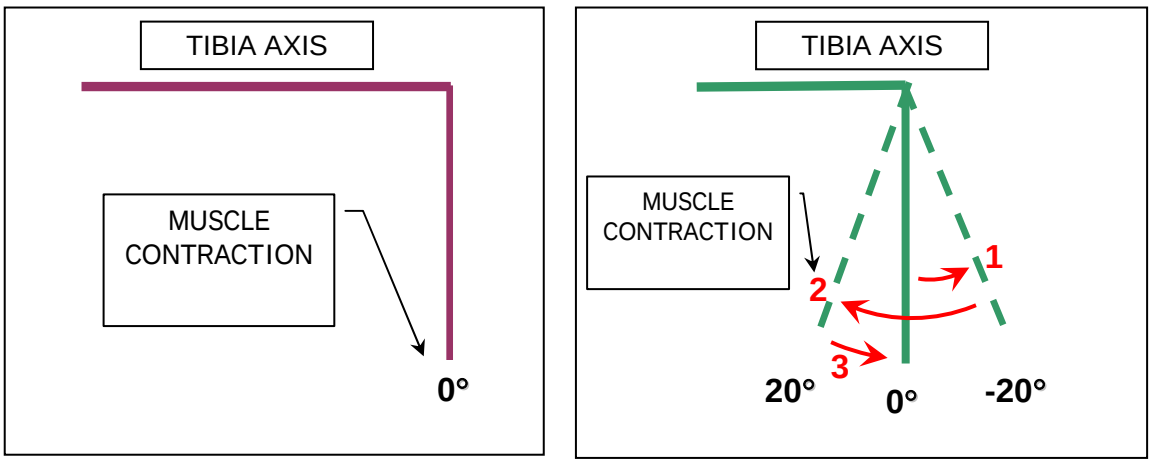

Figure 10 The previous protocol of Alcorn and Vyvial (2006). The isometric contractions (left) were done at 0°. Eccentric contractions (right) started with the foot at a right angle to the tibia, swept away from the tibia 20° (1), swept towards the tibia 40° (2-the muscle contracts during this motion), and returns to the starting position (3).

The duration of the eccentric contractions was increased from 500 ms to 1000ms. This change is illustrated in Figure 11. The number of contractions per session was decreased from 4 sets of 10 to 4 sets of 5. This maintains the same total contraction time. Because the new angle increases the torques recorded by the motor, the eccentric contractions are now done at 100% of PIT instead of 120% of PIT, as was done previously. This kept the intensity roughly equivalent. In the previous study, the eccentric contractions were spaced 10 seconds apart; in the current study they were spaced 12 seconds apart. The 2-minute rest between sets stayed the same.

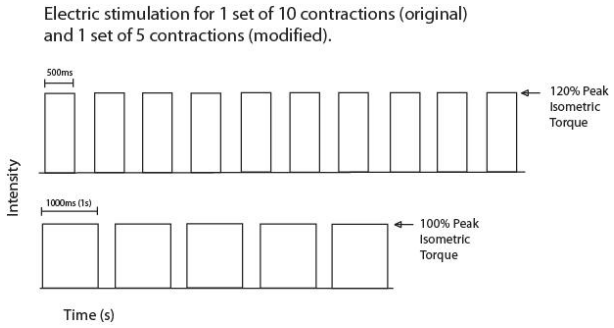

Figure 11 The new protocol increased from 500 ms contractions to 1 s eccentric contractions, but reduced the number by half. Note that the time axis does not represent the intervals between contractions.

Hindlimb Unloading

To simulate microgravity, hindlimb unloading was used. This is a widely accepted ground-based model for microgravity in that the hindlimbs are in a state of disuse, and a head down position creates a fluid shift similar to that in microgravity. Hindlimb unloading methodology is discussed in detail in a review by Emily R. Morey-Holton et al.[21].

To unload the hindlimbs of the experimental group, U-shaped harness were made of cloth tape and glued to the tail of each animal with Plumber's Goop adhesive. A paperclip hook at the top of each harness was attached to a swivel which runs along a

wire at the top of a specially designed cage. The height was adjusted to so that the animal's hind feet were lifted off the floor of the cage with the body in a slight head down position. This position allows the animal to ambulate, eat and groom normally after 1-2 days of acclimation (see Figure 12). Food intake was carefully monitored and the tail was checked as part of daily health monitoring. All animals in the hindlimb unloaded group remained healthy throughout the experiment.

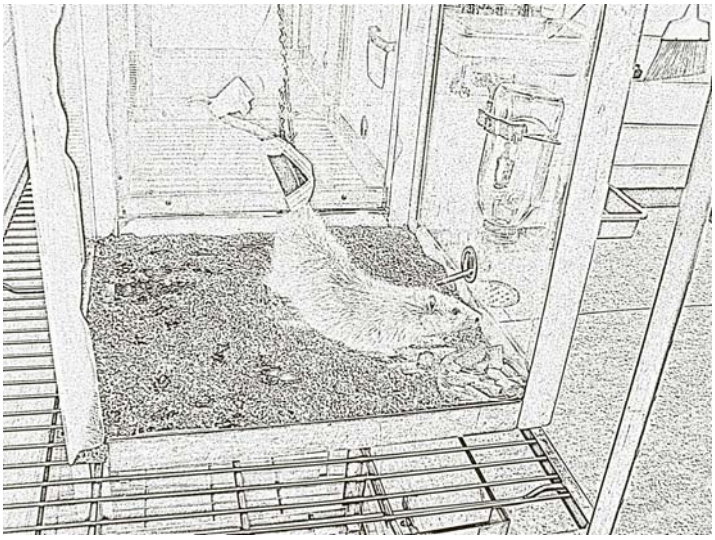

Figure 12 A hindlimb unloaded (HU) rat has the feet held off the floor by means of a tail harness, which is suspended from a wire at the top of the cage

Strain Measurement

The animal was anesthetized and the lower leg was shaved. A cut was made over the antero-medial aspect of the proximal tibia and the soft tissue on top of bone cleared from the strain gage site. The proximal tibia was the site chosen since it is a mixed site with both cortical and cancellous bone. Cancellous bone is typically lost first and most rapidly during disuse, so this site is the preferred place to detect early changes. The antero-medial aspect is located near the skin and implantation requires minimal tissue damage.

The strain gages used were Vishay model EA-06-015SE-120 (Measurements Group, NC). Leads were soldered to the gage prior to implantation and a polyurethane coating was applied. A prepared gage is shown in Figure 13. Gages were attached to the bone using cyanoacrylate adhesive. Data were collected on a Model 6100 Vishay scanner (Measurements Group, NC) and recorded to a computer using Strain Smart software (Measurements Group, NC).

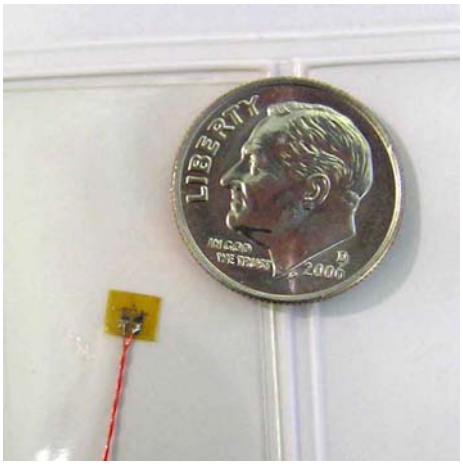

Figure 13 Strain gage used in the study with leads attached. Coin shown for scale.

In the work of Vyvial, strains were measured for eccentric contractions only, because these are considered to be the exercise countermeasure. The setup of the machine involves isometric contractions and has not traditionally been considered a part of the exercise. In the current study, strain is measured and considered for both types of contractions to more comprehensively understand what the bone experiences during the entire training session.

The stimulation procedure for measuring strain followed closely the procedure used during the resistive exercise sessions. Isometric contractions were done at increasing voltage until the torque saturated; this torque was the PIT. Once the voltage producing PIT was found, strain was recorded for 4 isometric contractions: 2 with the

foot at a right angle as in the previous protocol and 2 with the foot positioned 20^{o} towards the shin (dorsiflexed), as was done in the current protocol. These angles represent the middle point of the range used in their respective eccentric protocols and the angle where the voltage optimization in each session was performed. To vary the loading, strain was measured for eccentric contractions with stimulations at frequencies from 20 to 70 Hz in increments of 5 Hz. Some animals did not achieve torques of the same magnitude as was expected at these frequencies, so some animals were stimulated up to 90 Hz. The frequency to achieve a given torque value will vary with electrode placement, so the stimulation frequencies above and below those employed in the exercise protocol were used. Readings of torque were sampled at 10 kHz and strain was sampled at either 5 kHz or 10kHz. Immediately following the data collection, each animal was euthanized.

Data Analysis

Programs written in Matlab (The MathWorks, Natick, MA) were used to consolidate and filter the data sets. For the eccentric contractions, strain data was filtered with a Butterworth 10^{th} order filter and a cutoff frequency of 0.07. Isometric contraction strain data was filtered with a 1000^{th} order FIR1 filter and a cutoff frequency of 0.01. Due to the quarter Wheatstone bridge strain gage configuration's temperature sensitivity, the strain data had to be zeroed by subtracting the average of the first 0.1 seconds of data from each stain reading. Data preceding the start of the contraction was removed. Because torque and strain were recorded on independent computers, it was not possible to synchronize the torque data to the strain data in real time. To match up torque and strain in a repeatable way, the effective area in a torque versus strain curve with loading and unloading was minimized. This process and its implications are discussed in the Results section.

The data sets were loaded into Excel (Microsoft Corp.) for analysis. Strain values and rates were calculated. Plots were made to show differences between groups and find relationships between torque and strain. These values and relationships were imported into SigmaStat (Systat Software Inc., CA) for statistical analysis. Regressions

done in SigmaStat output P values for slopes and intercepts, which represent the statistical power of the regression. Also reported are P values comparing the 2 groups with t-tests. A two way ANOVA was used to compare eccentric and isometric contractions, which tested for the interactions between the 2 groups and the 2 types of contractions.

RESULTS

Eccentric Contractions

For each eccentric contraction at a given frequency, torque and strain measurements were recorded. Sample plots of torque and strain versus time are shown in Figure 14 and Figure 15, respectively. These show an increase in both torque and strain as the stimulation frequency increases.

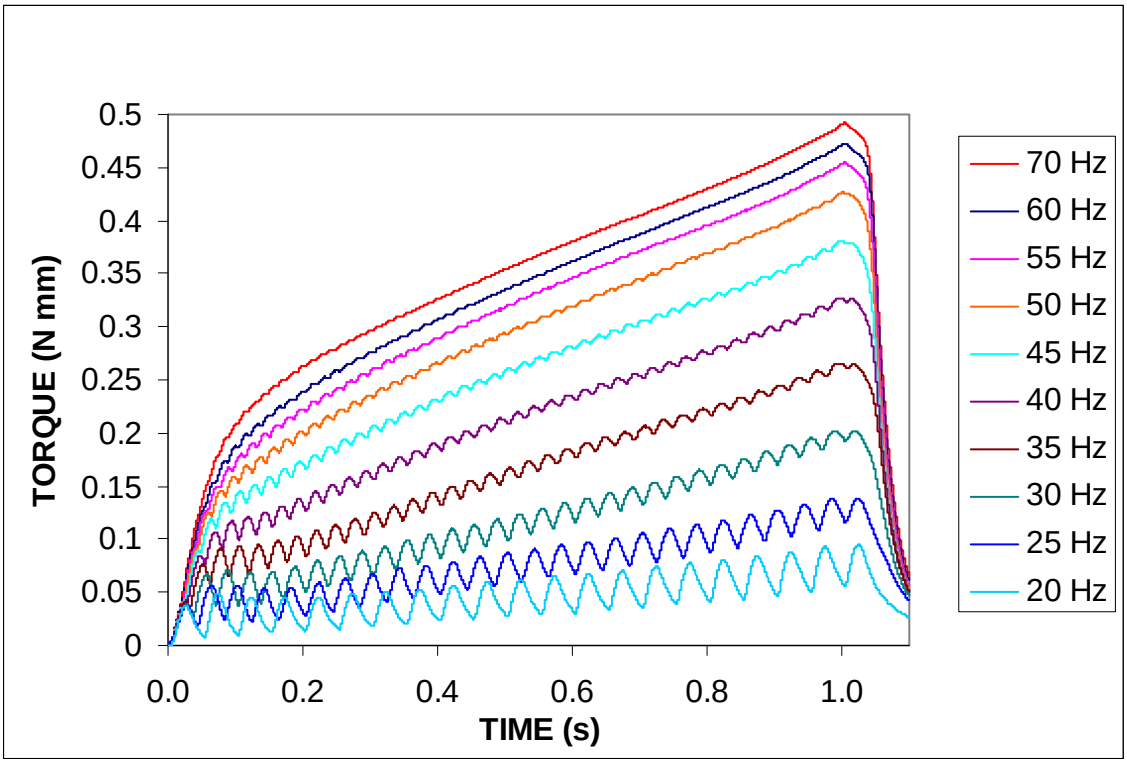

Figure 14 Torque at ankle from eccentric contractions at several stimulation frequencies.

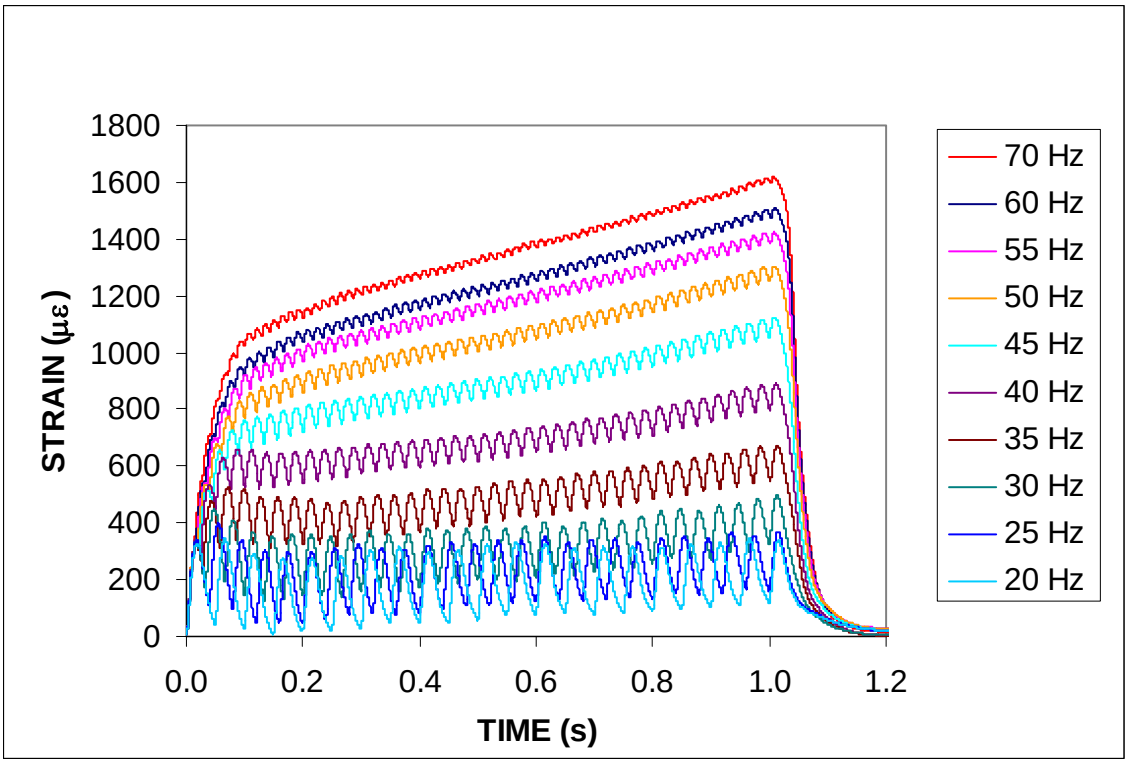

Figure 15 Strain on the tibia from eccentric contractions at several stimulation frequencies.

Stimulation frequencies appear in the torque and strain as nearly sinusoidal oscillations. The lines from higher frequencies tend to have lower oscillation magnitudes. The torques increased as the foot swept from a right angle to 40^{o} towards the shin in a fairly linear manner. The strain often increased during the stimulus delivery, but in some instances flattened out or even decreased. The cases where the strains peaked and did not increase during the stimulations were done with stimulation frequencies that exceeded those used in the exercise sessions (70 Hz).

The strain data were used to calculate peak strains, average strains, and strain rates, as illustrated in Figure 16. The peak strain is simply the highest strain recorded. The average strain was found by taking the mean of the strain values through the entire contraction. The initial strain rate was found by taking instantaneous slopes of the line and averaging these over the initial rise (0.01 seconds). Maximum oscillatory strain

rates were found by averaging the instantaneous slopes for 0.0012 seconds in the region where the strains exhibit sinusoidal-like behavior (0.2-0.8 seconds). In the work of Vyvial, secondary strain rates were reported. These were found by averaging the slopes of the entire middle portion of the curve. Secondary strain rates were calculated in this study, but as in the past study, did not correlate well with exercise intensity or demonstrate any physical significance. For this reason they are not reported here.

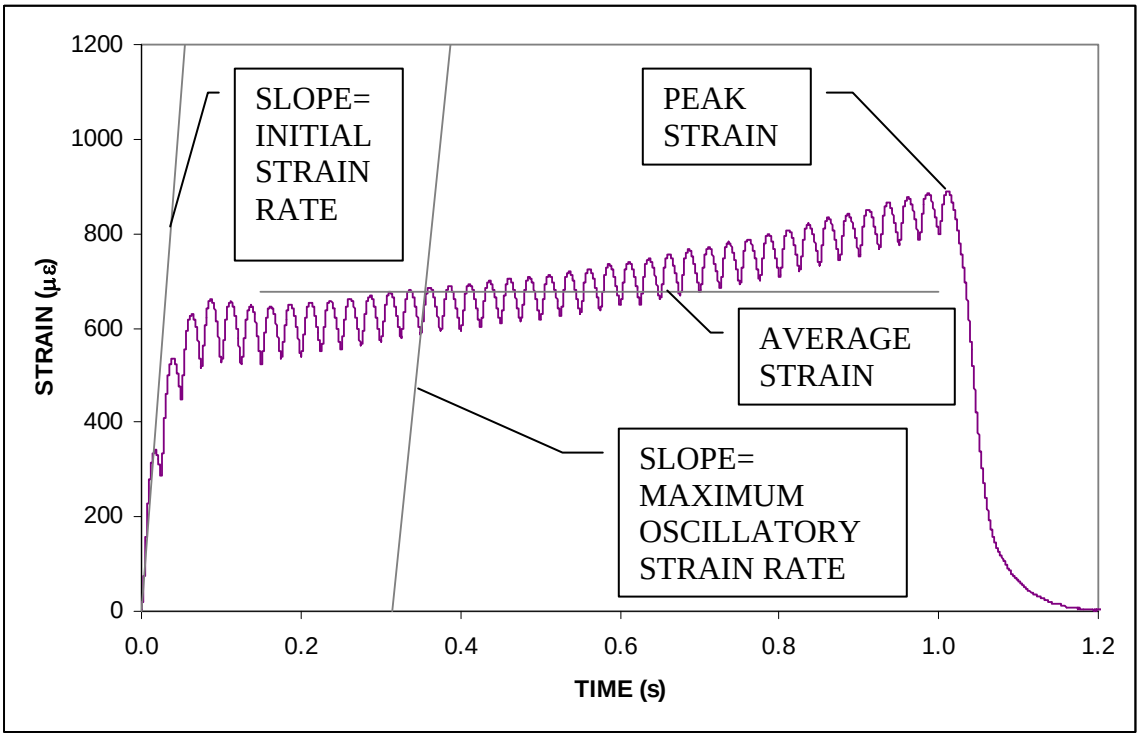

Figure 16 For each eccentric contraction, strains and strain rates were calculated.

The above-mentioned parameters were paired with the peak torque from the contraction and plotted. For example, the peak strain from a contraction with 30 Hz stimulation was plotted on the x-axis and the peak torque from the contraction was plotted on the y-axis (Figure 17). In the work of Vyvial, these plots had strain on the y-

axis. In this study, strains were plotted on the x-axis to comply with the stress-strain plotting convention common in the study of mechanics.

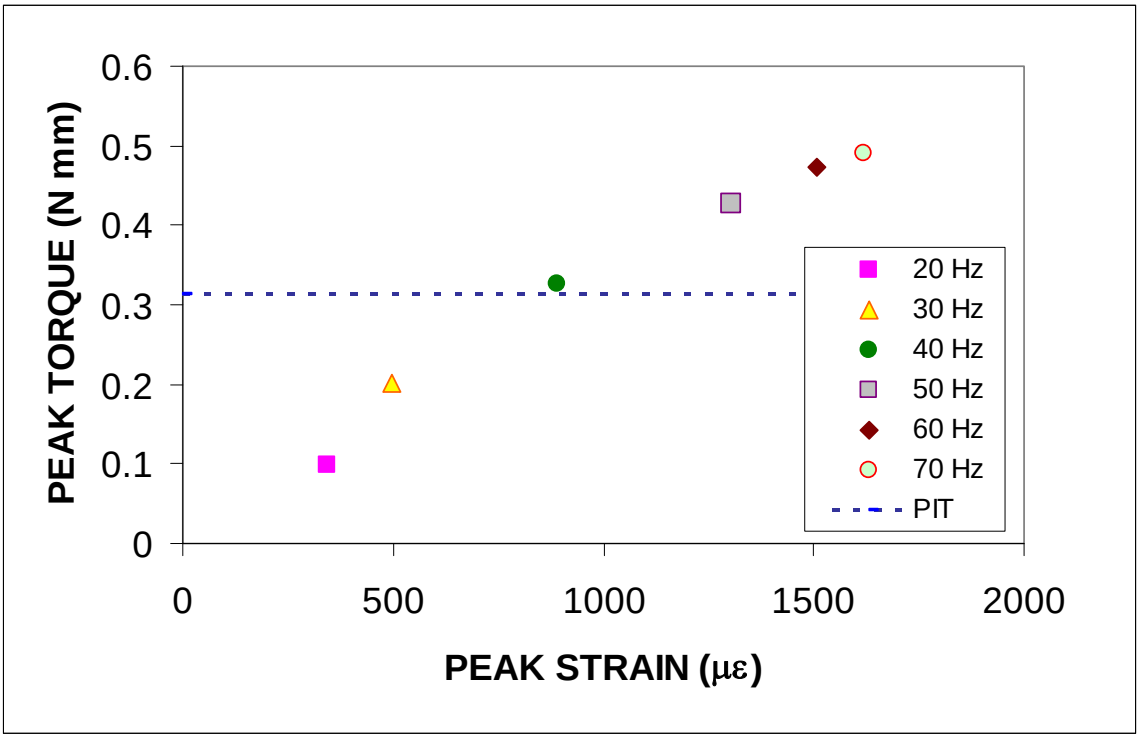

Figure 17 Eccentric contraction relationships for each animal were found by plotting peak torque and peak strain for each frequency.

These relationships appear generally linear in the region where the exercise is performed. However, nonlinearity is often observed at very low and at high torques. The nonlinearity is not consistent between animals in the shape or torque at which it begins. No clear physical meaning has been connected with these, so simple linear models are considered here. With this muscle stimulation set up, torques exhibit a saturation behavior where increasing the frequency affects torque values less towards the upper range, which eventually flatten out the curve. The strains do not seem to saturate

(at least not in the same way), which makes the torque versus strain curves plateau at the saturated torque value. The mechanism causing this remains unclear.

Linear regression trend lines for each animal were plotted together to compare groups. Regressions were performed with torque as the independent variable, the same as in the previous study of Vyvial. Torque here is presented on the y-axis, thus the slopes given are the inverse of what is shown on the plots, and the intercept corresponds to the x-axis. Peak strain versus peak torque for all the animals was plotted (Figure 18). The straight, thin lines are the trend lines from each animal's data set. The thicker lines represent trend lines from the groups. Results from the group regressions are shown in Table 1. No significant differences between groups were observed in the slopes or intercepts.

The data can also be plotted as a percentage of PIT versus strain (Figure 19). By plotting as a percentage of PIT, the torque values are normalized for the strength of activated muscles in the animal. Plotting this way also shows the strains experienced at the exercise intensity because the exercise sessions were done at 100% of PIT. Regression data can be seen in Table 2, and again there were no significant differences between groups.

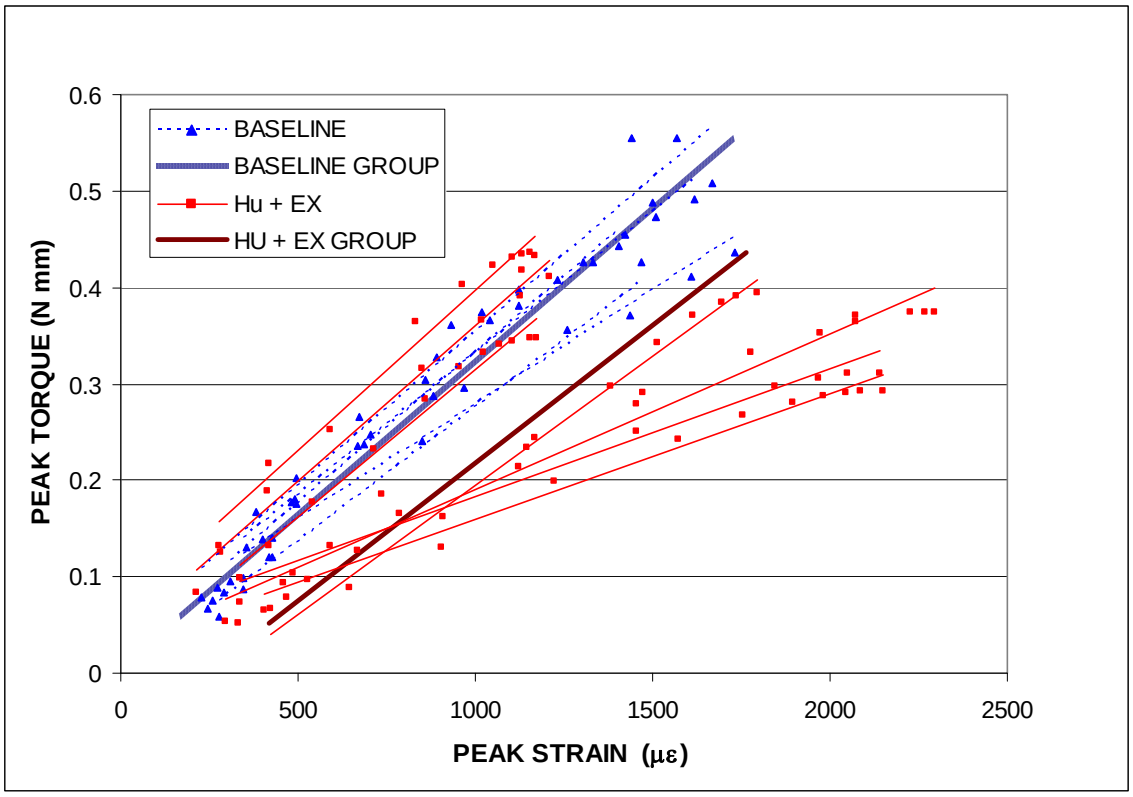

Figure 18 Peak eccentric torque and peak strain magnitudes. Each marker represents a single contraction. The baseline group is in blue, and the hindlimb unloading with exercise (HU + Ex) group is shown in red. The linear regressions for each individual animal are shown with the thin trend lines, and the group linear regressions are shown with the thicker trend lines.

Table 1 Eccentric Peak Torque vs. Peak Strain Regression

	Slope (με/N mm)	Intercept (με)	R^2	P (slope)	P (intercept)
Baseline	3115	-4.79	0.936	<0.001	0.9
HU + Ex	3512	233	0.444	<0.001	0.08
P (t-test)	0.493	0.156			

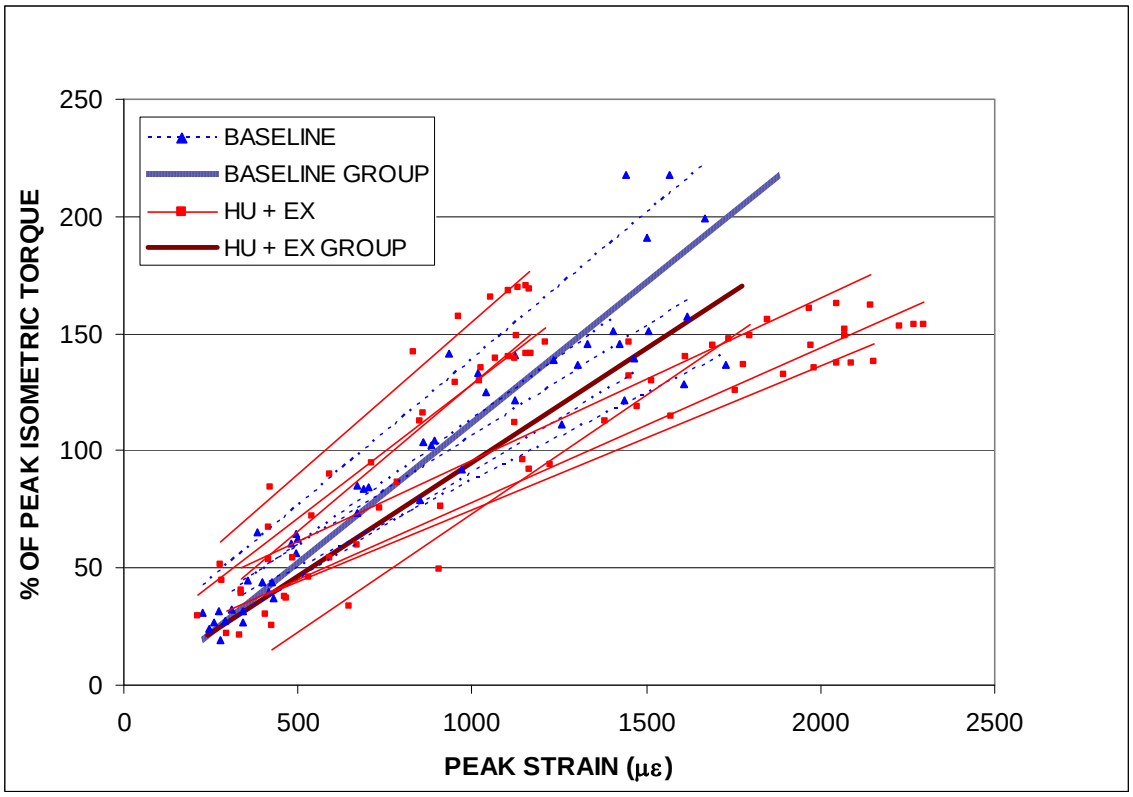

Figure 19 Peak eccentric strain plotted against peak torque normalized for PIT. The linear regressions for each individual animal are shown with the thin trend lines, and the group linear regressions are shown with the thicker trend lines. There is considerable overlap between groups. Note that 100% of PIT is the intensity at which the exercise sessions were performed.

Table 2 Eccentric % of PIT vs. Peak Strain Regression

	Slope (με)	Intercept (με)	R^2	P (slope)	P (intercept)
Baseline	8.27	75.8	0.866	<0.001	0.155
HU + Ex	10.3	21.4	0.614	<0.001	0.851
P (t-test)	0.099	0.713			

Peak average strains for the eccentric contractions are plotted in Figure 20. It looks similar to the peak strain plot. The regression coefficients are shown in Table 3, and no significant differences were found.

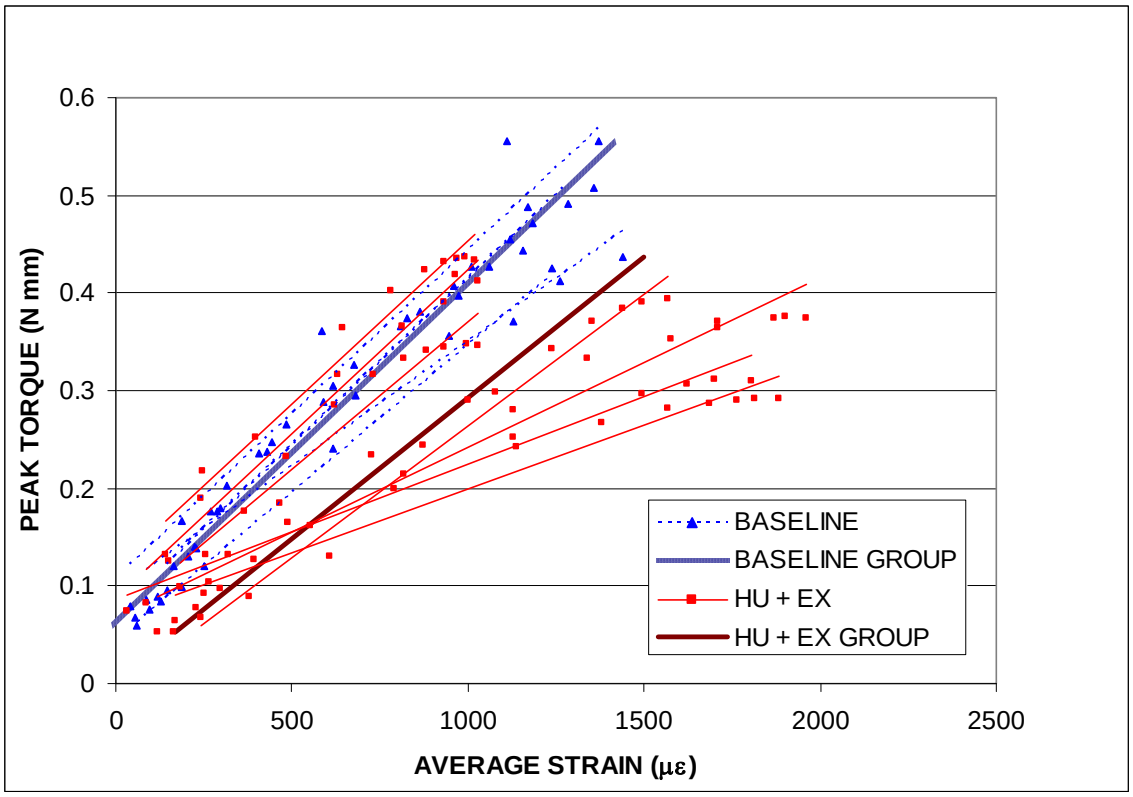

Figure 20 Peak eccentric torque plotted against average strain magnitudes. Individual trend lines are shown with the thin lines, and the group regressions are shown with the thicker lines. This plot closely resembles the plot for peak strain (Figure 18).

Table 3 Eccentric Torque vs. Average Strain Regression

	Slope (με/N mm)	Intercept (με)	R^2	P (slope)	P (intercept)
Baseline	2847	-167.859	0.935	<0.001	0.054
HU + Ex	3459	-10.22	0.51	<0.001	0.053
P (t-test)	0.223	0.277			

The average strains were also plotted with the torque normalized for PIT (Figure 21). Regression data for the percentage of PIT and average strains are shown in Table 4. Slopes were found to be higher in the HU + Ex group and this achieved statistical significance. The trend lines for both groups are nested together; it is difficult to know

whether this represents a change in the strain response to the loading or the difference is an artifact of the experimental procedures.

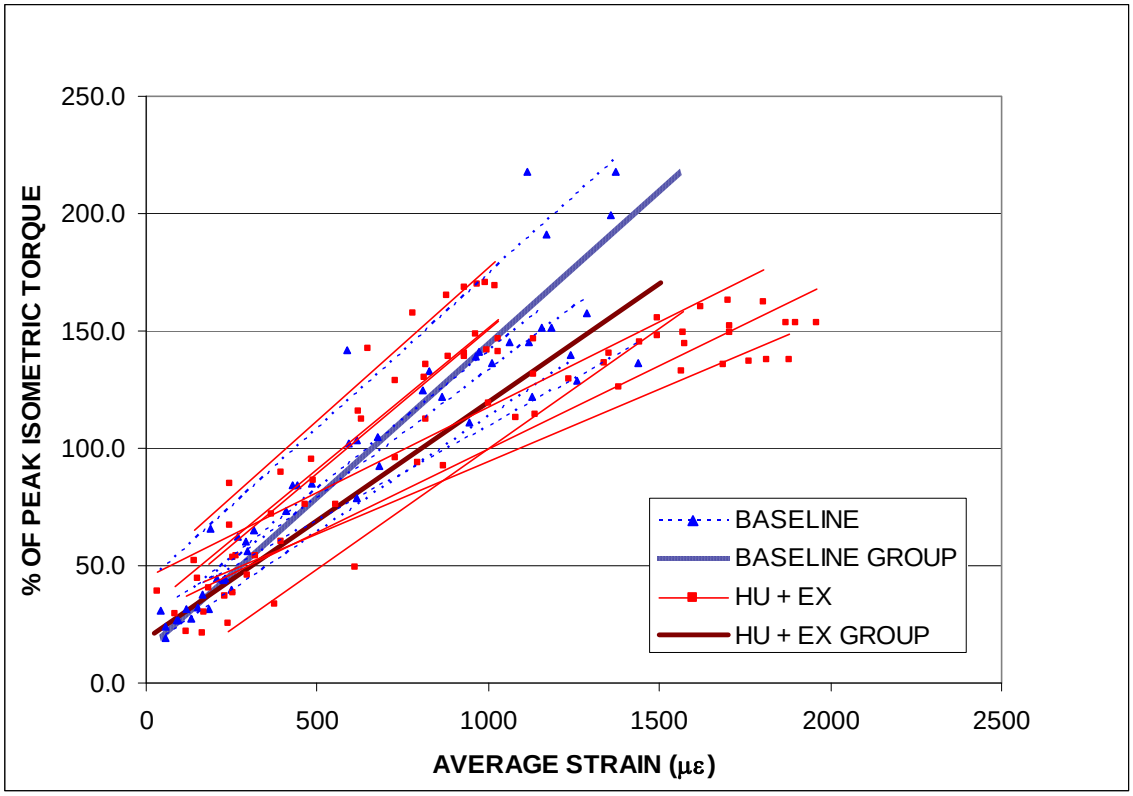

Figure 21 Average eccentric strain plotted against peak torque normalized for PIT. There is considerable overlap in the data between groups.

Table 4 Eccentric % of PIT vs. Average Strain Regression

	Slope (με)	Intercept (με)	R^2	P (slope)	P (intercept)
Baseline	7.57	-94.7	0.866	<0.001	<0.001
HU + Ex	9.94	-190	0.67	<0.001	0.929
P (t-test)	0.029#	0.452			

# indicates a significant difference at the 95% confidence level

Strain rate is an important parameter when considering the strain environment. The initial strain rate was plotted against peak torque in Figure 22. The scatter is high and this is reflected in the regression coefficients shown in Table 5. The variance in slopes is very high and no group trends are apparent. As can be noted in Figure 15, where the eccentric strains are plotted with time, the contraction lines start with similar slopes for all of the frequencies. Therefore there is little variation in initial strain rate with frequency for some of the data sets. Still, the initial strain rates generally increase with frequency and the slopes are positive.

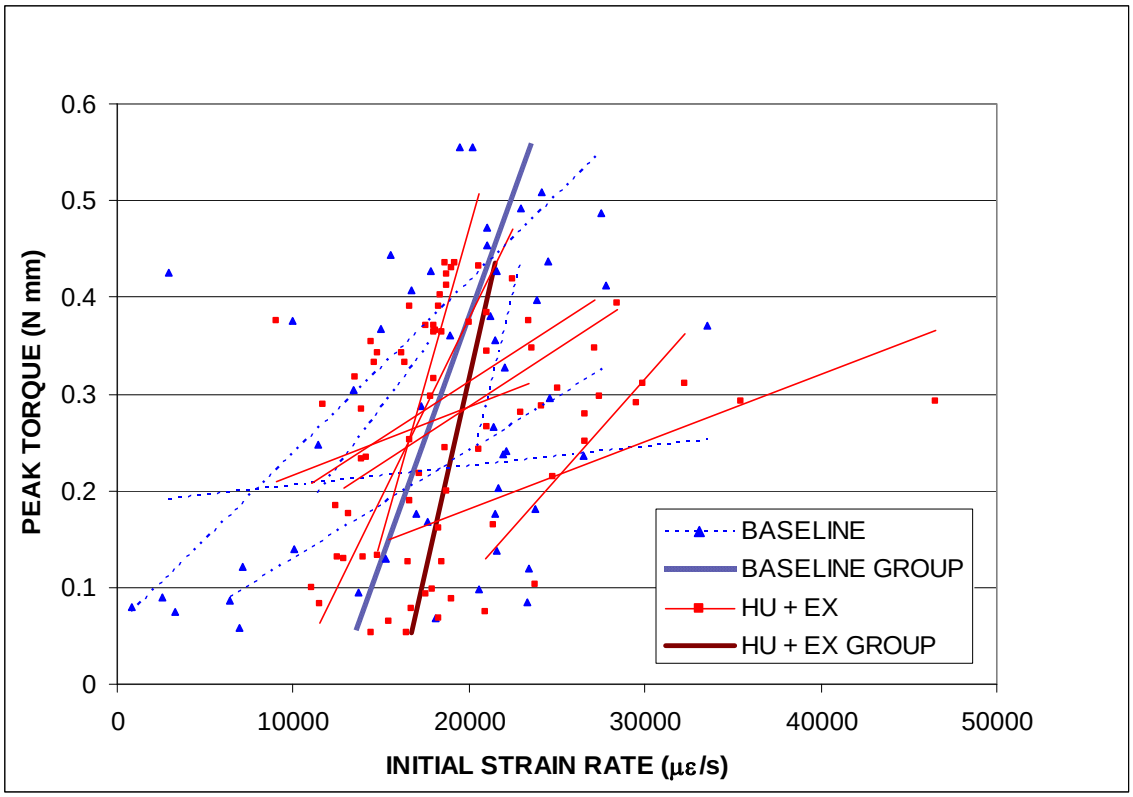

Figure 22 Initial strain rate plotted against peak torque. Scatter is high, and the data sets overlap.

Table 5 Eccentric Peak Torque vs. Initial Strain Rate Regression

	Slope (με/N mm)	Intercept (με)	R^2	P (slope)	P (intercept)
Baseline	20174	12311	0.177	0.003	<0.001
HU + Ex	12405	16091	0.0567	0.038	<0.001
P (t-test)	0.386	0.159			

The relationships are not improved when the initial strain rates are plotted against the peak torque normalized for PIT (Figure 23). Group differences are not significant and fit parameters are weak (Table 6).

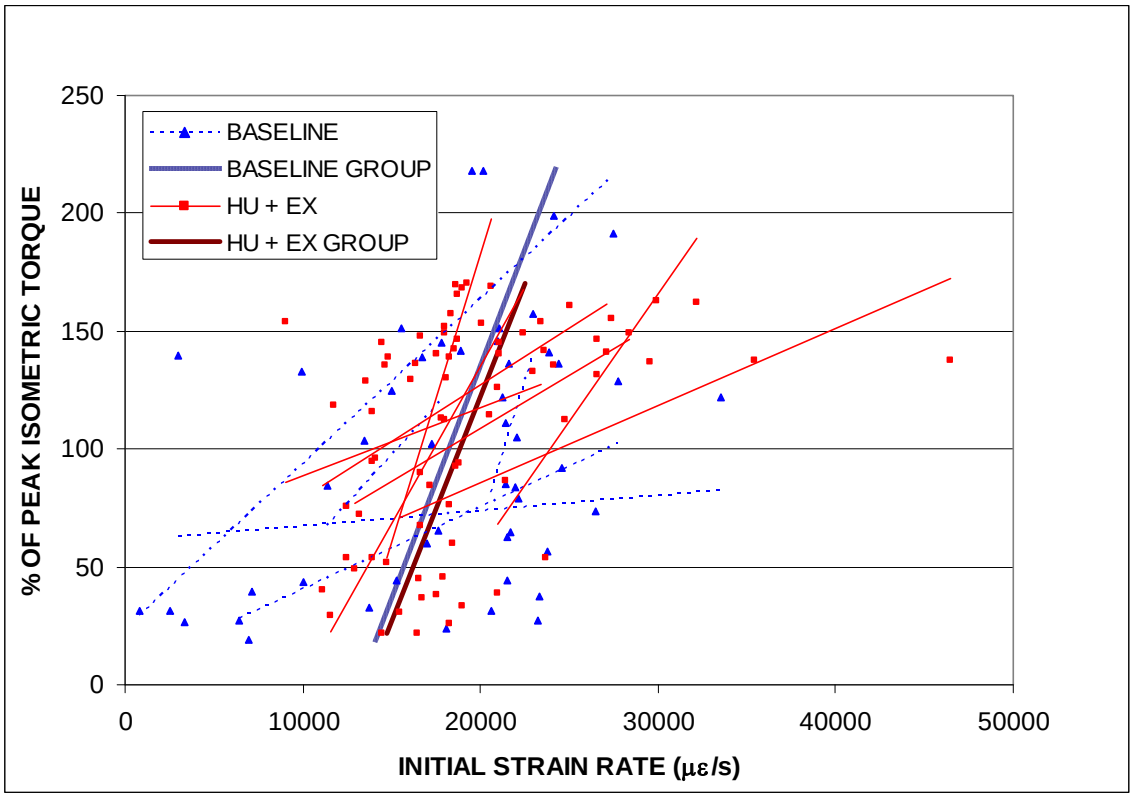

Figure 23 Eccentric torque normalized for PIT vs. initial strain rate. The scatter is high and there is substantial variance in the slopes.

Table 6 Eccentric % of PIT vs. Initial Strain Rate Regression

	Slope (με)	Intercept (με)	R^2	P (slope)	P (intercept)
Baseline	51.5	13036	0.151	0.006	<0.001
HU + Ex	52.4	13596	0.161	<0.001	<0.001
P (t-test)	0.967	0.83			

The highest strain rates found were not always in the initial rise, but were often in the oscillations induced by the stimulation frequency. The maximal value of the strain rate in the oscillatory region of the contraction is plotted against the peak torque in Figure 24. This plot shows some consistency in the slopes, but high spread otherwise. Regression data (Table 7) indicates a significant difference between the groups in slopes and intercepts; the HU + Ex slopes are over twice that of the baseline slopes. However, the spread is reflected in the low R^2 values. It is worth noting that the slopes are negative, meaning the strain rates in the oscillatory region decrease with stimulation frequency. Assuming the strain curves are true sinusoids, the maximum oscillatory strain rate would be the product of the amplitude and the frequency. Thus, a negative slope means that the amplitude of the oscillations decreases more than the frequency as the stimulation frequency is increased.

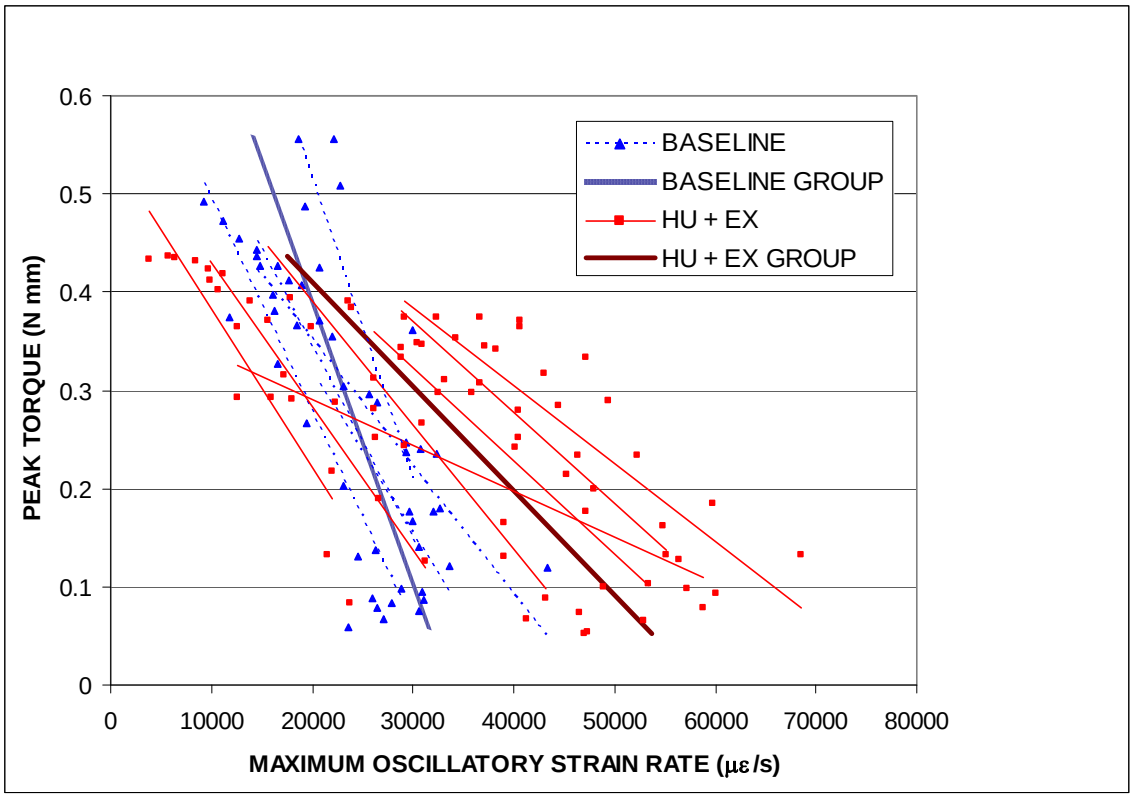

Figure 24 Maximum oscillatory strain rates decrease with frequency. Spread in the data is apparent, but most data sets show some general consistency in the slopes. The strain rates decrease with frequency, as shown by the negative slopes. The groups are statistically different.

Table 7 Eccentric Peak Torque vs. Maximum Oscillatory Strain Rate Regression

	Slope (με/N mm)	Intercept (με)	R^2	P (slope)	P (intercept)
Baseline	-35269	33632	0.549	<0.001	<0.001
HU + Ex	-94303	58637	0.493	<0.001	<0.001
P (t-test)	<0.001*	<0.001*			

*indicates a significant difference at the 99% confidence level

Normalizing for PIT does not noticeably decrease the spread in the maximum oscillatory strain rate data (Figure 25). Regression coefficients again show a significant differences between groups (Table 8).

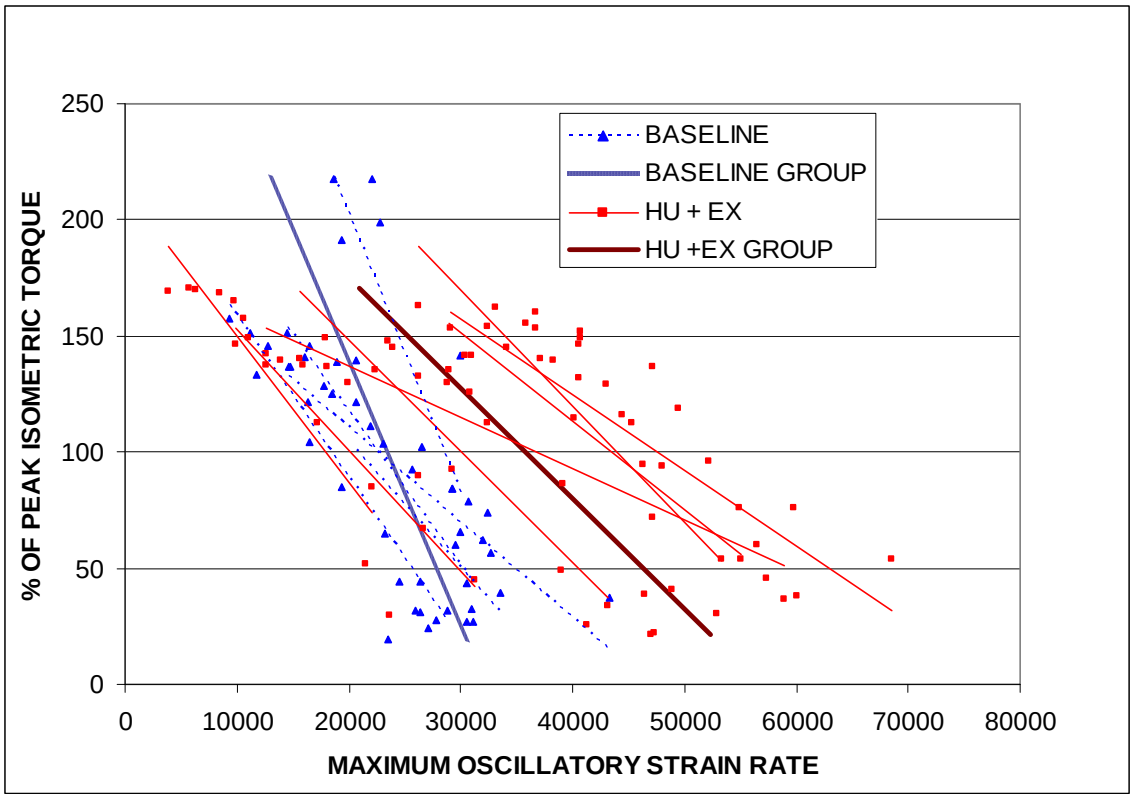

Figure 25 Eccentric torque normalized for PIT vs maximum oscillatory strain rate. The groups are statistically different.

Table 8 Eccentric % of PIT vs. Maximum Oscillatory Strain Rate Regression

	Slope (με)	Intercept (με)	R^2	P (slope)	P (intercept)
Baseline	-89.3	32295	0.461	<0.001	<0.001
HU + Ex	-211	56930	0.392	<0.001	<0.001
P (t-test)	<0.003*	<0.001*			

*indicates a significant difference at the 99% confidence level

Isometric Contractions

Sample plots of torque and strain from 4 separate isometric contractions are given in Figure 26 and Figure 27, respectively (from animal number 1444). Isometric contractions in the current protocol were done with the foot positioned at 20 degrees (see

Figure 9), while they were performed at 0 degrees in the previous study of Vyvial (see Figure 10). As expected, the torque and strain levels at 20 degrees were higher than those at 0 degrees.

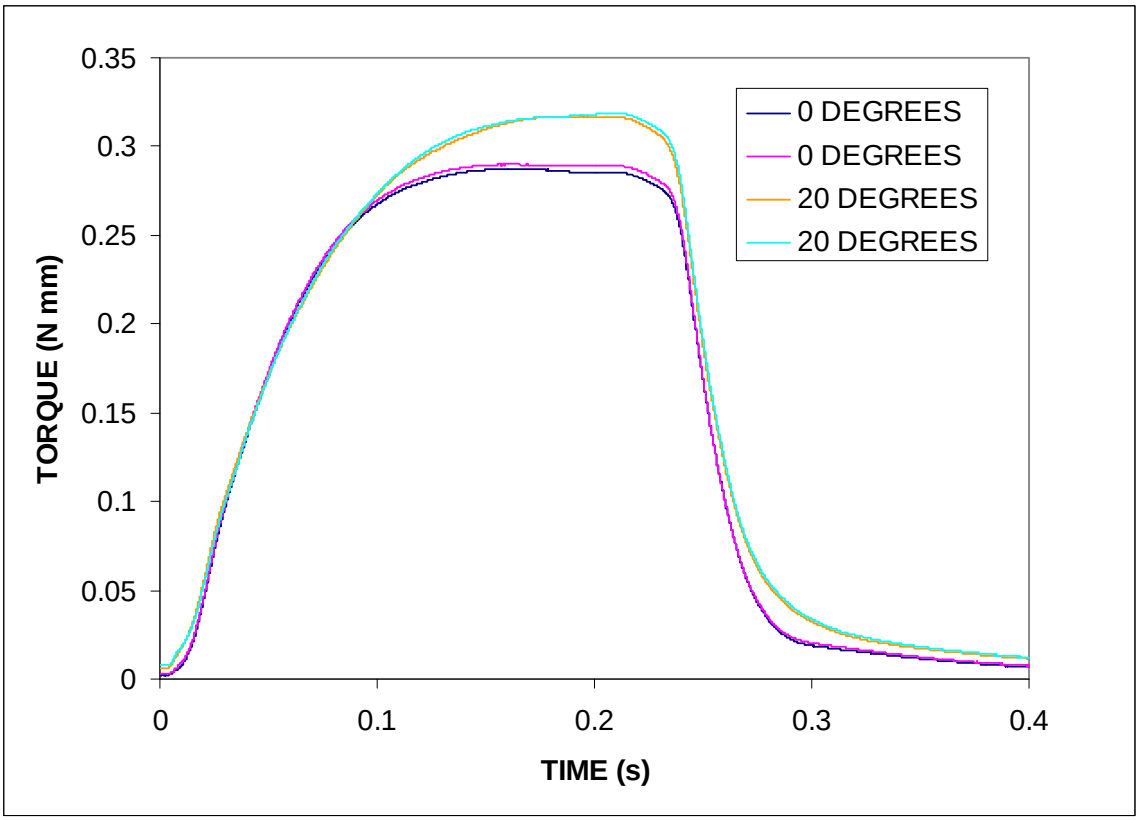

Figure 26 Isometric torques at PIT are lower at 0 degrees than at 20 degrees.

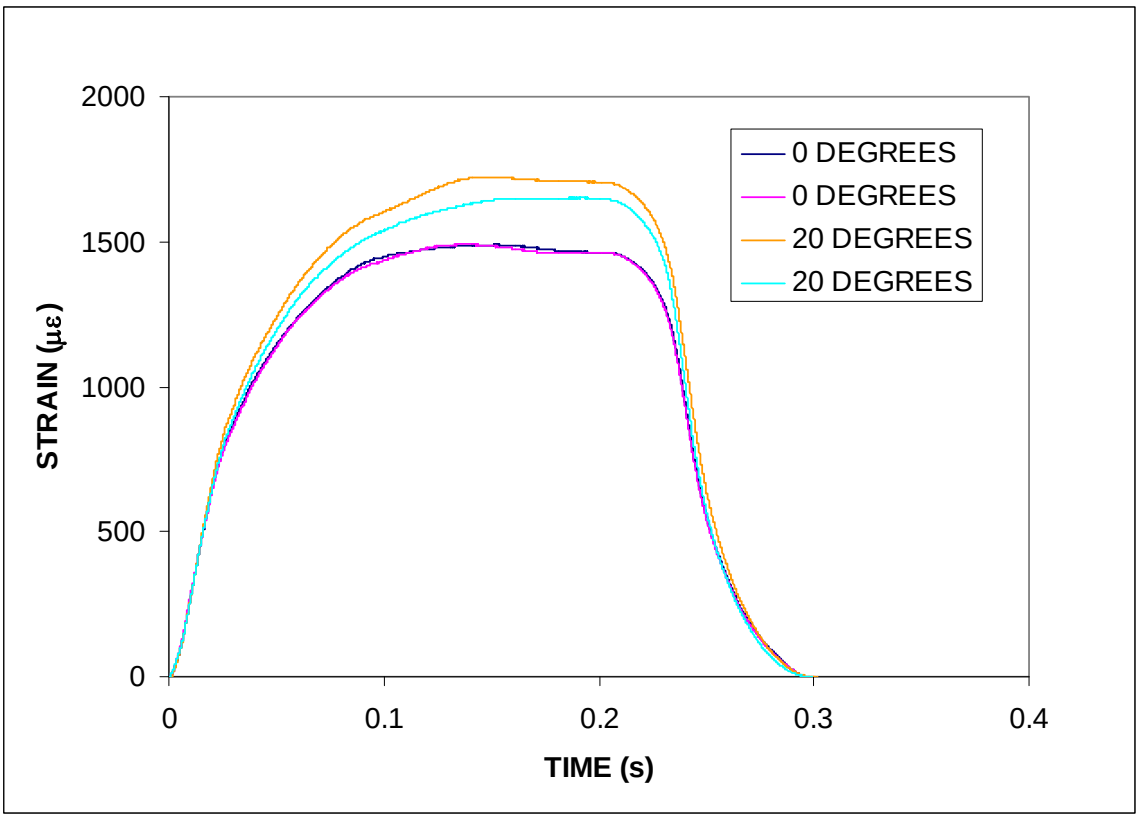

Figure 27 Strains at PIT are also lower at 0 degrees than at 20 degrees.

Torque and strain can be plotted on the same axes to show how they are related during the contraction. The biggest problem with such plots is synchronizing the torque and strain, since the data were collected on separate computers. A plot synchronized manually by starting with both curves departing from approximately zero together is shown in Figure 28. However, the shape of the curve is highly sensitive to the points chosen for time to start. Noise and floating zero point problems arising from the quarter bridge configuration gave inconsistent curve shapes. For the sake of repeatability and consistency, the data sets were shifted in time by an algorithm in a program written in Matlab, until the area inside the curve was minimized. A sample curve is shown in Figure 29. The curve resulting from this data point match up has the torque curve starting before the strain curve. The loading and unloading lines end up crossing each

other, sometimes more than once, which indicates that this match up does not represent a true synchronization of the data sets.

These plots may relate to constitutive properties of the bone. However, the loading in these relationships is not stress, but torque which is spatially removed from the site where strain is measured. Converting torque at the ankle joint to stress at the proximal tibia would require a thorough force and kinematic analysis that is beyond the scope of the current study.

The hysteresis (as shown by the area in the curve) appears consistent with the results from *ex vivo* tensile tests showing viscoelastic behavior in cortical bone at this strain magnitude[22]. However, connective tissue also exhibits viscoelastic behavior, which must be considered when loading the skeletal system *in vivo* and *in situ*.[23] Without having the data synchronized in real time, no reliable conclusions can be made. While these plots may fall short of showing intrinsic bone properties, relationships from these plots are useful for comparing groups.

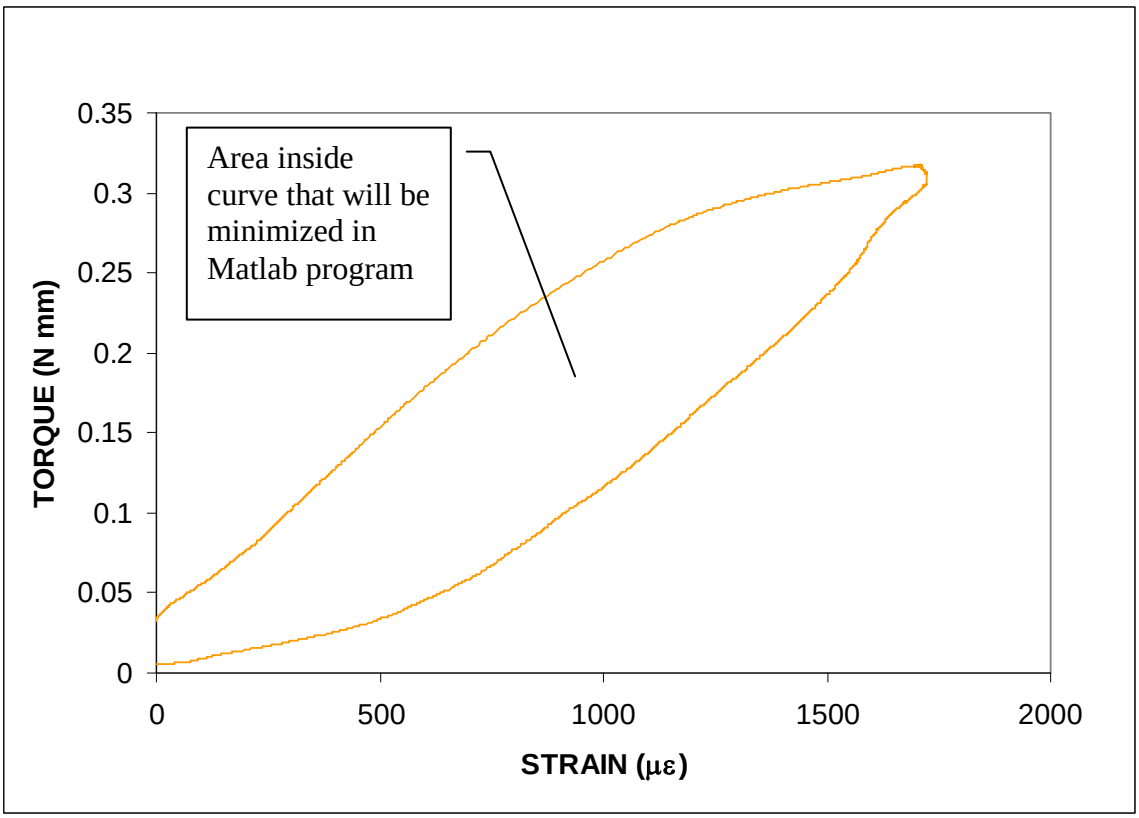

Figure 28 Torque and strain from an isometric contraction at 20 degrees were matched up manually. The resulting shapes are sensitive to the start points chosen. Drawing reliable conclusions is difficult.

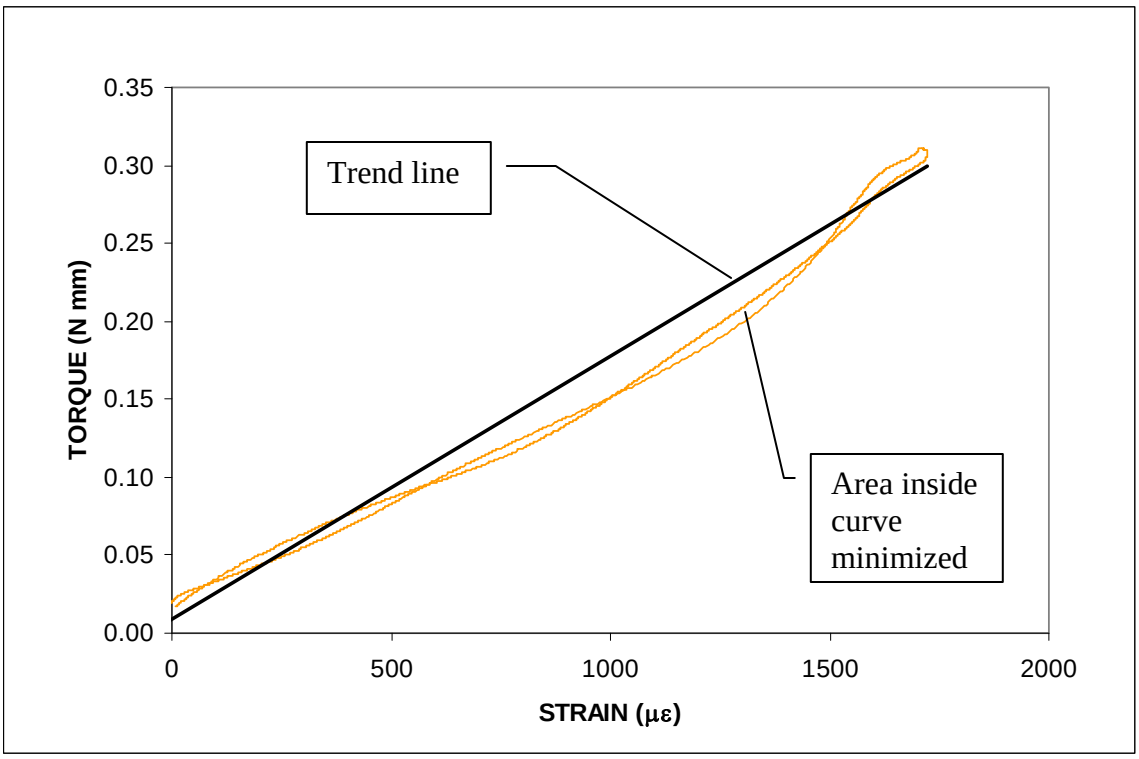

Figure 29 The same data set represented in Figure 28 with the torque and strain data points matched up using the Matlab program.

Linear trend lines were found for each of the 4 contractions, as shown in Figure 29. Plots for each animal can be found in Appendix A. From these trend lines were found slopes and intercepts, which were averaged for each animal. These parameters were used to compare groups (Table 9). Average trend lines from each of the animals are shown in Figure 30. This plot shows the peak magnitudes of torque and strain, as well as the trend line slopes and intercepts. There were no significant differences between group means for any of the regression parameters.

Other parameters considered were the strain magnitudes, strain rates and torques (Table 9). Initial strain rate was found by averaging the instantaneous slopes of the strain versus time curve for the initial rise (0.015 seconds). Group means for peak strain magnitudes and strain rates were not statistically different. Peak torques in the HU + Ex group were 20% lower with a confidence level of 95%.

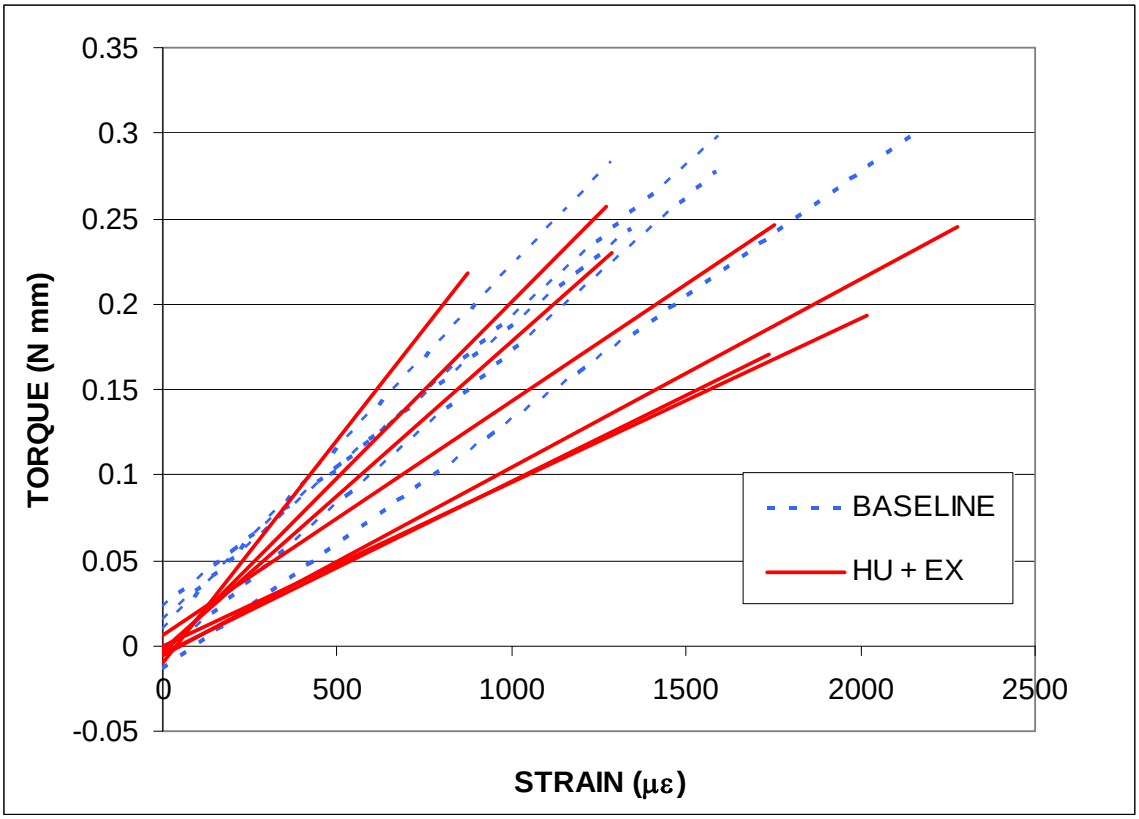

Figure 30 Trend lines for isometric contractions show no significant relationships between groups. The ends of the lines show peak torque (PIT) and peak strain.

Table 9 Isometric Contractions

	Peak Torque# (N mm)	Peak Strain (με)	Slope (N mm)	Intercept (N mm)	Initial Strain Rate (με/s)
Baseline	0.288	1593	1.76E-04	5.47E-03	48889
HU + Ex	0.230	1602	1.56E-04	-2.94E-03	50130

# denotes a statistical difference with P<0.01

Comparison Between Eccentric and Isometric Contractions

It should be stressed when referring to isometric and eccentric contractions, that these comparisons are specific to this exercise protocol and should not be generalized.

The objective of this study was to understand the loading and strain environment during this exercise. Because there are 2 types of contractions used during the exercise session, it is important to understand how the loading and strain environments differ during them.

Figure 31 illustrates strains for isometric and eccentric contractions, both at PIT. Some obvious features are that the isometric contraction is much shorter and that the strain magnitude is higher.

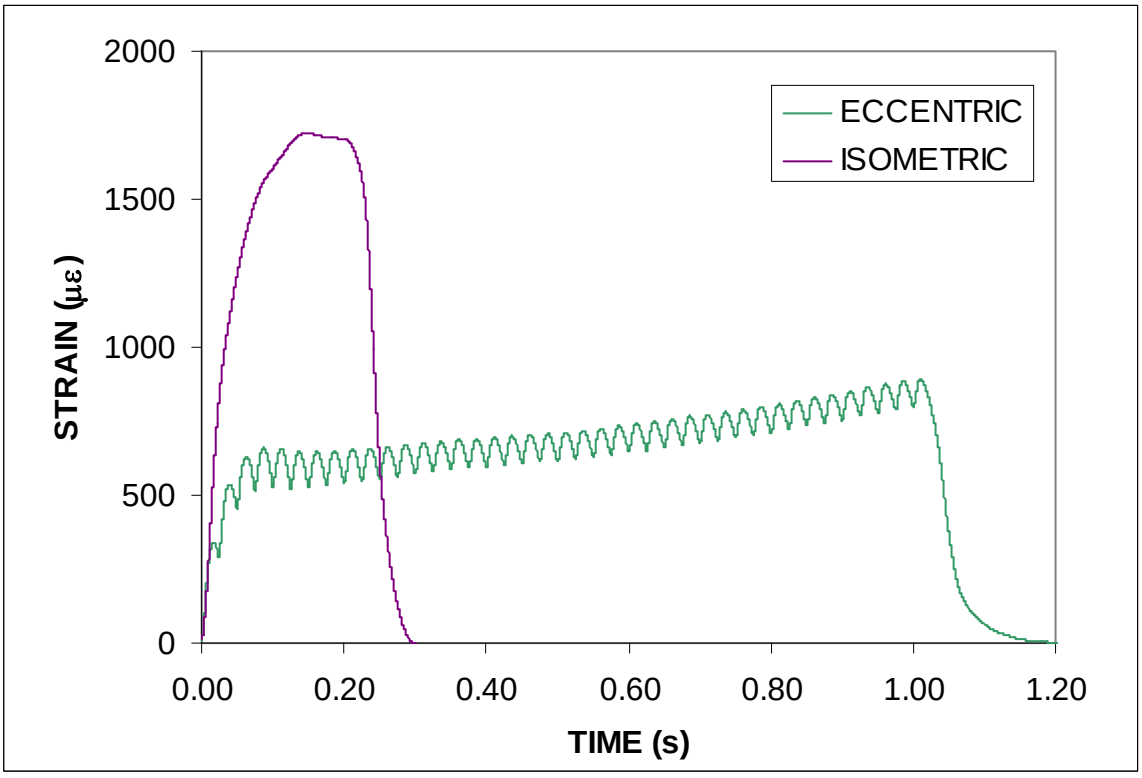

Figure 31 Eccentric and isometric strains shown on the same plot. Both are at PIT.

To compare isometric to eccentric contractions, eccentric strains and rates needed to be found for torque levels the same as those experienced during the isometric contractions and during the exercise sessions; linear regressions were used to approximate the eccentric strain magnitudes and strain rates at this level (PIT). Values

for peak strains and strain rates are given in Table 10. Statistical significance was checked for a difference between groups, between the contraction types and for an interaction between them. The differences were statistically significant.

Table 10 Strain Magnitude Comparisons at PIT

	Isometric Strain (με)	Eccentric Strain (με)	P (contraction)	
Baseline	1593	884	0.003*	<0.001*
HU + Ex	1602	1027	0.023#	
P (group)	0.971	0.386	0.66	
	0.616			

*indicates a significant difference at the 99% confidence level
#indicates a significant difference at the 95% confidence level

Strains for each animal are shown in Figure 32 to illustrate the differences between the contractions. Eccentric strain magnitudes were 39% lower than isometric strain magnitudes, with a standard deviation of 10%, showing the consistency of the difference.

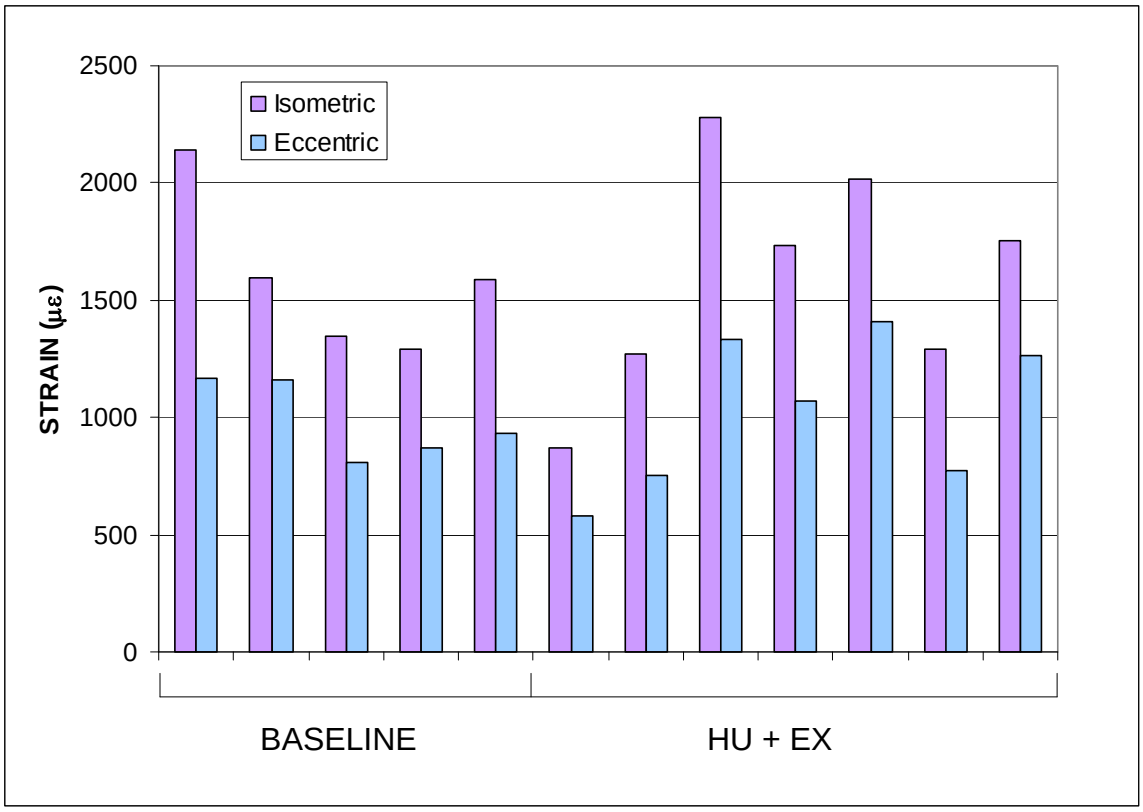

Figure 32 Peak strain magnitudes for both contractions compared animal by animal. Eccentric strain magnitudes were 38% lower than isometric strain magnitudes.

Isometric strain rates were compared to eccentric strain rates (Table 11) and to eccentric maximum oscillatory strain rates (Table 12); results from each animal are presented in Figure 33. Maximum oscillatory strain rate is found in the part of the eccentric contraction after the initial rise and is compared to the initial rise of isometric contraction to compare the highest strain rate experienced by the bone. A higher degree of variance was noted in the maximum oscillatory strain rate comparison. Eccentric initial strain rates were 62% lower than isometric strain rates, and eccentric maximum oscillatory strain rates were 41% lower. The standard deviations of these differences were respectively 10% and 18%. Several of the HU + Ex animals had maximum oscillatory strain rates which approached the isometric strain rates in magnitude, while most were much smaller. Whether this irregularity is due to a physiological change that

took place during the hindlimb unloading or the exercise, or is an artifact of the strain gaging procedures remains unclear.

Table 11 Isometric and Eccentric Initial Strain Rate Comparison at PIT

	Isometric Strain Rate (με/s)	Eccentric Initial Strain Rate (με/s)	P (contraction)	
Baseline	48889	16873	<0.001*	<0.001*
HU + Ex	50130	18922	<0.001*	
	0.86	0.336	0.911	
	0.65			

*indicates a significant difference at the 99% confidence level

Table 12 Isometric and Eccentric Oscillatory Strain Rate Comparison at PIT

	Isometric Strain Rate (με/s)	Eccentric Max Oscillatory Strain Rate (με/s)	P (contraction)	
Baseline	48889	22847	<0.001*	<0.001*
HU + Ex	50130	33764	0.032#	
P (group)	0.86	0.071	0.281	
	0.179			

*indicates a significant difference at the 99% confidence level
#indicates a significant difference at the 95% confidence level

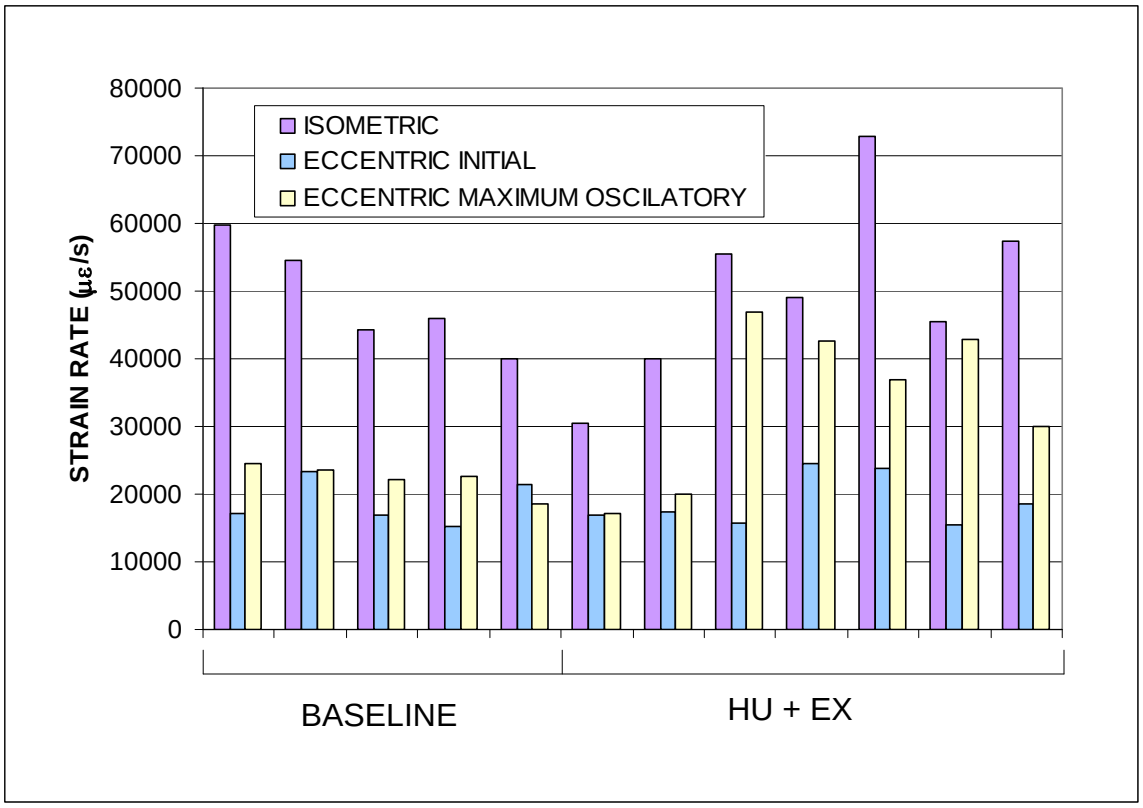

Figure 33 Strain rates for both contractions compared. On average, initial eccentric strain rates were 62% lower, and eccentric maximum oscillatory strain rates were 41% lower as compared to isometric strain rates.

DISCUSSION

Osteogenic Potential

The underlying goal of the current investigation is to better understand bone adaptation. This leads us to ask the questions, "Are these strain levels sufficient to prevent bone loss," and, "Are these strain levels sufficient to induce new bone formation (osteogenesis)?" These questions were answered in the parallel, contemporaneous study conducted by Sumner (2007). In her 28-day study using the same exercise protocol, it was found that the protocol prevented bone loss and even increased bone mass. At the metaphases of the proximal tibia, the hindlimb unloaded control group lost 11% total bone mineral content (BMC) while the hindlimb unloaded animals that received the exercise countermeasure (Hu + Ex) gained 7%. The BMC increase was not significantly greater than that of the aging cage control (CC) group, thus BMC was maintained. At the midshaft, total BMC values for the HU + Ex group were significantly higher than both control groups, which increased 15.3%. This indicates that the countermeasure is osteogenic. Mechanical testing also showed that the HU + Ex group had stronger cancellous bone (the bone which responds most to loading changes) than the CC and HU control groups. Thus the answer to these questions appears to be an empirical, "Yes." The study of Sumner focused on whether the exercise was effective, leaving the current study to address the question, "Why is the exercise osteogenic?"

According to basic mechanostat principles, two strain limits in bone tissue exists. As long as bone stays above a strain threshold, typically considered to be around 100-300 microstrain, bone mass will be maintained. The threshold above which bone will adapt to the loading is traditionally considered to be 1500-2500 microstrain[7]. These strain thresholds are generally applicable to the midshaft of long bones (where strain is the highest) and cannot be blindly applied to all parts of all bones. The role a bone plays will affect the strain threshold[24].

The strains in this study encountered at the exercise intensity ranged from 900-2200 microstrain during the isometric contractions and 600-1400 microstrain during the

eccentric contractions. These strain levels are somewhat borderline values and may fall within the osteogenic range. However, there is more to the issue than just strain magnitude, and other factors may better explain the bone response noted.

Diane M. Cullen et al. found in a study using the *in vivo* four point bending technique that cyclical loading at 1000 microstrain (at the tibial midshaft) was sufficient to note bone formation markers[25]. The study showed that increasing the number of loading cycles in each session increased the bone response.

Yeou-Fang Hsieh et al. conducted a study where rat ulnas were loaded in axial compression *in vivo*, and it was found that the osteogenic strain threshold varied with location on the bone[26]. The strain thresholds were 1343 microstrain 3mm proximal to the midshaft, 2284 microstrain at the midshaft and 3074 microstrain 3mm distal to the midshaft.

It is believed that the mechano-transduction mechanism that triggers bone formation is not so much sensitive to strain magnitude, but is sensitive to strain rate. Charles H. Turner reported in an *in vivo* four point bending study that loading applied at the same magnitude yielded a proportional relationship between strain rate and endocortical bone formation rate[27].

Sensitivity to frequency has also been noted. In a recent study, Stefan Judex et al. used a vibrating plate on which rats stood to induce bone formation[28]. Two frequencies were compared, only the higher of which was shown to be osteogenic. The 45 Hz vibrations did not trigger bone formation, despite having a strain magnitude and strain rate higher than the 90 Hz vibrations. Neither strain magnitude exceeded 100 microstrain; the strains were on the order of those experienced by a quiescent standing rat.

Sundar Srinivasan et al. investigated how rest insertion could make strain levels that would otherwise not be osteogenic form new bone[29]. Using a pinned turkey ulna model, 800 microstrain (ambulatory level) pulses were applied either in quick succession, or with a 10-second rest between them. The animals that had the loading

spaced out were reported to have experienced new bone formation, but the group without rest insertion did not.

Comparison to Normal Activity

Another question that bears addressing is, "How do the strain levels in this exercise compare with ambulatory activities?" Brian Rabkin et al. developed a technique for implanting strain gages for long term measurement without gage softening. In one study, gages similar to those used in this study were implanted on rat tibia at the same site used in this study; strain measurements were taken for walking activity[30]. The strain (i.e. breed) of the rats was Fischer, unlike the Sprague-Dawley rats used in the current study, and the animals were 3 month of age instead of 6. Mechanical strains reported were about 800-900 microstrain, measured peak to peak.

Unpublished findings within our lab group using the same strain of rat (Sprague-Dawley), strain gage and bone site as the current study found a range of 600-800 microstrain measured peak to peak for a walking rat. In our experience, cage activities such as standing on the hindlimbs result in 400-500 microstrain peak to peak. It should be noted that possible adhesive softening could reduce the strains measured, and that procedures employed by our lab to prevent softening in survival implantations have not been validated. Still, the strain levels are almost certainly higher during the these stimulated muscle contractions than during normal cage activity and ambulation.

Contraction Comparisons

The long-term objective of the larger investigation in the Bone Biology Lab, of which this study is a part, is to understand exercise disuse countermeasures, antiresorptive pharmacological disuse countermeasures, and how these can be combined to prevent bone loss. This will entail combining variable doses of medications with variable doses of exercise, then measuring the combined effect on bone. Developing an exercise that allows variable dosing of the exercise is an important element of this investigation.

This leads us to ask, “Which parts of the exercise contribute most to the bone response and how can this response be adjusted?” The different stages of an exercise session are illustrated in Figure 34, with average strain parameters shown. Since the number and intensity of the contractions in the voltage optimization stage and the frequency tuning stage will vary, the overall volume of the exercise session will inevitably vary.

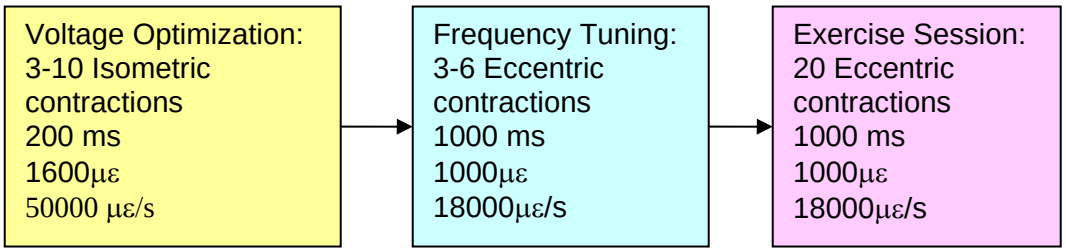

Figure 34 Osteogenic factors during the stages of a training session indicate that the strongest stimulus might occur early in the session.

Several possibilities exist regarding which elements of the training session responsible for the bone response.

- The isometric contractions may provide the strain environment to promote a response, while the eccentric contractions may not.
- The eccentric contractions may provide the proper stimulus to trigger a response and may be responsible for the response.
- The response may saturate during the isometric contractions.
- Both types of muscle contractions may contribute to the response.

In Figure 31 an isometric contraction and an eccentric contraction were shown on the same plot. The torque levels were both at peak isometric torque as they would be in an exercise session. It is immediately obvious from this figure, Figure 32, and Figure 33 that strain magnitudes and strain rates are higher in the isometric contractions by

significant margins. This observation suggests that the isometric contractions could provide the dominate stimulus to bone.

The stimulation frequency at which the eccentric contractions were performed was between 30 and 50 Hz (one session was done at 60 Hz). The isometric electrical stimulus was administered at 175 Hz; however, it is unclear whether this frequency content in the strain is modulated into a steady pulse. The number of loading cycles during the eccentric stages of an exercise session is typically much higher than in the isometric stage. The eccentric contraction may play a significant role in the response if the number of loading cycles or their frequency is an important part of the stimulus.

Rest insertion is more complicated to compare. During the voltage optimization phase with isometric contractions and during the frequency tuning phase with eccentric contractions, there is a 45-second rest between contractions and a 2-minute rest between the voltage optimization and frequency tuning phases of the protocol. During the exercise portion, there is a 12-second rest between the 5 eccentric contractions in each set, and 2 minutes of rest between each of the 4 sets. While there are differences in rest insertion, it is unclear whether this would cause one contraction type to stimulate a response better than the other in the current protocol.

If the bone response is coming from the voltage optimization stage with the isometric contractions, reducing the eccentric contractions in the exercise phase will not be an effective way of reducing the dosing of mechanical stimulus. The voltage optimization, however, is a necessary part of the current muscle stimulation procedure. It may not be practical to reduce the exercise stimulus by eliminating or attempting to reduce the isometric portion of the protocol.

Comparison to Previous Work

This study sought to extend the work of Vyvial (2006) in characterizing the strain on the rat tibia during muscle stimulation. His protocol differed from the current protocol in the length of the contraction and the range through which the foot rotated (see Figure 10). He used fewer animals and measured strain at 0, 7 and 21 days of hindlimb unloading with an exercise countermeasure.

In his study, eccentric strains measured at the exercise intensity (120% of PIT) ranged from about 400-1200 microstrain. In the current study (at 100% PIT and angles changed), these strains range from 600-1400 microstrain. These ranges are very close and this indicates a degree of repeatability or similarity between these studies.

One of the outcomes from the study of Vyvial (2006) was an apparent trend in which the eccentric torque versus strain relationship changed with time. This apparent trend can be seen in a plot excerpted from his study (Figure 35). The trend line for the baseline group sits on top, followed by the 7 day HU + Ex and the 21 day HU + Ex group is on the bottom. These trendlines were not statistically different, but this could have been explained by the small numbers of animals in each group.

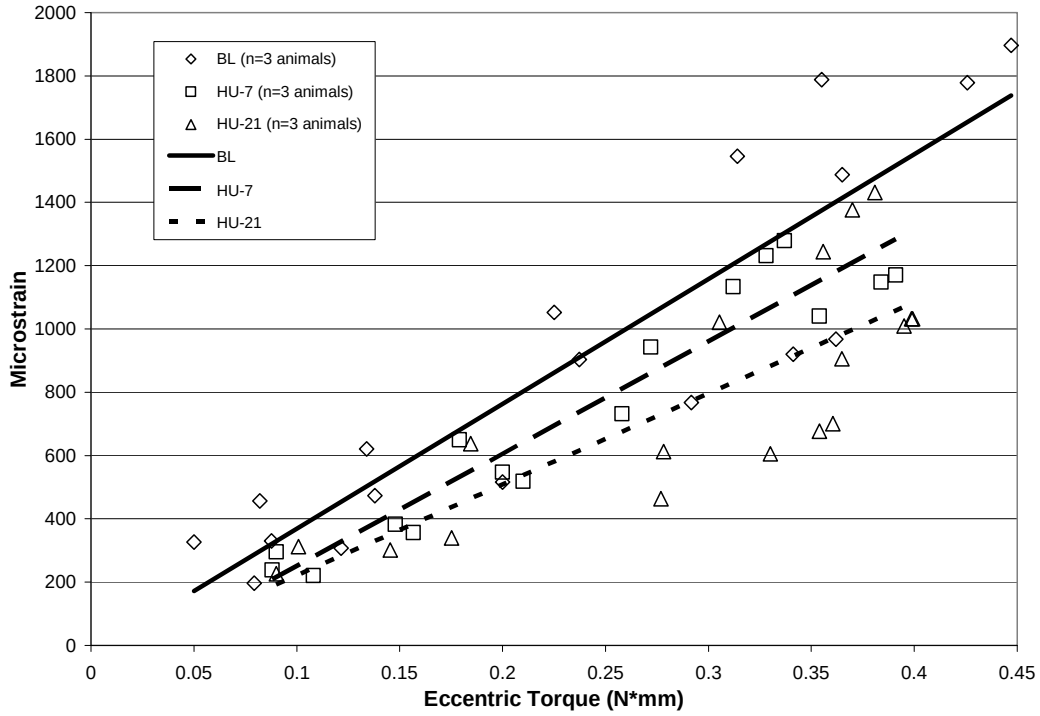

Figure 35 Eccentric torque vs. strain plot from the previous study by Vyvial[1]. A trend was noticed where the hindlimb unloaded groups' trend lines seemed to move down with time. This trend was not significant.

In the current study, a similar plot was presented and is shown in Figure 18 on page 25, but with the axes opposite those of Figure 35. The same data, but with axes consistent with the work of Vyvial, are presented in Figure 36. In the graph from the current study the data sets have too much overlap to consider their differences significant, and the statistical results support this. In the current study, the 21 day HU + Ex group's trend line is on top, the opposite of the trend observed by Vyvial. Thus it appears likely that the trends noticed may have been the result of random variations or experimental artifacts.

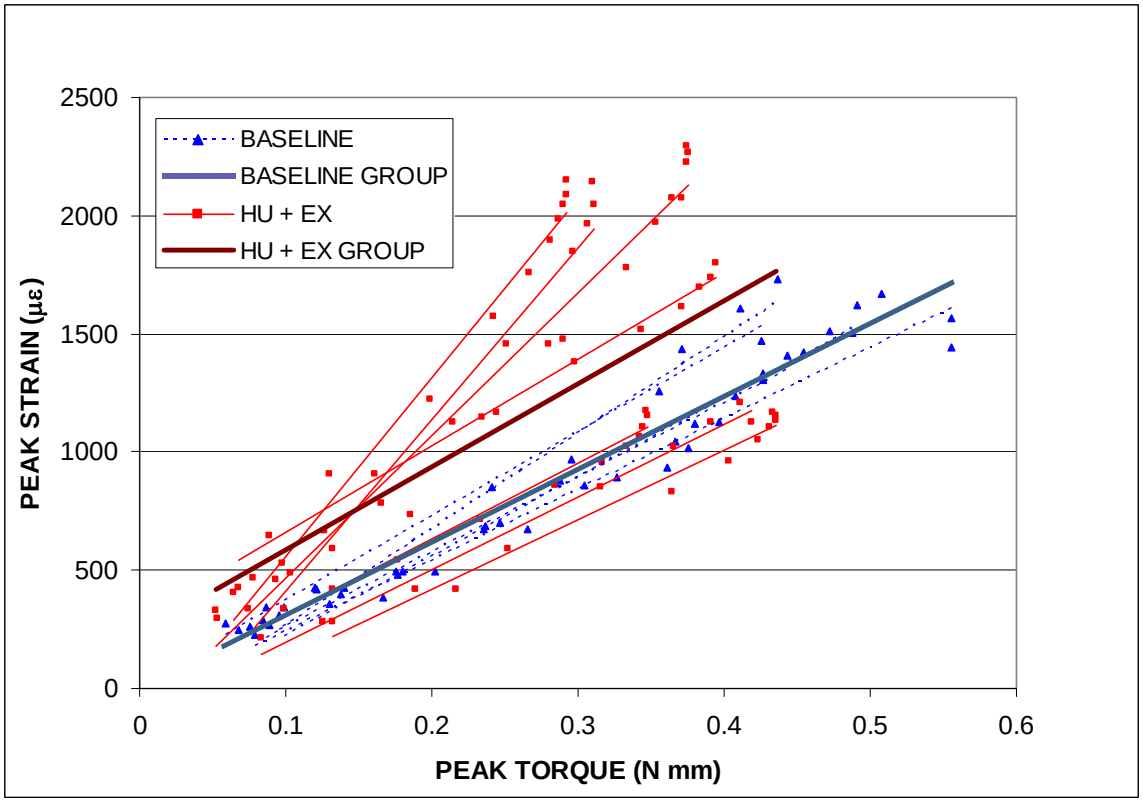

Figure 36 Strain vs. eccentric torque plot from the current study with axes consistent with the study of Vyvial. In this case the hindlimb unloaded group spreads on both sides of the baseline group and its trend line is above the trend line for the baseline group.

Group Differences

The purpose of the experimental groups in this project was to note any changes that might occur during the period of hindlimb unloading and exercise. No meaningful differences were found between the groups, with the exception of eccentric maximum oscillatory strain rate and peak isometric torque. The question here might be, "Why weren't there any other differences, and should any differences have been expected?" If the countermeasure was effective at maintaining bone, this might be evident in the absence of group differences. However, this study was not designed to test the efficacy of the countermeasure in that it lacked a hindlimb unloaded control group that did not receive the countermeasure.

The duration of the study was 21 days. Bone studies using hindlimb unloading, including the study of Sumner, which noted an osteogenic response, typically last 28 days. The current study may not have unloaded the rats long enough to realize a measurable response.

Another possible reason that no change in the bone was noticed is related to where on the bone strain was measured. Figure 37 shows a radiograph of a tibia from this study with the gage attached and radiographs for many of the animals are given in Appendix C. The gage region of the strain gage is too small to be seen, but the solder tabs on the gage mark its location. The antero-medial aspect of the proximal tibia was chosen as the implantation site because the proximal tibia has both cortical and cancellous bone. Since cancellous bone is more responsive to changes in loading; this site would be expected to be particularly sensitive to changes in the bone architecture. A careful inspection of the site on the radiograph, however, reveals that little or no cancellous bone is present below the gage. It should be noted that the gage was placed in the same location in the study of Vyvial.

The other reason this site was chosen was to minimize disrupting the function of the leg musculature. Implanting a strain gage above the cancellous bone may not be practical for a procedure that utilizes animal effort. End effects in the strain distribution

from implanting a gage close to the joint would also need to be considered if a gage were implanted proximal the current site.

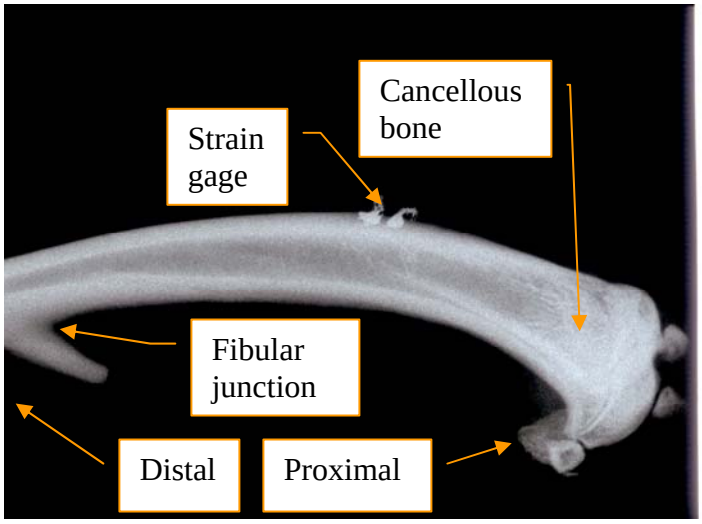

Figure 37 Radiograph of excised tibia with strain gage attached. Note that there is no cancellous bone under the gage.

CONCLUSIONS AND RECOMMENDATIONS

Contraction Comparison

It appears this study raises as many questions as it answers. The loading environment in the current protocol is an effective disuse countermeasure and even appears to be osteogenic, but it remains unclear exactly why. A study to identify which aspects of the exercise are contributing to the bone response would be useful to help better understand how the countermeasure could be effectively dosed. To determine whether the isometric contractions dominate the response, a study could include a group that just receives the voltage optimization portion of the exercise session. This group could be compared to a group that receives the complete exercise session. Isolating the effects of stimulation frequency would be more complicated since it is adjusted to achieve the torque value in the exercise. Stimulation voltage or some other aspect of the input would need to be adjusted to achieve a standard eccentric torque. This may involve stepper motor feedback in the stimulation.

Rosette Strain Gages

The weakness of using unidirectional strain gages is that strain is only known in the direction of the gage. In this case, strain is only measured along the axis of the bone. This assumes that the gage is glued on straight, which is difficult to achieve and even more difficult to detect *in situ*. To minimize impairing leg muscle function, the space on the tibia cleared for gage implantation needs to be very small. Without a large portion of bone visible, the axis of the bone can be difficult to accurately identify. One animal in this study had strain readings much lower than any other animal, which was attributed to a rotated gage, and the data were deemed invalid. It is unknown how much experimental scatter in the current protocol can be attributed to gage alignment.

Uniaxial strain gages are often used in rodent studies because of their small size. *In vivo* methods that load bone externally, such as axial compression or 4-point bending, allow the direction of principle (highest) strain to be predicted because the mechanics of

the loading are fairly straight forward (anisotropy aside). The current protocol uses muscles to load the bone and may have a more complicated strain state than can be observed using a uniaxial gage.

If 3-element rosette strain gages were used, strain would be known in 3 linearly independent directions. From 3 directions, the full strain tensor could be calculated and the principle strain known. The alignment of the axis of the gage also becomes inconsequential in determining principle strain.

Muscle Stimulation as a Mechanical Test

Mechanical testing of skeletal tissue is typically done with tests adapted from metallic materials testing standards. These do a fine job of isolating material properties, but they do not load the bone in the manner it was adapted to be loaded. The procedures presented here could be used to design mechanical tests that characterize skeletal tissue with physiological relevance. If the isometric torque versus strain plots could be synchronized in real time, viscoelastic properties could be possibly quantified. If the kinematics could be worked out to estimate stress on the bone from ankle torque, stress-strain curves could be made. From these, material properties could be estimated. To synchronize the data in real time, the strain and torque need only be recorded at the same time in the same program. For isometric contractions, the foot pedal need not be attached to a motor, but could be attached to a rigid shaft with a torque transducer. The strategy employed in this study to synchronize the data after the fact was only useful for comparing groups; the test has the potential to provide more meaningful data.

Final Remark

It can be difficult attempting to apply results from the current mix of studies to general bone adaptation. Variations in the loading mechanisms and protocols, the strain gage designs and implantation locations, the specific bones studied, the strain and age of rats studied, the disuse model employed, and basic biological variance inherent in animal studies make results difficult to compare. Still, the insights from these studies help us

develop skeletal adaptation models and better models will eventually lead to better skeletal heath for astronauts and the rest of us.

REFERENCES

1. Vyvial BA 2006 Characterizing strain in the proximal rat tibia during electrical muscle stimulation. MS Thesis, Texas A&M University.

2. Sumner LR 2007 Osteogenic effect of optimized muscle stimulation exercise as a countermeasure during hindlimb unloading. MS Thesis, Texas A&M University.

3. Alcorn JD 2006 Osteogenic effect of electric muscle stimulation as a countermeasure during hindlimb unloading. MS Thesis, Texas A&M University.

4. Morey-Holton ER, Globus RK 1998 Hindlimb unloading of growing rats: a model for predicting skeletal changes during spaceflight. Bone **22**: 83S-88S.

5. U.S. National Cancer Institute's Surveillance, Epidemiology and End Results Program. Anatomy and Physiology 4 July 2007 http://training.seer.cancer.gov/module_anatomy/unit3_4_bone_classification.html.

6. U.S. National Cancer Institute's Surveillance, Epidemiology and End Results Program. Anatomy and Physiology 4 July 2007 http://training.seer.cancer.gov/module_anatomy/unit3_2_bone_tissue.html.

7. Frost HM 1987 Bone “mass” and the “mechanostat”: A proposal. Anatomical Record **219**:1-9.

8. Lang T, LeBlanc A, Evans H, Lu H, Genant H, Yu A 2004 Cortical and trabecular bone mineral loss from the spine and hip in long-duration spaceflight. J Bone Miner Res **19**:1006-1012.

9. Collet PH, Uebelhart D, Vico L, Moro L, Hartmann D, Roth M, Alexandre C 1997 Effects of 1- and 6-month spaceflight on bone mass and biochemistry in two humans. Bone **20**:547-551.

10. Robling AG, Burr, DB, Turner, CH 2001 Skeletal loading in animals. J Musculoskel Neuron Interact **1**:249-262.

11. Rubin CT and Lanyon LE 1984 Regulation of bone formation by applied dynamic loads. J. Bone Jt. Surg. **66**-A(3): 397-402.

12. Forwood MR, Bennett MB, Blowers AR, Nadorfi RL 1998 Modification of the in vivo four-point loading model for studying mechanically induced bone adaptation. Bone **23**:307-310.

13. Fritton JC, Myers ER, Wright TM, Van der Meuken MCH 2005 Loading induces site-specific increases in mineral content assessed by microcomputed tomography of mouse tibia. Bone **36**:1030-1038.

14. De Souza RL, Matsuura M, Eckstein F, Rawlinson SCF, Lanyon LE, Pitsillides AA 2005 Non-invasive axial loading of mouse tibiae increases cortical bone formation and modifies trabecular organization: A new model to study cortical and cancellous compartments in a single loaded element. Bone **37**(6):810-818.

15. Fluckey JD, Dupont-Versteegden EE, Montague DC, Knox M, Tesch P, Peterson CA, Gaddy-Kurten D 2002 A resistance exercise regimen attenuates losses of musculoskeletal mass during hindlimb suspension. Acta Physiol Scand **176**:293-300.

16. Fritton SP, Rubin CT 2001. In vivo measurement of bone deformations using strain gauges. Bone Mechanics Handbook. 2nd ed. CRC Press, Boca Raton, FL, USA, 8.1-8.41.

17. Bloomfield SA, Allen MR, Hogan HA, Delp MD 2002 Site- and compartment-specific changes in bone with hindlimb unloading in mature adult rats. Bone **31**:149-157.

18. Ashton-Miller JA, He Y, Kadhiresan VA, McCubbrey DA, Faulkner JA 1992 An apparatus to measure in vivo biomechanical behavior of dorsi- and plantarflexors of mouse ankle. J Appl Phsiol **92**:1205-1211.

19. Cutlip RG, Stauber WT, Willison RH, McIntosh TA, Means KH 1997 Dynamometer for rat plantar flexor muscles in vivo. Med Biol Eng Comput **35**:540-543.

20. Warren GL, Stallone JL, Allen MR, Bloomfield SA 2004 Functional recovery of the plantorflexor muscle group after hindlimb unloading in the rat. Eur J Appl Physiol **93**: 130-138.

21. Morey-Holton ER, Globus RK 2002 Hindlimb unloading rodent model: Technical aspects. J Appl Physiol **92**: 1367-1377.

22. Fondrk M, Bahniuk D, Davy DT, Michaels C 1986 Some viscoplastic characteristics of bovine and human cortical bone. J. Biomechanics **21**:623-630.

23. Hsieh YF, Wang T, Turner CH 1999 Viscoelastic response of the rat loading model: Implications for studies of strain-adaptive bone formation. Bone **25**:379-382.

24. Turner CH 1999 Toward a mathematical description of bone biology: The principle of cellular accommodation. Calcif Tissue Int **65**:466-471.

25. Cullen D, Smith R, Akhter MP 2001 Bone-loading response varies with strain magnitude and cycle number. J Appl Physiol **91**:1971-1976.

26. Hsieh YF, Robling AG, Ambrosius WT, Burr DB, Turner CH 2001 Mechanical loading of Diaphyseal bone in vivo: The strain threshold for an osteogenic response varies with location. J Bone Miner Res **16**:2291-2297.

27. Turner CH, Owan I, Takano Y 1995 Mechanotransduction in bone: Role of strain rate. Am J Physiol **269** (Endocrinol Metab **32**):E438-E442.

28. Judex S, Lei X, Han D, Rublin C 2007 Low-magnitude mechanical signals that stimulate bone formation in the ovarectimized rat are dependent on the applied frequency but not on the strain magnitude. J Biomech **40**:1333-1339.

29. Srinivasan S, Weimer D, Agans S, Bain S, Gross T 2002 Low-magnitude mechanical loading becomes osteogenic when rest is inserted between each load cycle. J Bone Miner Res **17**:1613-1619.

30. Rabkin BA, Szivek JA, Schonfeld JE, Halloran BP 2001 Long-term measurement of bone strain in vivo: The rat tibia. J Biomed Mater Res **58**:277-281.

APPENDIX A

Data plots by animal

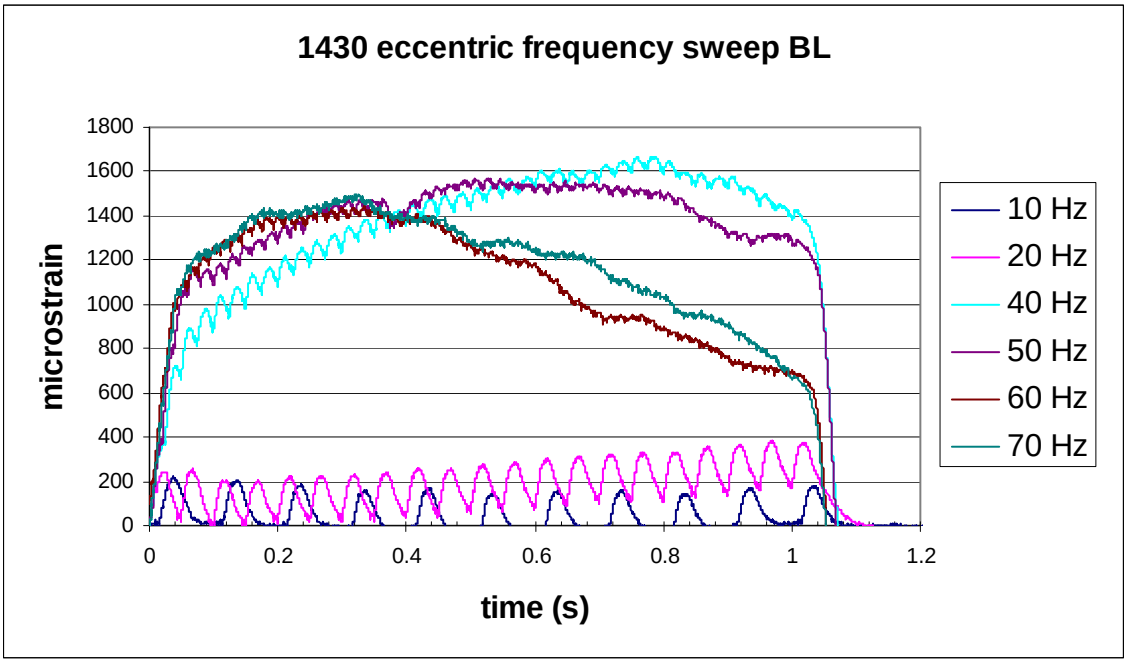

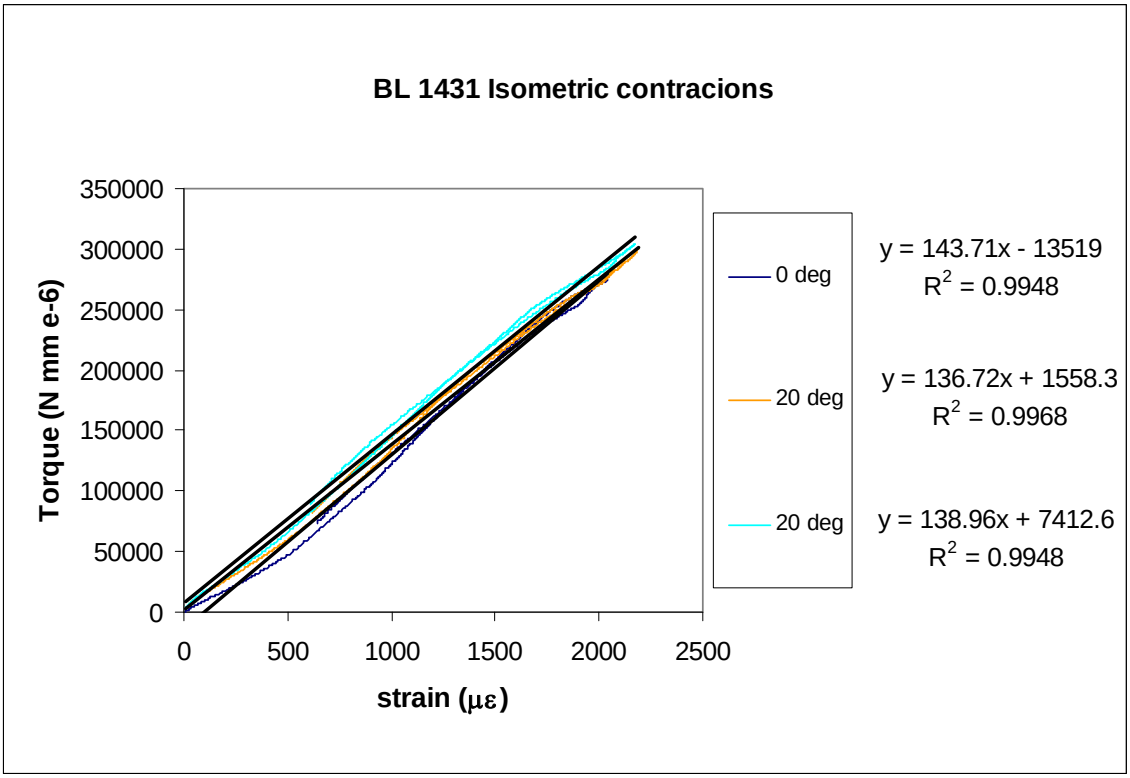
BL 1431 Isometric contracions
Torque (N mm e-6)
350000
300000
250000
200000
150000
100000
50000
0
0
500
1000
1500
2000
2500
strain (με)
0 deg
20 deg
20 deg
y = 143.71x - 13519
R2 = 0.9948
y = 136.72x + 1558.3
R2 = 0.9968
y = 138.96x + 7412.6
R2 = 0.9948

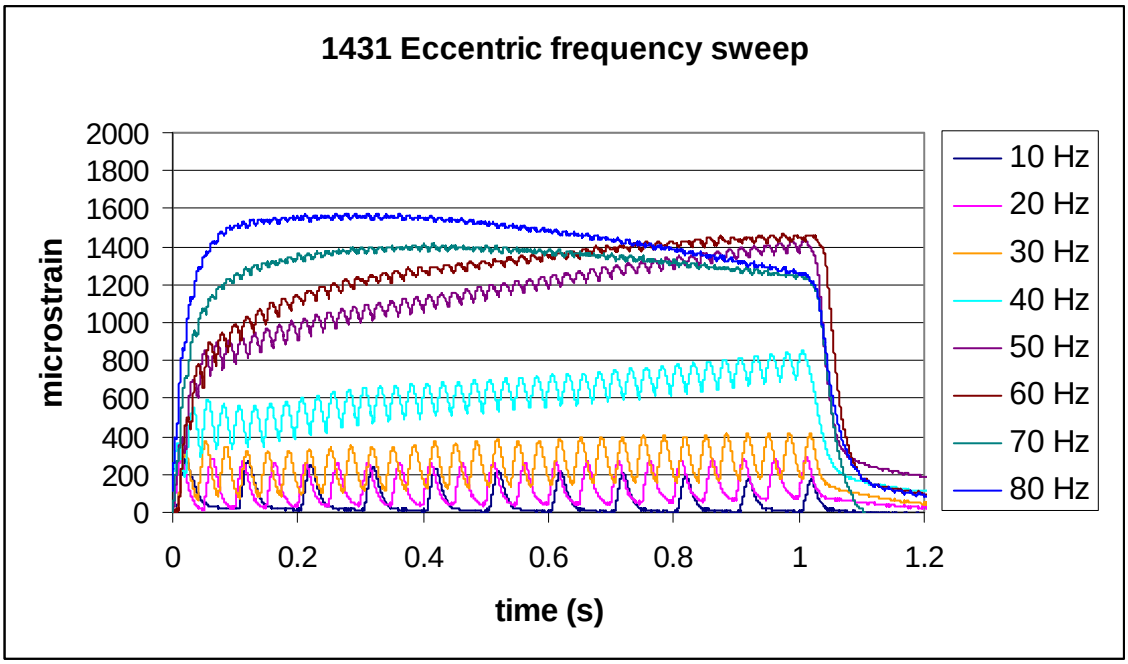
1431 Eccentric frequency sweep
microstrain
2000
1800
1600
1400
1200
1000
800
600
400
200
0
0
0.2
0.4
0.6
0.8
1
1.2
time (s)
10 Hz
20 Hz
30 Hz
40 Hz
50 Hz
60 Hz
70 Hz
80 Hz

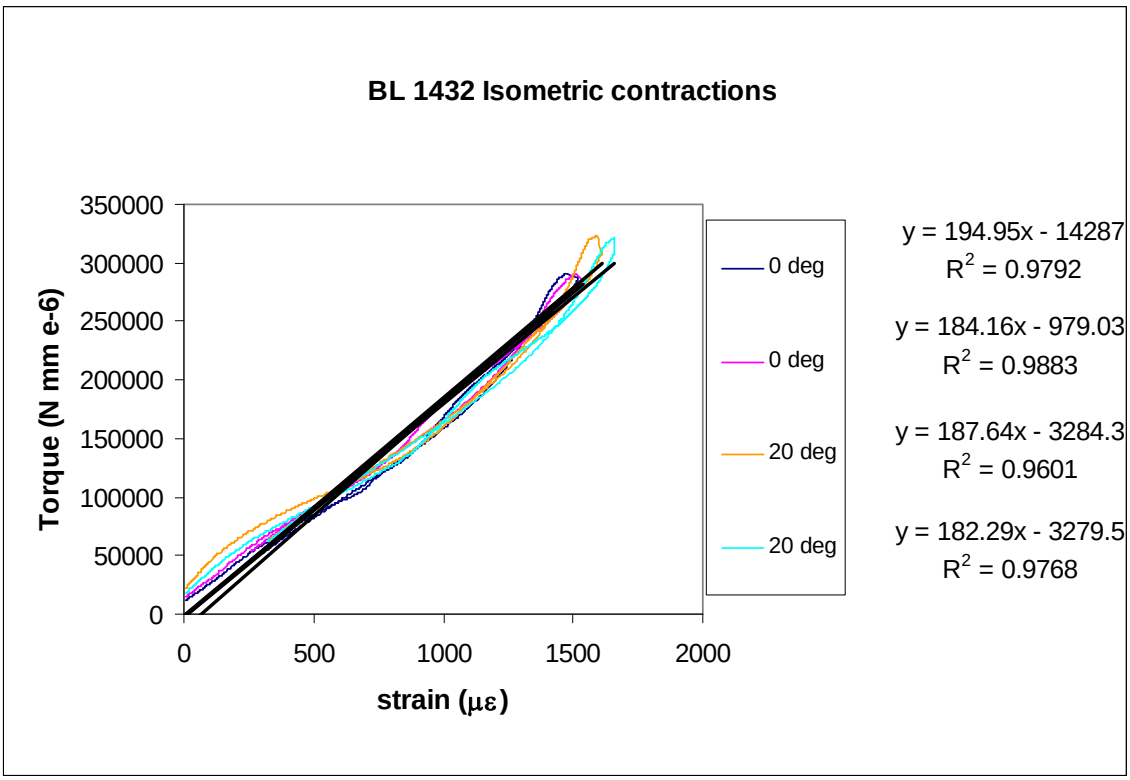
BL 1432 Isometric contractions
Torque (N mm e-6)
350000
300000
250000
200000
150000
100000
50000
0
0
500
1000
1500
2000
strain (με)
0 deg
0 deg
20 deg
20 deg
y = 194.95x - 14287
R2 = 0.9792
y = 184.16x - 979.03
R2 = 0.9883
y = 187.64x - 3284.3
R2 = 0.9601
y = 182.29x - 3279.5
R2 = 0.9768

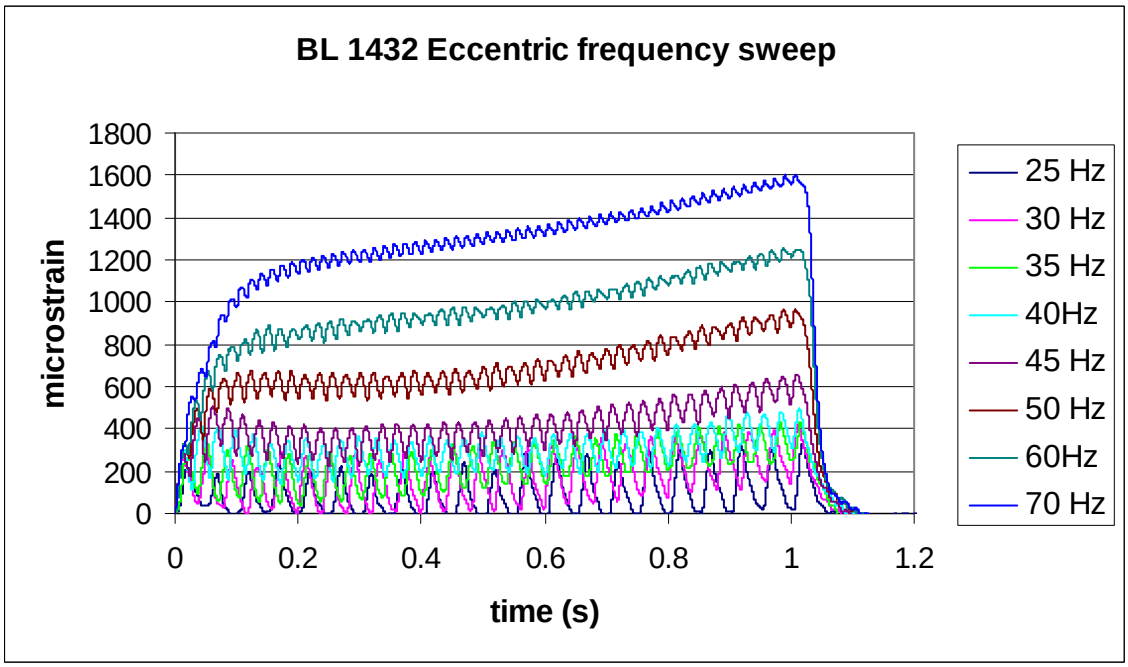
BL 1432 Eccentric frequency sweep
microstrain
1800
1600
1400
1200
1000
800
600
400
200
0
0
0.2
0.4
0.6
0.8
1
1.2
time (s)
25 Hz
30 Hz
35 Hz
40Hz
45 Hz
50 Hz
60Hz
70 Hz

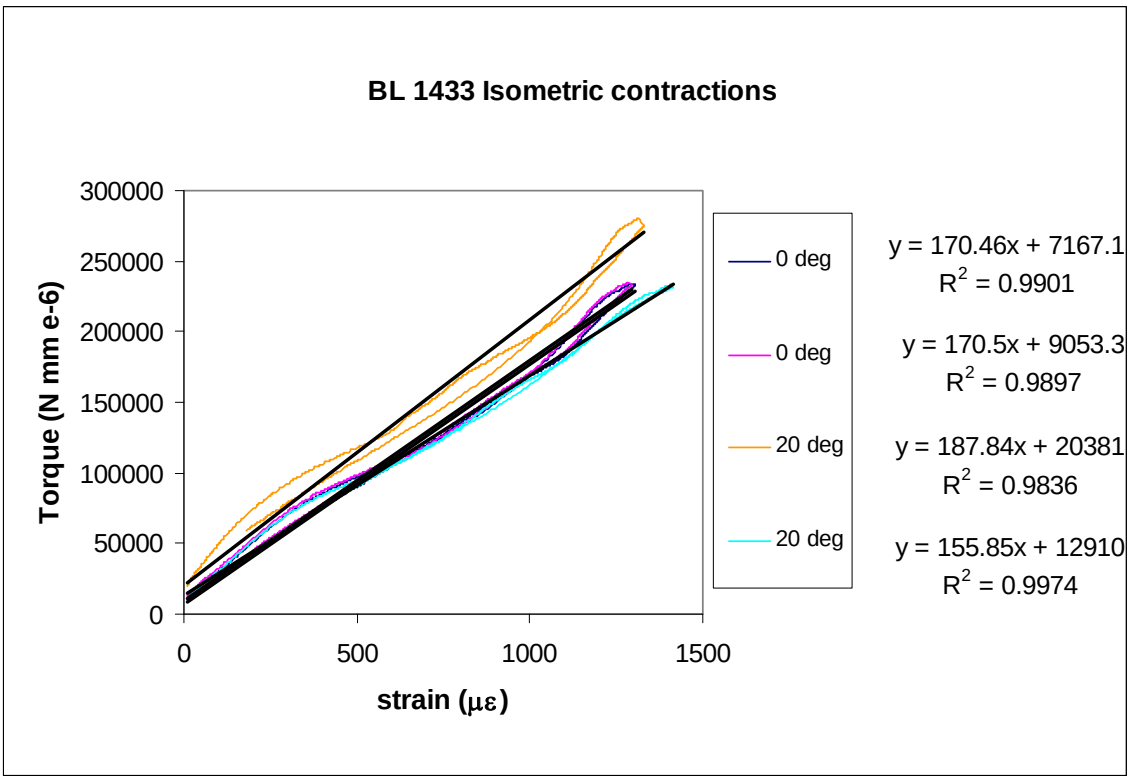
BL 1433 Isometric contractions
Torque (N mm e-6)
300000
250000
200000
150000
100000
50000
0
0
500
1000
1500
strain (με)
0 deg
0 deg
20 deg
20 deg
y = 170.46x + 7167.1
R2 = 0.9901
y = 170.5x + 9053.3
R2 = 0.9897
y = 187.84x + 20381
R2 = 0.9836
y = 155.85x + 12910
R2 = 0.9974

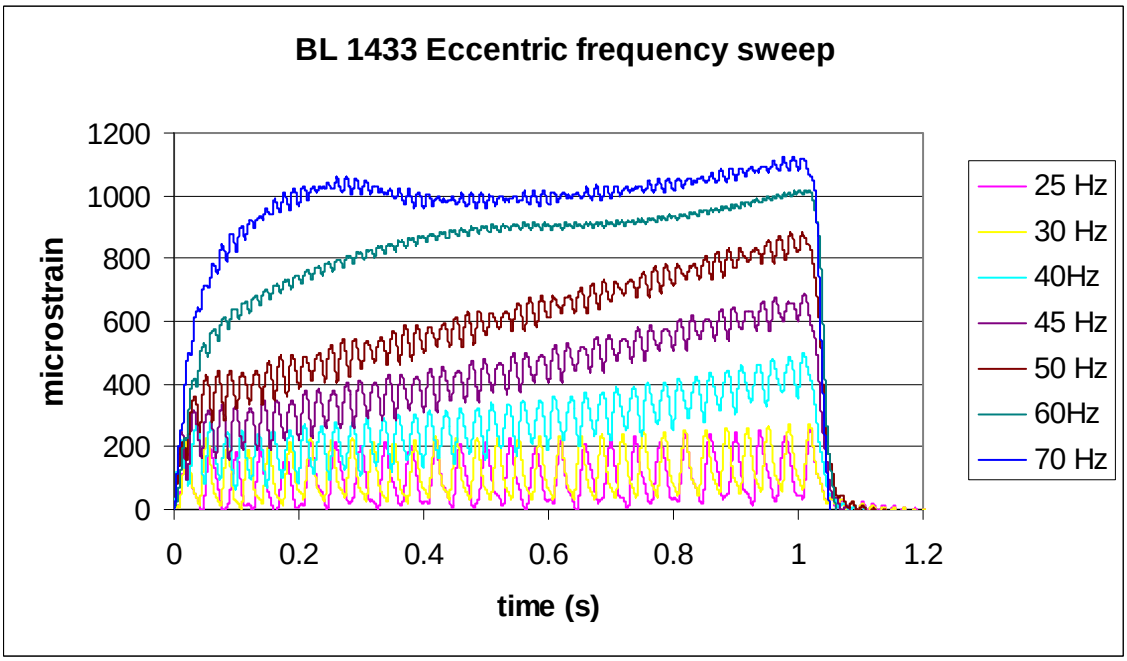
BL 1433 Eccentric frequency sweep
microstrain
1200
1000
800
600
400
200
0
0
0.2
0.4
0.6
0.8
1
1.2
time (s)
25 Hz
30 Hz
40Hz
45 Hz
50 Hz
60Hz
70 Hz

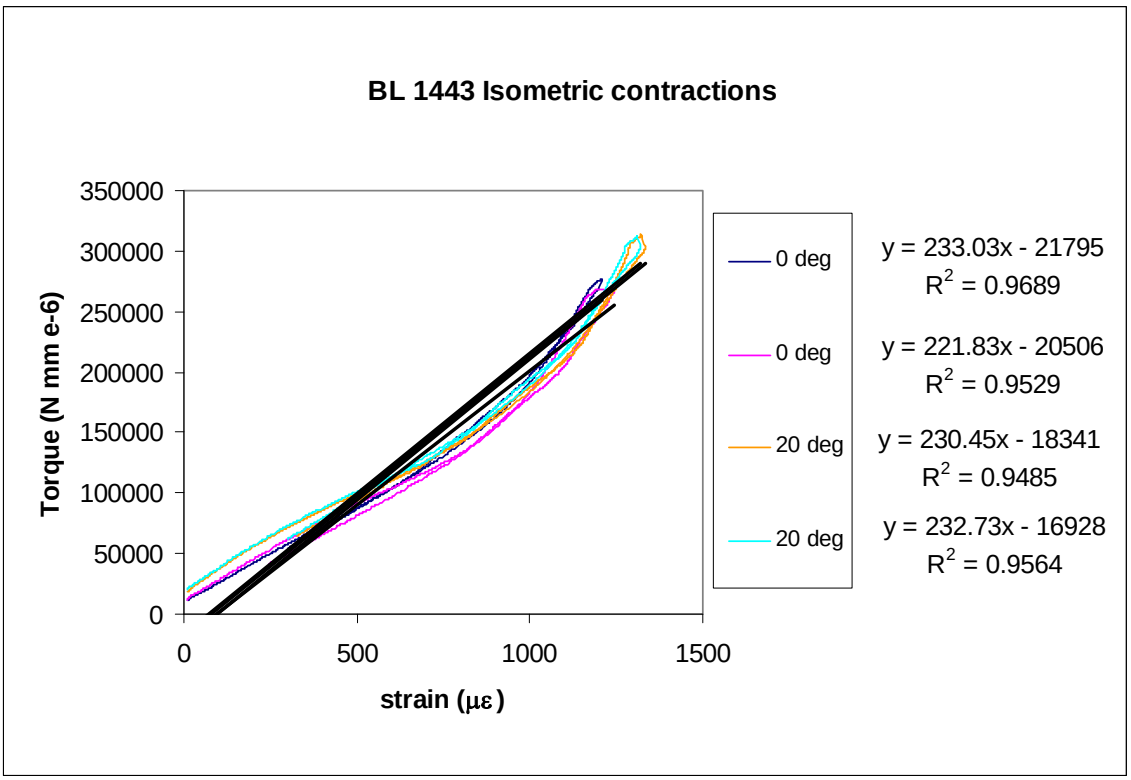
BL 1443 Isometric contractions
Torque (N mm e-6)
350000
300000
250000
200000
150000
100000
50000
0
0
500
1000
1500
strain (με)
0 deg
0 deg
20 deg
20 deg
y = 233.03x - 21795
R2 = 0.9689
y = 221.83x - 20506
R2 = 0.9529
y = 230.45x - 18341
R2 = 0.9485
y = 232.73x - 16928
R2 = 0.9564

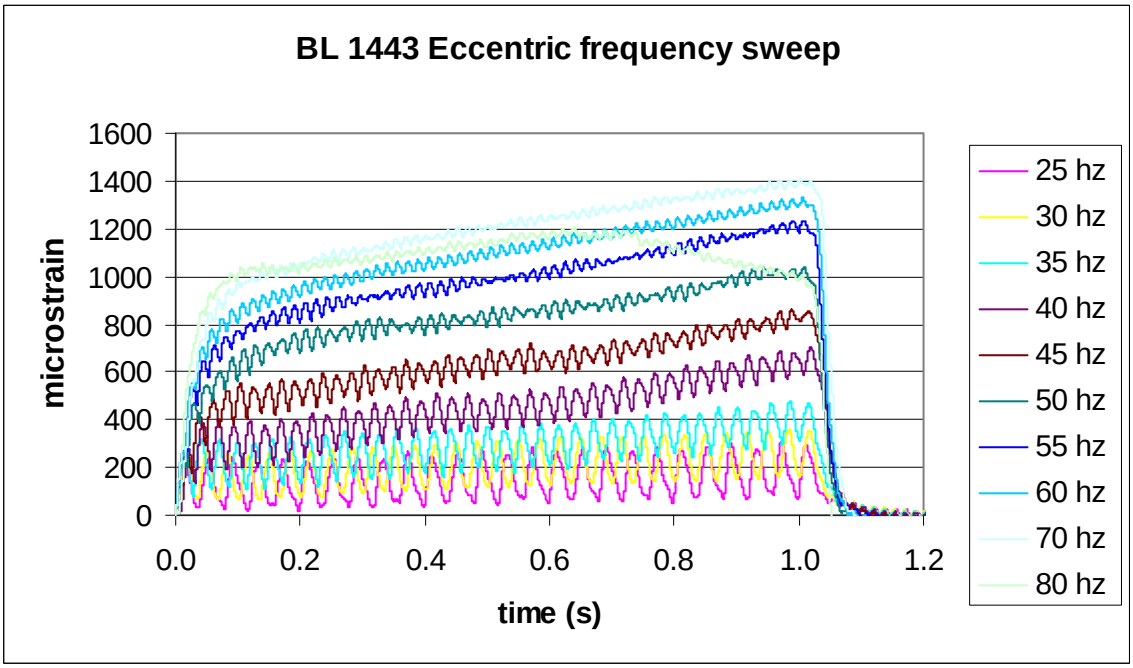
BL 1443 Eccentric frequency sweep
microstrain
1600
1400
1200
1000
800
600
400
200
0
0.0
0.2
0.4
0.6
0.8
1.0
1.2
time (s)
25 hz
30 hz
35 hz
40 hz
45 hz
50 hz
55 hz
60 hz
70 hz
80 hz

Note: Plots of 1444 were used for all example figures in text

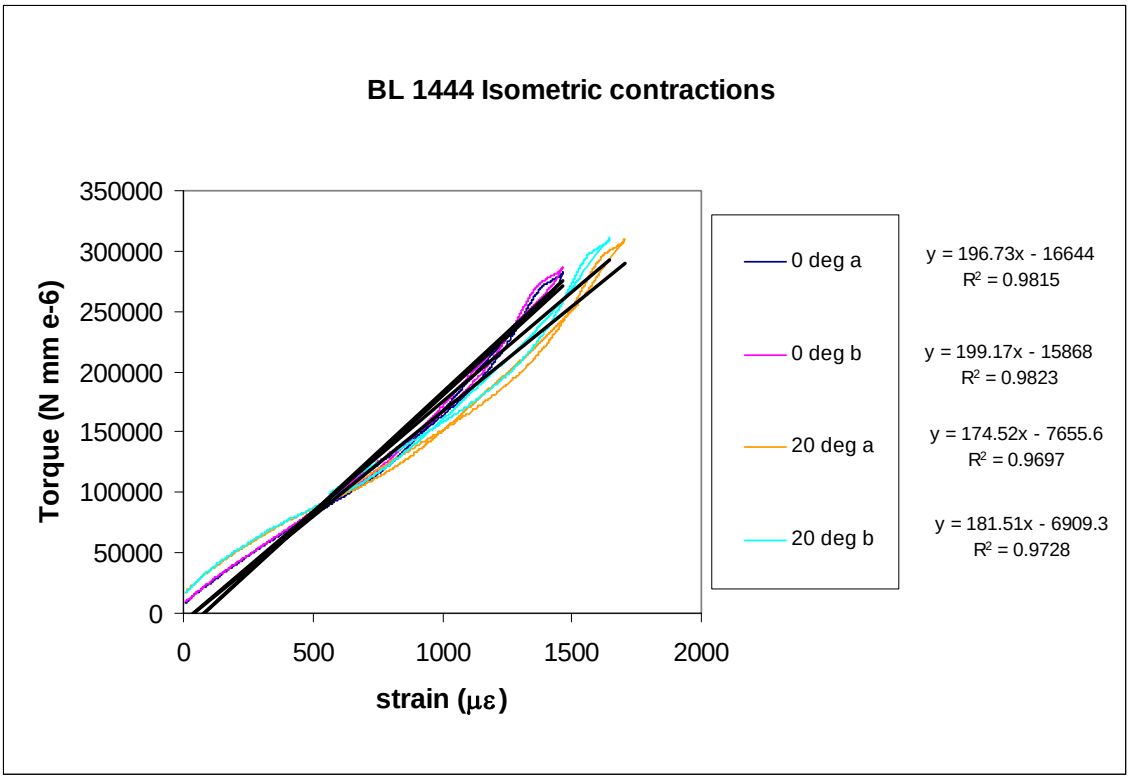

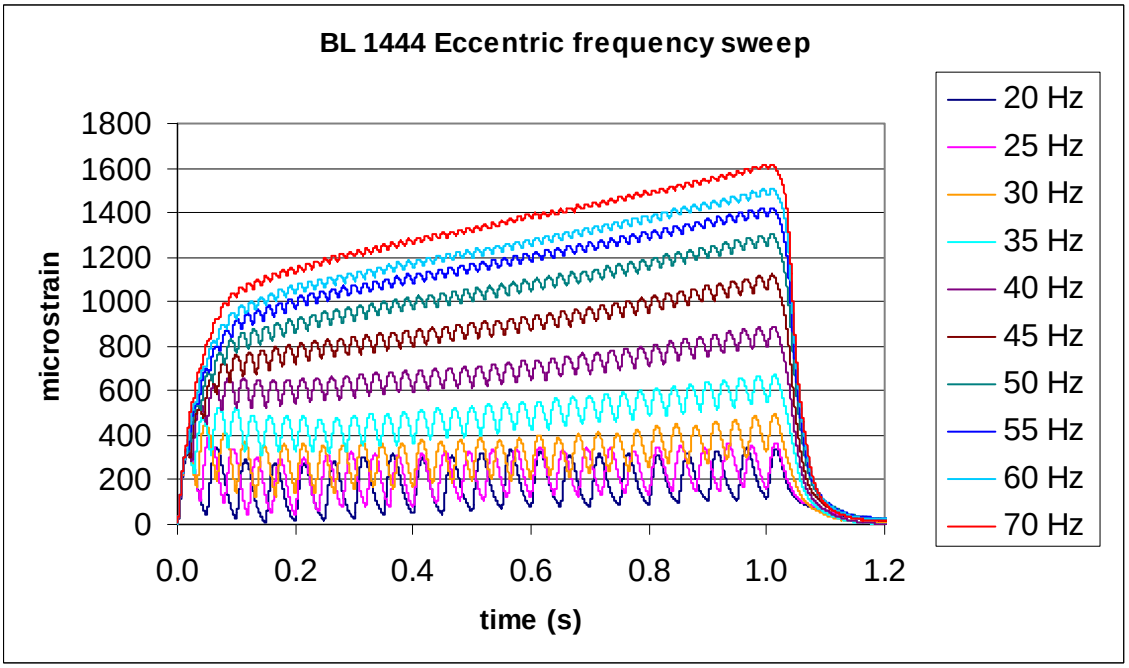

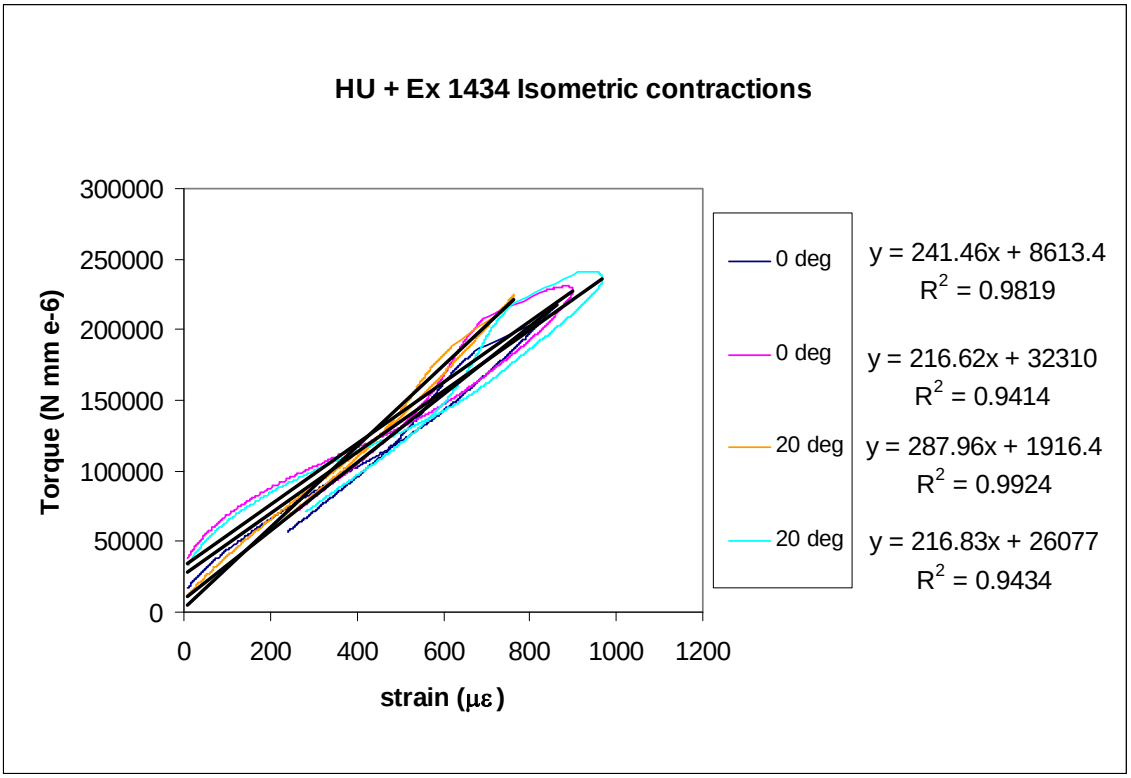
HU + Ex 1434 Isometric contractions
Torque (N mm e-6)
300000
250000
200000
150000
100000
50000
0
0
200
400
600
800
1000
1200
strain (με)
0 deg
0 deg
20 deg
20 deg
y = 241.46x + 8613.4
R2 = 0.9819
y = 216.62x + 32310
R2 = 0.9414
y = 287.96x + 1916.4
R2 = 0.9924
y = 216.83x + 26077
R2 = 0.9434

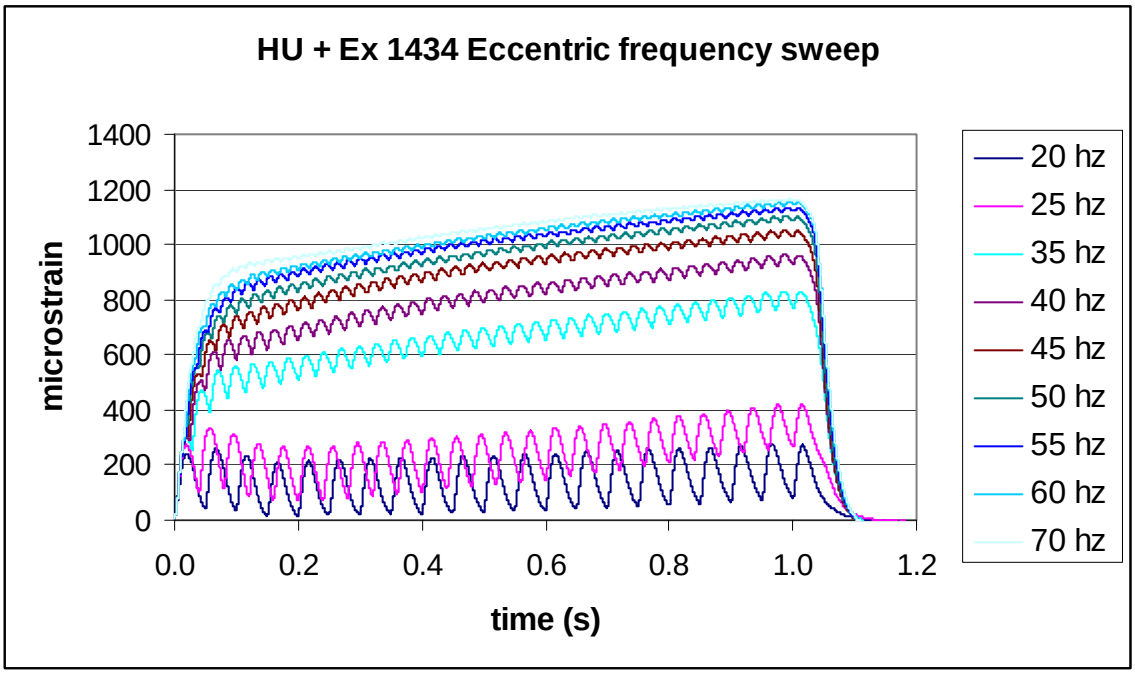
HU + Ex 1434 Eccentric frequency sweep
microstrain
1400
1200
1000
800
600
400
200
0
0.0
0.2
0.4
0.6
0.8
1.0
1.2
time (s)
20 hz
25 hz
35 hz
40 hz
45 hz
50 hz
55 hz
60 hz
70 hz

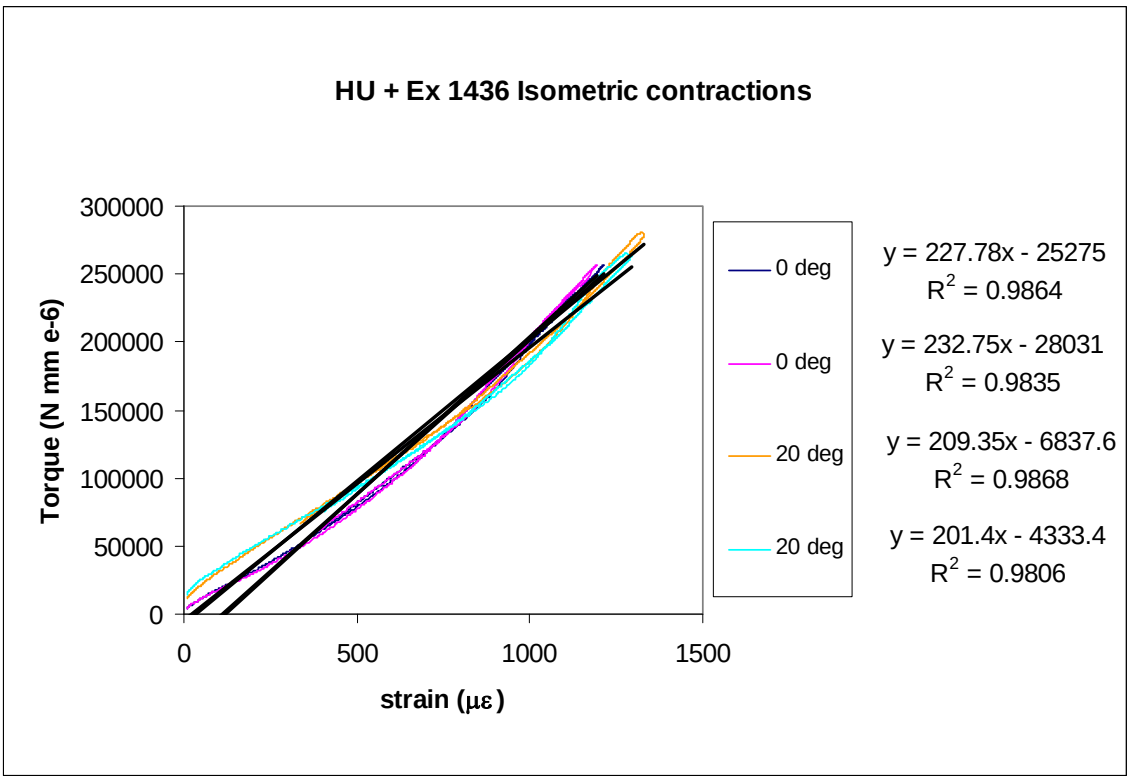
HU + Ex 1436 Isometric contractions
Torque (N mm e-6)
300000
250000
200000
150000
100000
50000
0
0
500
1000
1500
strain (με)
0 deg
0 deg
20 deg
20 deg
y = 227.78x - 25275
R2 = 0.9864
y = 232.75x - 28031
R2 = 0.9835
y = 209.35x - 6837.6
R2 = 0.9868
y = 201.4x - 4333.4
R2 = 0.9806

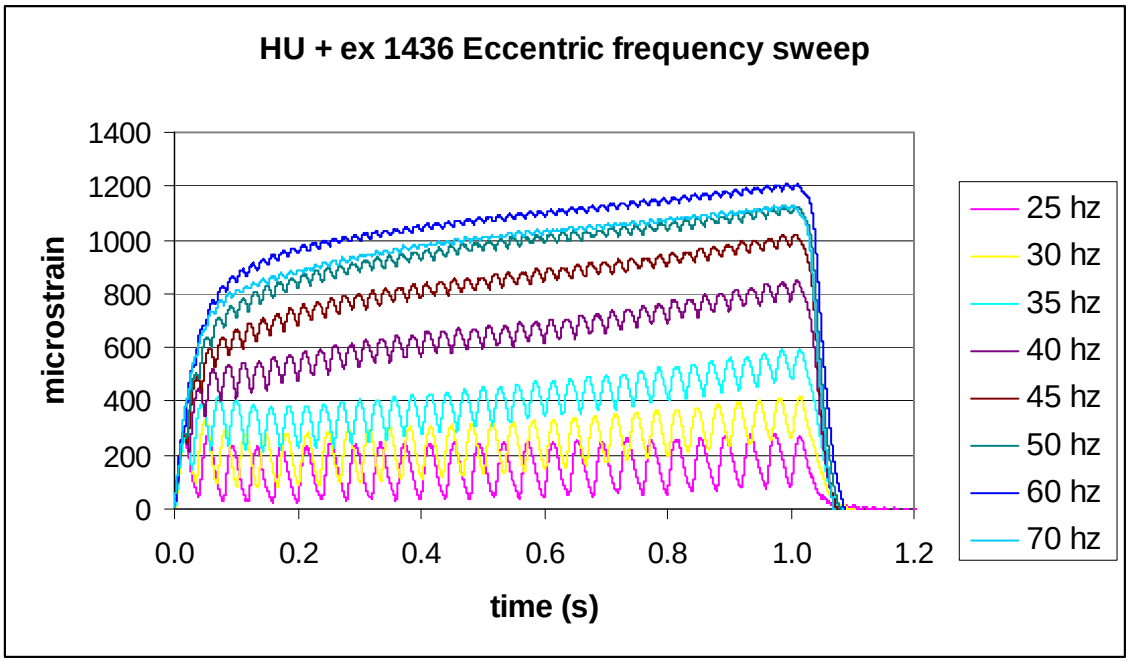
HU + ex 1436 Eccentric frequency sweep
microstrain
1400
1200
1000
800
600
400
200
0
0.0
0.2
0.4
0.6
0.8
1.0
1.2
time (s)
25 hz
30 hz
35 hz
40 hz
45 hz
50 hz
60 hz
70 hz

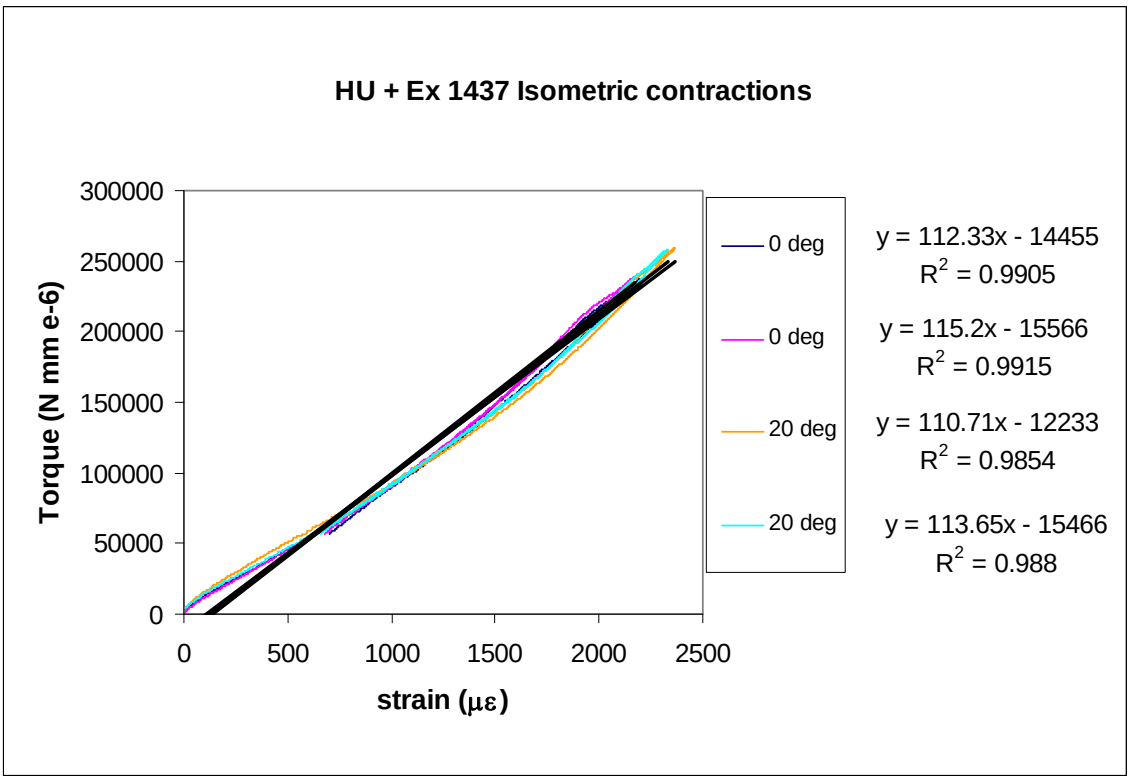
HU + Ex 1437 Isometric contractions
Torque (N mm e-6)
300000
250000
200000
150000
100000
50000
0
0
500
1000
1500
2000
2500
strain (με)
0 deg
0 deg
20 deg
20 deg
y = 112.33x - 14455
R2 = 0.9905
y = 115.2x - 15566
R2 = 0.9915
y = 110.71x - 12233
R2 = 0.9854
y = 113.65x - 15466
R2 = 0.988

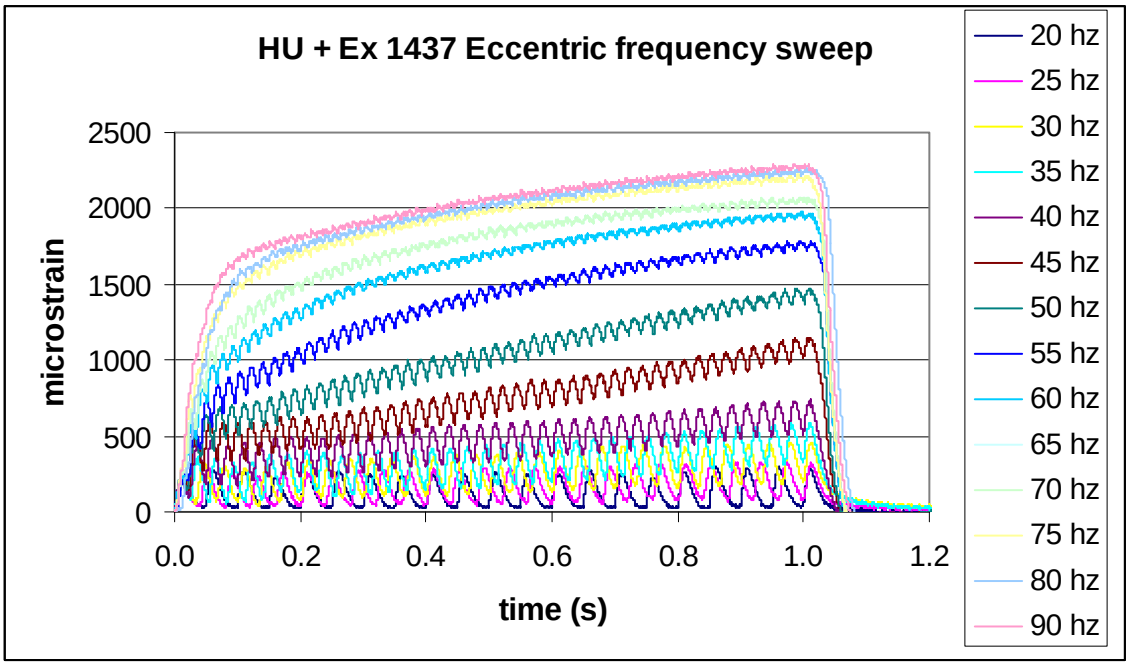
HU + Ex 1437 Eccentric frequency sweep
microstrain
2500
2000
1500
1000
500
0
0.0
0.2
0.4
0.6
0.8
1.0
1.2
time (s)
20 hz
25 hz
30 hz
35 hz
40 hz
45 hz
50 hz
55 hz
60 hz
65 hz
70 hz
75 hz
80 hz
90 hz

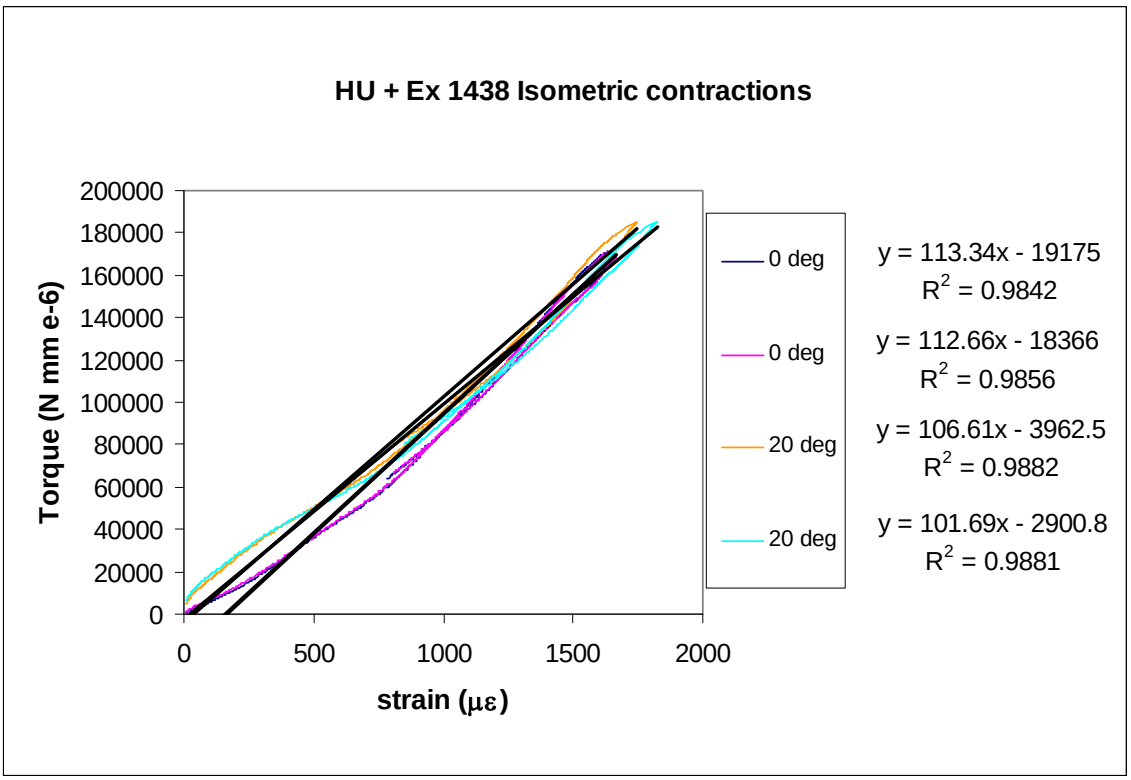
HU + Ex 1438 Isometric contractions
Torque (N mm e-6)
200000
180000
160000
140000
120000
100000
80000
60000
40000
20000
0
0
500
1000
1500
2000
strain (με)
0 deg
0 deg
20 deg
20 deg
y = 113.34x - 19175
R2 = 0.9842
y = 112.66x - 18366
R2 = 0.9856
y = 106.61x - 3962.5
R2 = 0.9882
y = 101.69x - 2900.8
R2 = 0.9881

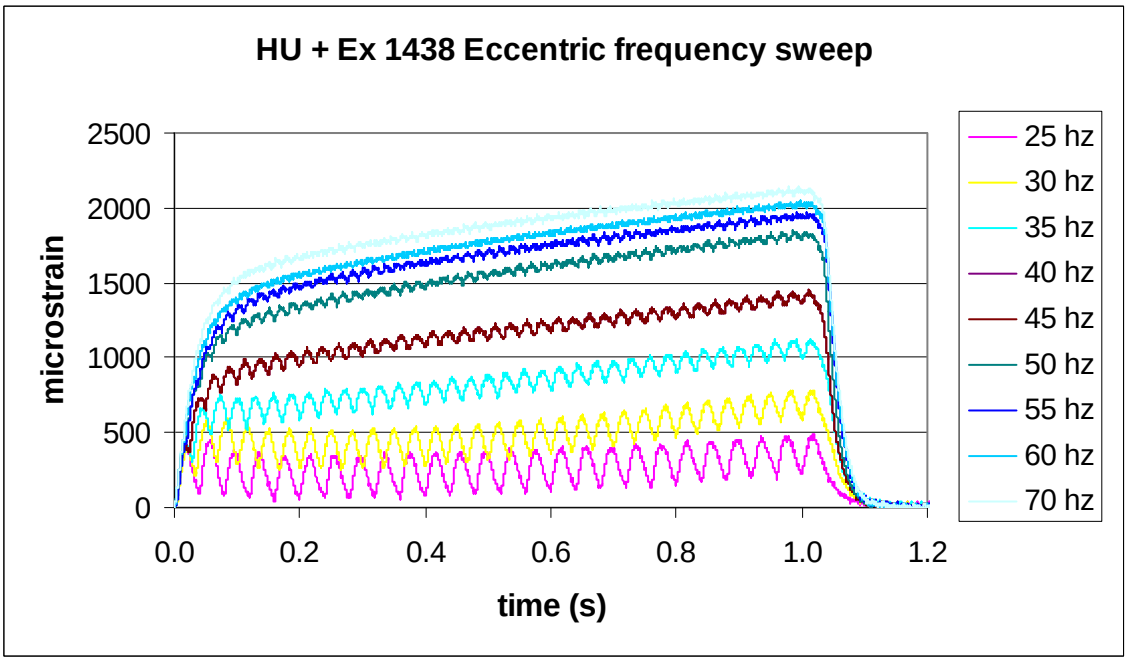
HU + Ex 1438 Eccentric frequency sweep
microstrain
2500
2000
1500
1000
500
0
0.0
0.2
0.4
0.6
0.8
1.0
1.2
time (s)
25 hz
30 hz
35 hz
40 hz
45 hz
50 hz
55 hz
60 hz
70 hz

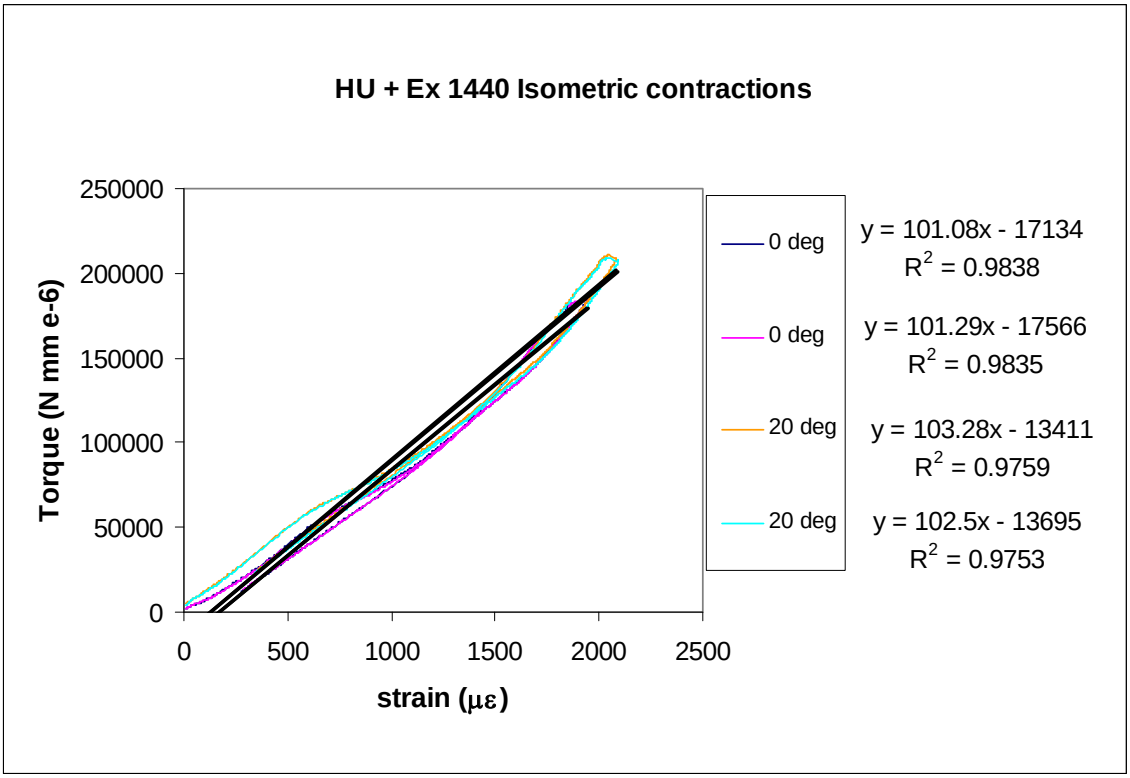
HU + Ex 1440 Isometric contractions
Torque (N mm e-6)
250000
200000
150000
100000
50000
0
0
500
1000
1500
2000
2500
strain (με)
0 deg
0 deg
20 deg
20 deg
y = 101.08x - 17134
R2 = 0.9838
y = 101.29x - 17566
R2 = 0.9835
y = 103.28x - 13411
R2 = 0.9759
y = 102.5x - 13695
R2 = 0.9753

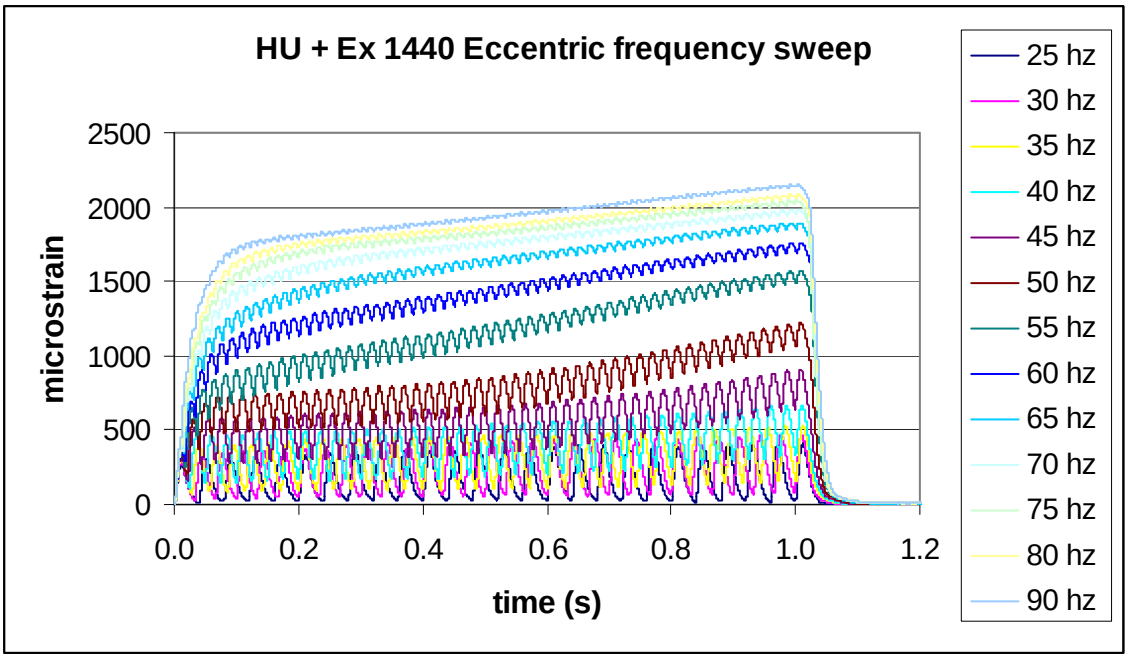
HU + Ex 1440 Eccentric frequency sweep
microstrain
2500
2000
1500
1000
500
0
0.0
0.2
0.4
0.6
0.8
1.0
1.2
time (s)
25 hz
30 hz
35 hz
40 hz
45 hz
50 hz
55 hz
60 hz
65 hz
70 hz
75 hz
80 hz
90 hz

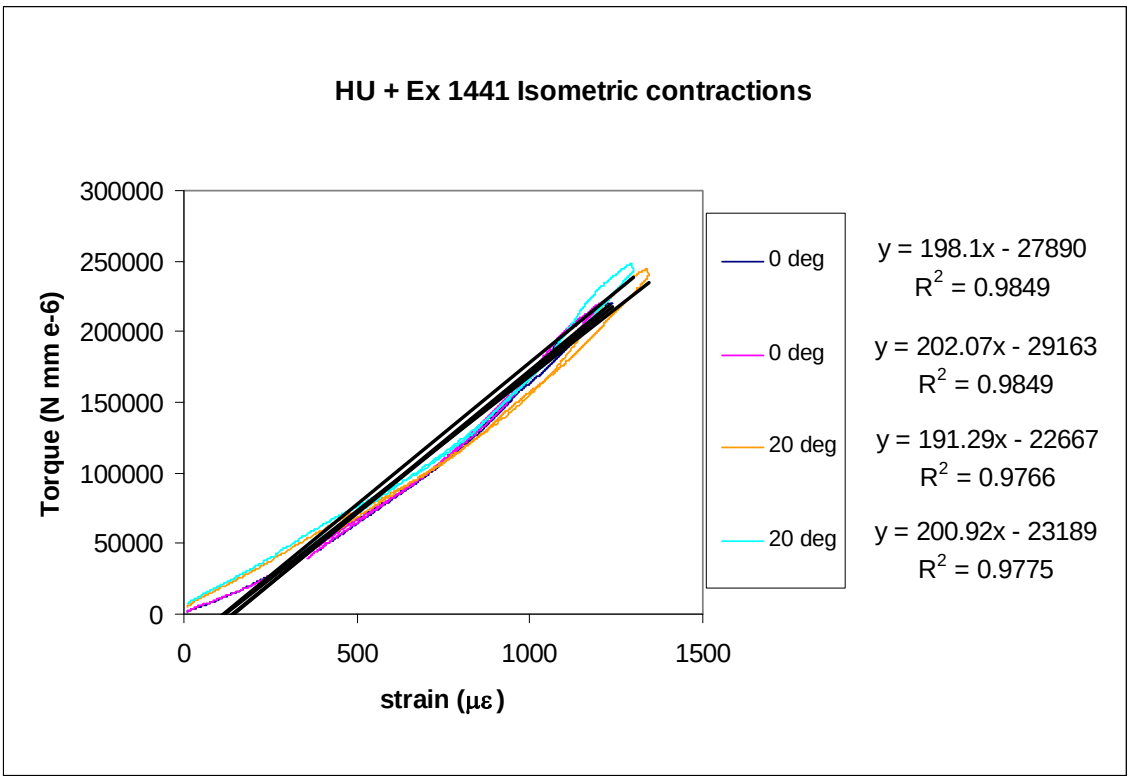
HU + Ex 1441 Isometric contractions
Torque (N mm e-6)
300000
250000
200000
150000
100000
50000
0
0
500
1000
1500
strain (με)
0 deg
0 deg
20 deg
20 deg
y = 198.1x - 27890
R2 = 0.9849
y = 202.07x - 29163
R2 = 0.9849
y = 191.29x - 22667
R2 = 0.9766
y = 200.92x - 23189
R2 = 0.9775

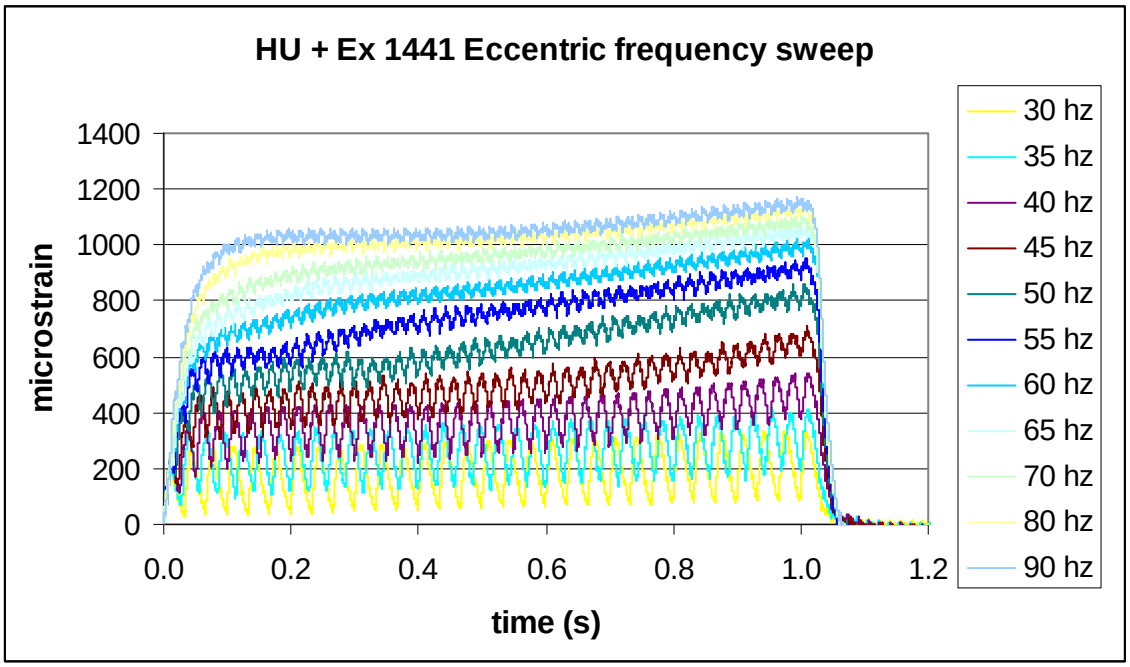
HU + Ex 1441 Eccentric frequency sweep
microstrain
1400
1200
1000
800
600
400
200
0
0.0
0.2
0.4
0.6
0.8
1.0
1.2
time (s)
30 hz
35 hz
40 hz
45 hz
50 hz
55 hz
60 hz
65 hz
70 hz
80 hz
90 hz

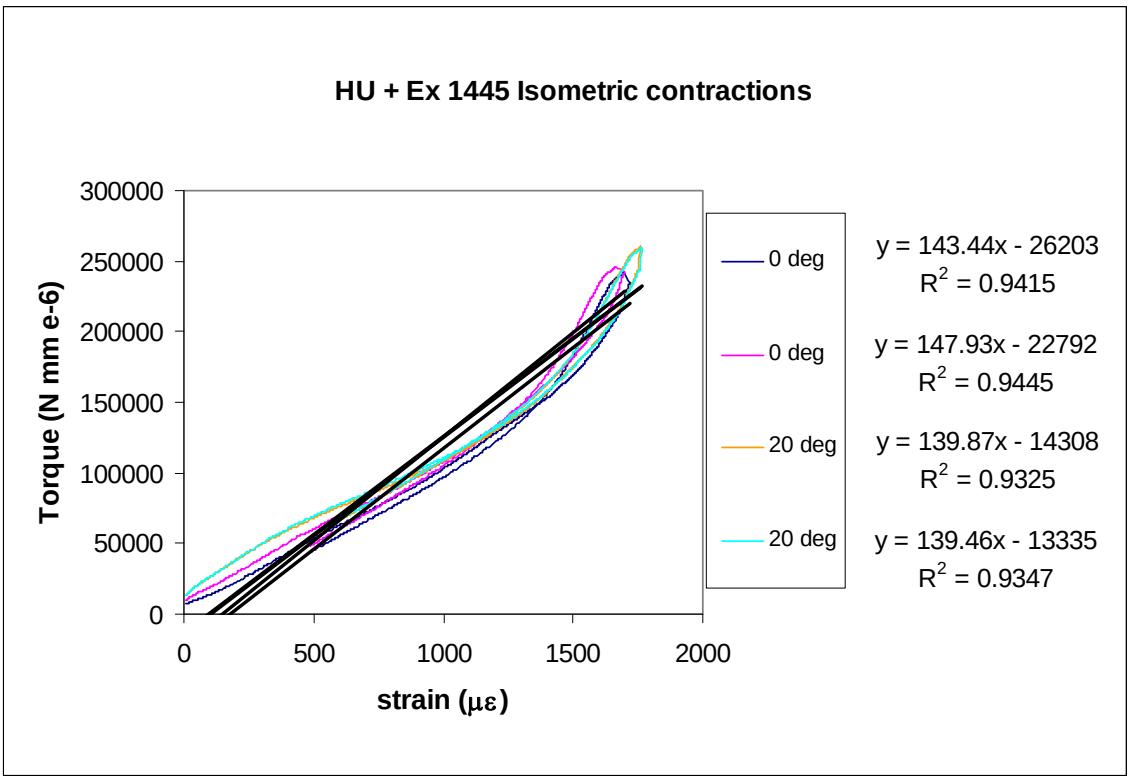
HU + Ex 1445 Isometric contractions
Torque (N mm e-6)
300000
250000
200000
150000
100000
50000
0
0
500
1000
1500
2000
strain (με)
0 deg
0 deg
20 deg
20 deg
y = 143.44x - 26203
R2 = 0.9415
y = 147.93x - 22792
R2 = 0.9445
y = 139.87x - 14308
R2 = 0.9325
y = 139.46x - 13335
R2 = 0.9347

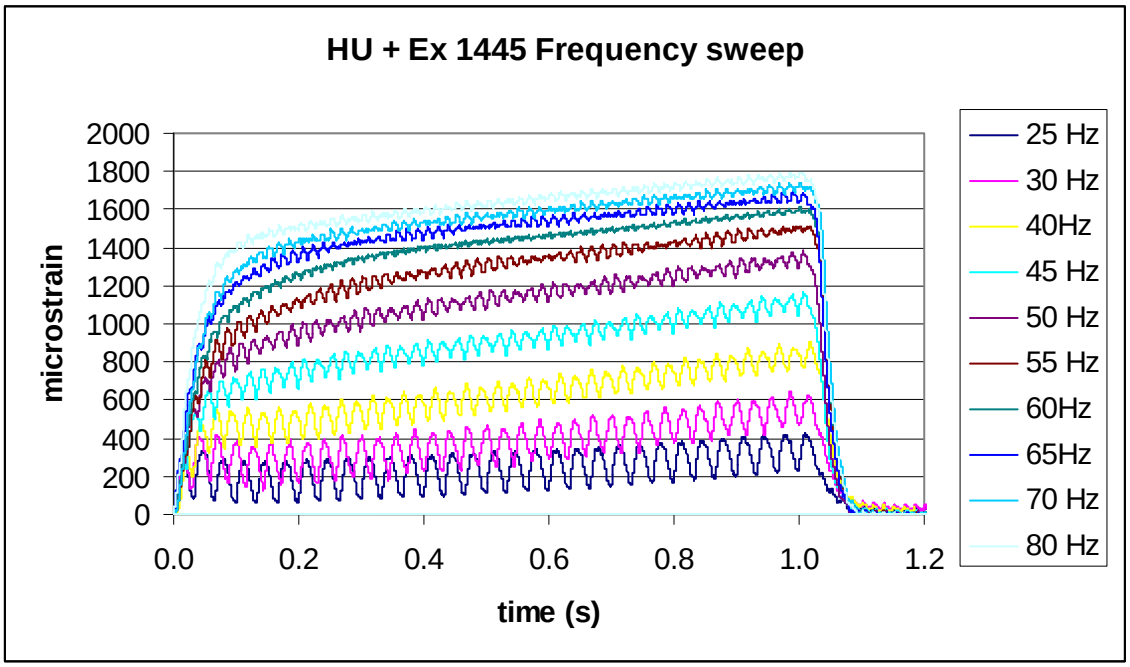
HU + Ex 1445 Frequency sweep
microstrain
2000
1800
1600
1400
1200
1000
800
600
400
200
0
0.0
0.2
0.4
0.6
0.8
1.0
1.2
time (s)
25 Hz
30 Hz
40Hz
45 Hz
50 Hz
55 Hz
60Hz
65Hz
70 Hz
80 Hz

APPENDIX B

Group data tables

Baseline Isometric contraction data

	Individual contractions			Animal average		
Animal	Peak strain	Peak torque	Strain rate	Peak strain	Peak torque	Strain rate
1431	2044	0.2775	61923	2144	0.2964	59754
1431	2199	0.3032	61240			
1431	2190	0.3084	56099			
1432	1523	0.2909	54796	1596	0.3068	54464
1432	1547	0.2905	52299			
1432	1629	0.3238	56647			
1432	1687	0.3220	54116			
1433	1311	0.2354	45059	1345	0.2465	44397
1433	1301	0.2356	44699			
1433	1338	0.2810	41899			
1433	1431	0.2340	45932			
1443	1234	0.2793	37397	1289	0.2941	45932
1443	1242	0.2702	48735			
1443	1350	0.3143	48370			
1443	1328	0.3128	49227			
1444	1489	0.2848	39824	1588	0.2984	39896
1444	1491	0.2871	38797			
1444	1724	0.3109	41652			
1444	1650	0.3109	39311			

HU + Ex Isometric contraction data

	Individual contractions			Animal average		
Animal	Peak strain	Peak torque	Strain rate	Peak strain	Peak torque	Strain rate
1434	865	0.2202	30506	873	0.2293	30416
1434	900	0.2307	32411			
1434	763	0.2248	24446			
1434	967	0.2413	34300			
1436	1216	0.2578	41233	1269	0.2678	40087
1436	1199	0.2578	38258			
1436	1347	0.2836	42642			
1436	1312	0.2720	38215			
1437	2208	0.2387	56017	2278	0.2498	55592
1437	2187	0.2409	55104			
1437	2376	0.2599	53687			
1437	2341	0.2596	57560			
1438	1674	0.1716	51094	1735	0.1793	49072
1438	1679	0.1720	51609			
1438	1756	0.1867	44282			
1438	1833	0.1869	49301			
1440	1940	0.1851	70435	2016	0.1982	72822
1440	1946	0.1855	72048			
1440	2082	0.2118	73534			
1440	2095	0.2104	75270			
1441	1246	0.2220	44540	1289	0.2354	45493
1441	1237	0.2243	43821			
1441	1359	0.2457	47815			
1441	1315	0.2495	45796			
1445	1734	0.2429	54701	1754	0.2528	57427
1445	1707	0.2476	59177			
1445	1785	0.2607	57453			
1445	1792	0.2601	58375			

Eccentric contraction data

Group	Animal	Body weight	Freq	Peak torque	PIT	Peak strain	Ave strain	Initial strain rate	Max oscl strain rate
Baseline	1430	445	10	0.079	0.255	226	43	800	26429
Baseline	1430	445	20	0.167	0.255	382	187	17600	30000
Baseline	1430	445	30	0.361	0.255	932	586	18900	30000
Baseline	1430	445	40	0.508	0.255	1667	1357	24100	22857
Baseline	1430	445	50	0.555	0.255	1567	1370	20200	22143
Baseline	1430	445	60	0.555	0.255	1443	1112	19500	18571
Baseline	1430	445	70	0.488	0.255	1502	1172	27500	19286
Baseline	1431		10	0.059	0.305	277	57	6939	23571
Baseline	1431		20	0.084	0.305	289	130	23265	27857
Baseline	1431		30	0.121	0.305	418	250	7143	33571
Baseline	1431		40	0.241	0.305	849	616	22143	30714
Baseline	1431		50	0.371	0.305	1435	1129	33571	20714
Baseline	1431		60	0.426	0.305	1467	1240	2959	20714
Baseline	1432	455	20	0.086	0.32	344	88	6388	31071
Baseline	1432	455	25	0.120	0.32	428	165	23361	43277
Baseline	1432	455	30	0.140	0.32	425	224	10045	30561
Baseline	1432	455	35	0.180	0.32	493	295	23765	32707
Baseline	1432	455	40	0.235	0.32	670	409	26517	32336
Baseline	1432	455	45	0.295	0.32	969	679	24575	25629
Baseline	1432	455	50	0.355	0.32	1258	947	21436	22004
Baseline	1432	455	60	0.412	0.32	1608	1262	27771	17738
Baseline	1432	455	70	0.437	0.32	1730	1439	24453	14555
Baseline	1433	449	20	0.068	0.282	247	56	18084	27043
Baseline	1433	449	25	0.075	0.282	259	96	3326	30596
Baseline	1433	449	30	0.089	0.282	271	119	2556	26009
Baseline	1433	449	40	0.176	0.282	497	270	21501	32028
Baseline	1433	449	45	0.237	0.282	687	429	21940	29303
Baseline	1433	449	50	0.288	0.282	882	590	17254	26512
Baseline	1433	449	60	0.375	0.282	1019	828	9939	11745
Baseline	1433	449	70	0.397	0.282	1124	974	23893	16089
Baseline	1443	489	25	0.095	0.293	309	148	13727	30981
Baseline	1443	489	30	0.130	0.293	356	206	15264	24490
Baseline	1443	489	35	0.176	0.293	481	289	16995	29582
Baseline	1443	489	40	0.247	0.293	703	441	11386	29254
Baseline	1443	489	45	0.304	0.293	859	617	13444	23146
Baseline	1443	489	50	0.366	0.293	1041	811	15033	18487
Baseline	1443	489	55	0.408	0.293	1234	961	16697	18914
Baseline	1443	489	60	0.427	0.293	1331	1060	17797	16501
Baseline	1443	489	70	0.443	0.293	1405	1157	15522	14434

Eccentric contraction data (cont.)

Group	1443	Body weight	Freq	Peak torque	PIT	Peak strain	Ave strain	Initial strain rate	Max oscl strain rate
Baseline	1444	486	20	0.099	0.312	344	185	20587	28871
Baseline	1444	486	25	0.138	0.312	398	228	21561	26356
Baseline	1444	486	30	0.202	0.312	496	313	21658	23183
Baseline	1444	486	35	0.266	0.312	672	484	21386	19393
Baseline	1444	486	40	0.327	0.312	890	677	22060	16495
Baseline	1444	486	45	0.381	0.312	1123	863	21215	16306
Baseline	1444	486	50	0.426	0.312	1303	1012	21610	14761
Baseline	1444	486	55	0.455	0.312	1423	1121	20989	12776
Baseline	1444	486	60	0.472	0.312	1508	1186	21064	11159
Baseline	1444	486	70	0.492	0.312	1617	1286	22956	9286
HU + Ex	1434	457	20	0.132	0.256	279	142	14774	21557
HU + Ex	1434	457	25	0.217	0.256	419	245	17173	22050
HU + Ex	1434	457	35	0.365	0.256	830	646	18496	12554
HU + Ex	1434	457	40	0.403	0.256	963	781	18353	10652
HU + Ex	1434	457	45	0.423	0.256	1052	878	18750	9770
HU + Ex	1434	457	50	0.431	0.256	1105	930	19010	8502
HU + Ex	1434	457	55	0.435	0.256	1134	969	18662	6300
HU + Ex	1434	457	60	0.436	0.256	1156	991	19221	5708
HU + Ex	1434	457	70	0.433	0.256	1166	1020	20586	3860
HU + Ex	1436	434	20	0.083	0.281	212	86	11540	23697
HU + Ex	1436	434	25	0.126	0.281	280	151	16505	31203
HU + Ex	1436	434	30	0.189	0.281	416	243	16605	26665
HU + Ex	1436	434	35	0.253	0.281	592	396	16627	26233
HU + Ex	1436	434	40	0.316	0.281	850	631	18016	17192
HU + Ex	1436	434	45	0.365	0.281	1020	812	18105	19944
HU + Ex	1436	434	50	0.391	0.281	1125	931	18280	13853
HU + Ex	1436	434	60	0.412	0.281	1209	1029	18717	9943
HU + Ex	1436	434	70	0.418	0.281	1130	962	22446	11106

Eccentric contraction data (cont.)

Group	1436	Body weight	Freq	Peak torque	PIT	Peak strain	Ave strain	Initial strain rate	Max oscl strain rate
HU + Ex	1437	417	20	0.053	0.244	296	120	14470	47286
HU + Ex	1437	417	25	0.052	0.244	331	164	16435	46987
HU + Ex	1437	417	30	0.093	0.244	461	253	17559	60081
HU + Ex	1437	417	35	0.132	0.244	590	319	13958	68520
HU + Ex	1437	417	40	0.185	0.244	737	466	12439	59738
HU + Ex	1437	417	45	0.234	0.244	1148	726	14147	52233
HU + Ex	1437	417	50	0.290	0.244	1474	1002	11721	49430
HU + Ex	1437	417	55	0.333	0.244	1779	1339	16342	47216
HU + Ex	1437	417	60	0.353	0.244	1974	1576	14464	34188
HU + Ex	1437	417	65	0.364	0.244	2071	1707	18013	40707
HU + Ex	1437	417	70	0.371	0.244	2071	1707	18013	40707
HU + Ex	1437	417	75	0.375	0.244	2226	1870	20062	36699
HU + Ex	1437	417	80	0.375	0.244	2270	1900	9060	32389
HU + Ex	1437	417	90	0.375	0.244	2295	1961	23396	29091
HU + Ex	1438	346	20	0.074	0.191	337	31	20953	46484
HU + Ex	1438	346	25	0.103	0.191	487	265	23728	53385
HU + Ex	1438	346	30	0.165	0.191	784	487	21418	39088
HU + Ex	1438	346	35	0.214	0.191	1125	816	24784	45317
HU + Ex	1438	346	40	0.252	0.191	1453	1130	26570	40532
HU + Ex	1438	346	45	0.280	0.191	1453	1130	26570	40532
HU + Ex	1438	346	50	0.297	0.191	1847	1496	27380	35901
HU + Ex	1438	346	55	0.307	0.191	1967	1623	25083	36687
HU + Ex	1438	346	60	0.312	0.191	2049	1700	29928	26215
HU + Ex	1438	346	70	0.310	0.191	2143	1804	32227	33164
HU + Ex	1440	348	25	0.065	0.212	406	170	15442	52935
HU + Ex	1440	348	30	0.078	0.212	468	230	16718	58861
HU + Ex	1440	348	35	0.097	0.212	530	296	17873	57279
HU + Ex	1440	348	40	0.127	0.212	669	395	18487	56437
HU + Ex	1440	348	45	0.162	0.212	910	553	18256	54858
HU + Ex	1440	348	50	0.199	0.212	1223	792	18784	48040
HU + Ex	1440	348	55	0.243	0.212	1572	1138	20555	40209
HU + Ex	1440	348	60	0.267	0.212	1757	1381	20986	30861
HU + Ex	1440	348	65	0.281	0.212	1894	1566	22938	26178
HU + Ex	1440	348	70	0.287	0.212	1983	1685	24113	22345
HU + Ex	1440	348	75	0.291	0.212	2047	1765	29547	18019
HU + Ex	1440	348	80	0.292	0.212	2087	1813	35467	15953
HU + Ex	1440	348	90	0.292	0.212	2152	1882	46515	12636

Eccentric contraction data (cont.)

Group	1440	Body weight	Freq	Peak torque	PIT	Peak strain	Ave strain	Initial strain rate	Max oscl strain rate
HU + Ex	1441	384	30	0.099	0.246	338	183	11081	48875
HU + Ex	1441	384	35	0.132	0.246	417	255	12506	55062
HU + Ex	1441	384	40	0.177	0.246	542	365	13172	47123
HU + Ex	1441	384	45	0.233	0.246	711	485	13913	46348
HU + Ex	1441	384	50	0.285	0.246	858	622	13907	44467
HU + Ex	1441	384	55	0.317	0.246	953	730	13555	42956
HU + Ex	1441	384	60	0.333	0.246	1024	818	14621	28912
HU + Ex	1441	384	65	0.342	0.246	1068	881	14793	38235
HU + Ex	1441	384	70	0.344	0.246	1106	933	21050	37161
HU + Ex	1441	384	80	0.348	0.246	1154	995	23624	30435
HU + Ex	1441	384	90	0.347	0.246	1171	1027	27140	30956
HU + Ex	1445	441	20	0.068	0.264	425	241	18270	41287
HU + Ex	1445	441	25	0.089	0.264	645	378	18978	43109
HU + Ex	1445	441	30	0.130	0.264	904	609	12895	38968
HU + Ex	1445	441	40	0.244	0.264	1166	871	18619	29195
HU + Ex	1445	441	45	0.298	0.264	1381	1080	17789	32463
HU + Ex	1445	441	50	0.343	0.264	1515	1237	16135	28791
HU + Ex	1445	441	55	0.371	0.264	1612	1354	17522	15613
HU + Ex	1445	441	60	0.384	0.264	1694	1441	21051	23905
HU + Ex	1445	441	65	0.391	0.264	1738	1492	16648	23573
HU + Ex	1445	441	70	0.394	0.264	1797	1569	28388	17920

Eccentric contraction aproximations at PIT

Group	Animal	Peak strain	Ave strain	Initial strain rate	Max oscil strain rate
Baseline	1431	704	463	13848	26576
Baseline	1432	1102	863	17073	24430
Baseline	1433	808	600	16833	22106
Baseline	1443	873	646	15123	22664
Baseline	1444	933	697	21488	18457
Hu + Ex	1434	583	423	16921	17198
Hu + Ex	1436	751	575	17377	20116
Hu + Ex	1437	1336	1013	15650	46857
Hu + Ex	1438	1072	769	24573	42506
Hu + Ex	1440	1406	1094	23915	36980
Hu + Ex	1441	775	590	15462	42752
Hu + Ex	1445	1263	1003	18553	29938
Baseline Average		884	654	16873	22847
HU +Ex Average		1027	781	18922	33764
Overall Average		967	728	18068	29215

APPENDIX C

Radiographs

Some bones were lost and were not available for radiography. Images were inverted. See Figure 37 for identifying markers.

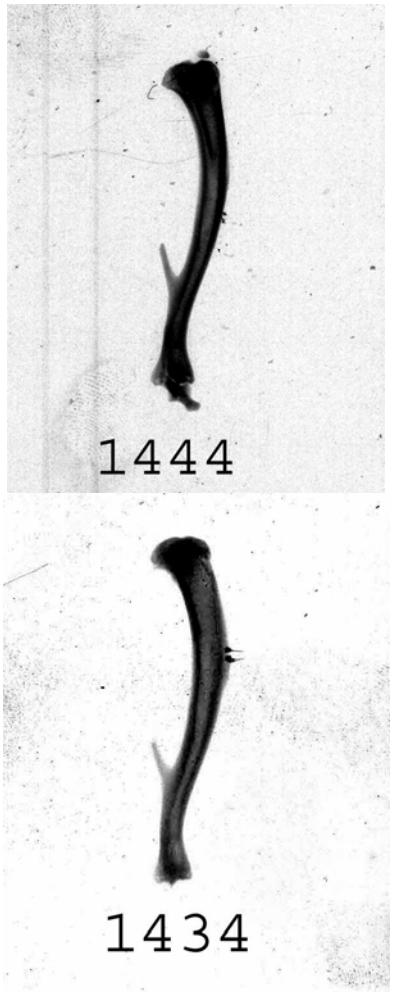

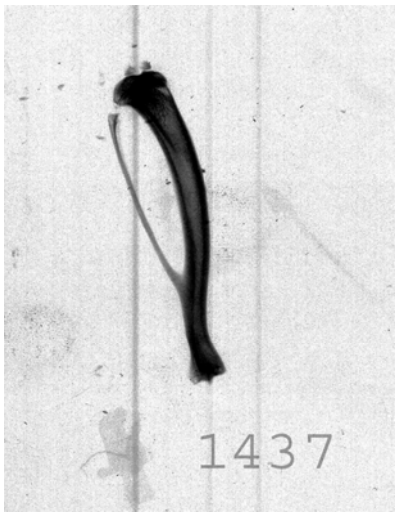
1437

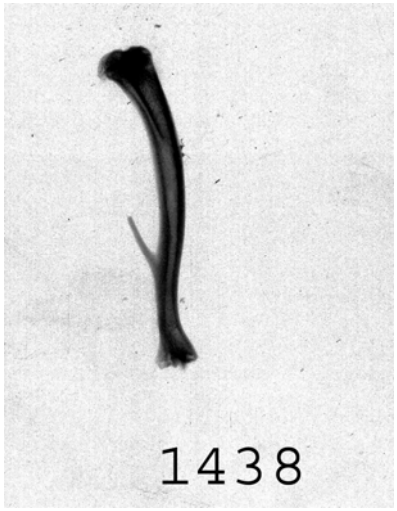
1438


1440

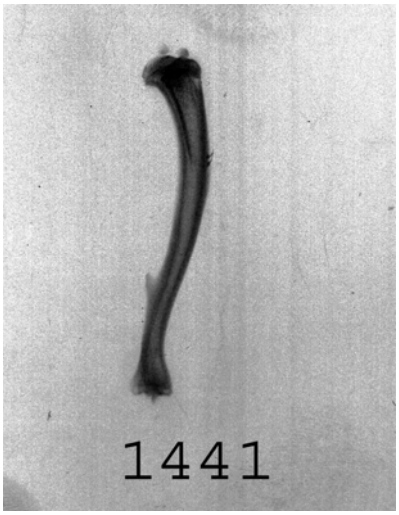
1441

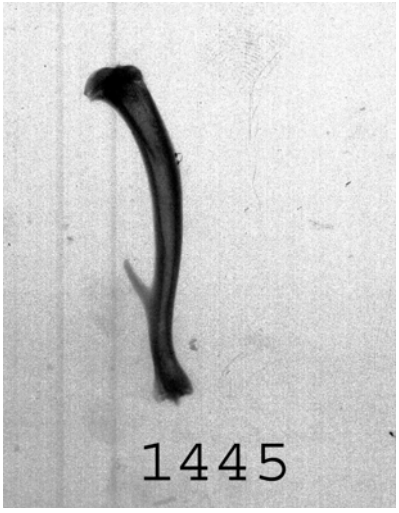
1445

VITA

Name: Jay Melvin Jeffery

Address: Department of Mechanical Engineering
c/o Dr. Harry Hogan
Texas A&M University MS 3123
College Station, TX 77843

Email: jaymjeffery@yahoo.com

Education: M.S., Mechanical Engineering
Texas A&M University, College Station, TX, December 2007
B.S., Mechanical Engineering
Brigham Young University, Provo, UT, April 2004

Publications: Jeffery JM, Murphy MC, Stallone JL, Bloomfield SA, Hogan HA Characterizing strain in the tibia of rats exposed to hindlimb unloading with an exercise countermeasure, Abstract Proceedings of the ASME 2007 Summer Bioengineering Conference (SBC2007) June 20-24, Keystone Resort & Conference Center, Keystone, Colorado, USA